

**PYROGLUTAMATE FORMATION AND HYDROGEN-DEUTERIUM  
EXCHANGE IN LYOPHILIZED THERAPEUTIC PROTEINS**

by

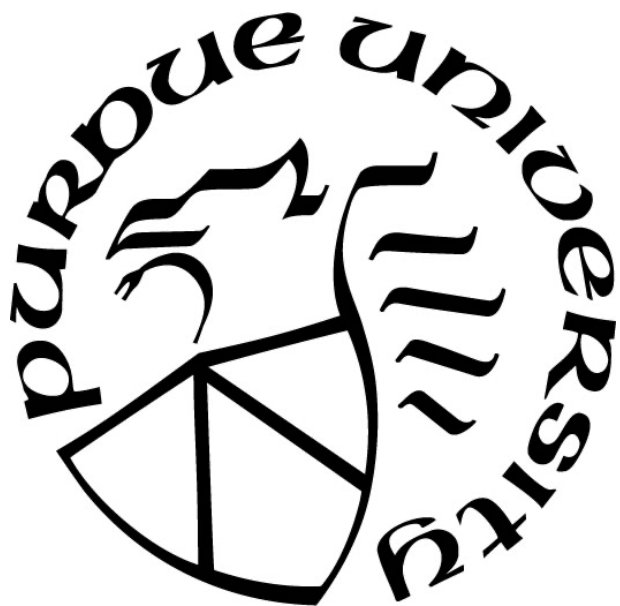
**Lia M. Bersin**

**A Dissertation**

*Submitted to the Faculty of Purdue University*

*In Partial Fulfillment of the Requirements for the degree of*

**Doctor of Philosophy**



Department of Industrial and Physical Pharmacy

West Lafayette, Indiana

December 2021

**THE PURDUE UNIVERSITY GRADUATE SCHOOL**  
**STATEMENT OF COMMITTEE APPROVAL**

**Dr. Elizabeth Topp, Chair**

Department of Industrial and Physical Pharmacy

**Dr. Sajal M. Patel**

AstraZeneca

**Dr. Lynne S. Taylor**

Department of Industrial and Physical Pharmacy

**Dr. Qi Tony Zhou**

Department of Industrial and Physical Pharmacy

**Approved by:**

Dr. Eric Munson

*To Juju and Bebo*

## ACKNOWLEDGMENTS

While completing a doctoral dissertation is undoubtedly an exercise in independence, it cannot be achieved alone. I would not be here today without the support and encouragement of many people both here at Purdue and those farther afield. I will be forever grateful to those who helped me reach this milestone.

I would like to express my sincerest thanks to my advisor Dr. Elizabeth Topp, who guided me gracefully while also challenging me to build independence. Due to her mentorship, I am now a more inquisitive and confident scientist and professional. An advisor that truly supports pursuit of your own interests is a unique gift, as is one that encourages fostering a life outside of the lab. I am fortunate to have found both in Dr. Topp.

I am thankful to my committee members Dr. Sajal Patel, Dr. Lynne Taylor, and Dr. Q. Tony Zhou for their guidance.

This research would not have been possible without contributions from AstraZeneca. The discussions with and advice from Dr. Sajal Patel shaped my research considerably. I am grateful that these interactions helped maintain the balance between industry and academia in my research that I strived for. I am also thankful for the financial support provided by the PhRMA Foundation Pre-Doctoral Fellowship in Pharmaceutics and the Bilsland Dissertation Fellowship from the College of Pharmacy.

It has been a pleasure to work with all members of the Topp lab over the past five years. I am thankful for the friendly and supportive environment where advice could equally be given and received, and scientific discussion was aplenty. For every challenge faced during my research I will have a memory of laughter and joy thanks to this group. Specific thanks are due to Dr. Rishabh Tukra, with whom I completed this journey in tandem. I am grateful for the camaraderie, support, and all that we have learned from each other over the years.

Most importantly, I would not be here today without the love and support of my friends and family. I owe so much to them. To my friends and colleagues at GSK for encouraging me to embark on this wild journey. To the WRCC, where I have found a newfound love of cycling, a wonderful community and a group of friends that make leaving Indiana harder than I could have ever imagined. The support on and off the bike was exactly what I needed during challenging times. To Ali, for always viewing me as the most outstanding and capable version of myself. To my dear

Julian for his love and support, and for always encouraging me to be a better scientist and human.  
To my sister, Emily, for being the perfect role model and friend for as long as I can remember.  
Finally, to my parents for their unwavering support, for reassuring me when I am uncertain, for teaching me the value of hard work, and for believing the world in me.

## TABLE OF CONTENTS

ACKNOWLEDGMENTS .....	4
LIST OF TABLES.....	10
LIST OF FIGURES .....	11
LIST OF ABBREVIATIONS.....	14
ABSTRACT.....	15
CHAPTER 1. INTRODUCTION .....	17
1.1 Therapeutic Proteins.....	17
1.2 Mechanisms of Protein Stability in the Solid State .....	18
1.3 Formulating to Achieve Stability in Lyophilized Proteins.....	20
1.3.1 Sugars and Carbohydrates.....	21
1.3.2 Buffer Salts and pH control.....	22
1.3.3 Amino Acids and Osmolytes.....	22
1.3.4 Moisture Content.....	23
1.4 Pyroglutamate Formation .....	24
1.5 Solid-State Hydrogen-Deuterium Exchange Mass Spectrometry .....	29
1.6 Conclusions .....	34
1.7 Research Scope.....	34
1.8 Dissertation Overview .....	34
1.9 References .....	36
CHAPTER 2. EFFECT OF 'PH' ON RATE OF PYROGLUTAMATE FORMATION IN SOLUTION AND LYOPHILIZED SOLIDS.....	43
2.1 Abstract.....	43
2.2 Introduction .....	43
2.3 Experimental Section.....	46
2.3.1 Materials.....	46
2.3.2 Preparation of Model Peptide Solutions.....	47
2.3.3 Preparation of Buffer Solutions.....	47
2.3.4 Preparation of Formulations in the Solid and Solution States .....	48
2.3.5 Accelerated Stability Studies .....	48

2.3.6	Sample Analysis .....	49
2.3.7	Kinetic Analysis .....	49
2.3.8	Moisture Content of Lyophilized Solids .....	50
2.4	Results .....	51
2.4.1	EVQL and pGlu-VQL Peptide Analysis.....	51
2.4.2	pH Effect on Accelerated Stability.....	51
2.4.3	Buffer Catalysis.....	55
2.4.4	Rate Constants.....	56
2.5	Discussion.....	58
2.6	Conclusions .....	61
2.7	References .....	62
CHAPTER 3. FORMULATION APPROACH TO INHIBIT PYROGLUTAMATE FORMATION IN A MODEL PEPTIDE .....		64
3.1	Abstract.....	64
3.2	Introduction .....	64
3.3	Experimental Section.....	66
3.3.1	Materials.....	66
3.3.2	Sample Preparation .....	67
3.3.3	Accelerated Stability Studies .....	69
3.3.4	Kinetic Analysis .....	69
3.3.5	Solid-State HDX-MS .....	70
3.3.6	Moisture Content of Lyophilized Solids .....	71
3.3.7	Modulated Differential Scanning Calorimetry (DSC) .....	71
3.4	Results .....	71
3.4.1	Excipient and 'pH' Effects.....	71
3.4.2	ssHDX-MS Analysis of Excipient and 'pH' Effects.....	74
3.4.3	Moisture Content and Tg Effects .....	78
3.5	Discussion.....	80
3.6	Conclusions .....	83
3.7	References .....	84

CHAPTER 4. EFFECTS OF TEMPERATURE AND RELATIVE HUMIDITY ON SOLID-STATE HYDROGEN DEUTERIUM EXCHANGE (SSHDX-MS) OF A MONOCLONAL ANTIBODY 87

4.1	Abstract.....	87
4.2	Introduction .....	87
4.3	Experimental Section.....	90
4.3.1	Materials.....	90
4.3.2	Experimental Design.....	90
4.3.3	Statistical Analysis .....	91
4.3.4	Sample Preparation .....	91
4.3.5	Solid-State Hydrogen-Deuterium Exchange Mass Spectrometry (ssHDX-MS) ....	92
4.3.6	Moisture Content by Karl Fischer Titration (KF).....	93
4.3.7	Modulated Differential Scanning Calorimetry (DSC).....	93
4.3.8	Solid-State Fourier Transform Infrared Spectroscopy (FTIR).....	93
4.3.9	Powder X-ray Diffraction (PXRD).....	94
4.3.10	Dynamic Vapor Sorption (DVS).....	94
4.4	Results .....	94
4.4.1	Secondary Structure by FTIR.....	94
4.4.2	Physical Characterization by PXRD .....	95
4.4.3	Water Vapor Sorption Behavior by DVS.....	95
4.4.4	Moisture Content by KF.....	95
4.4.5	Modulated DSC.....	97
4.4.6	ssHDX-MS .....	97
4.5	Discussion.....	105
4.6	Conclusions .....	111
4.7	References .....	112
CHAPTER 5. CONCLUSIONS AND RECOMMENDATIONS.....		115
5.1	Main Findings.....	115
5.2	Recommendations for Future Research.....	117
5.3	References .....	119
APPENDIX A. SUPPORTING INFORMATION FOR CHAPTER 2 .....		120

APPENDIX B. SUPPORTING INFORMATION FOR CHAPTER 3 ..... 130  
APPENDIX C. SUPPORTING INFORMATION FOR CHAPTER 4 ..... 135

## LIST OF TABLES

Table 3-1. Composition of EVQL peptide formulations for study of excipient and 'pH' effects.	68
Table 3-2. Composition of EVQL peptide formulations for moisture content and mobility investigation.	69
Table 4-1. ANOVA of the treatment variables RH, temperature, and glycerol content on ssHDX-MS kinetic parameters $D_{\text{fast}}$ and $k_{\text{fast}}$ . Treatment variables with $p > 0.05$ were eliminated from the fit model.	103

## LIST OF FIGURES

Figure 1-1. Reaction pathways for the formation of pGlu through cyclization of N-terminal Gln or Glu (A). The reaction from Gln results in the loss of ammonia while the reaction from Glu results in the loss of a water molecule. Proposed mechanism of pGlu formation from Glu through a tetrahedral intermediate (B). .....	24
Figure 1-2. pH effects on pyroglutamate formation of the light chain (LC) and heavy chain (HC) of a mAb after storage as a lyophilized powder for 3 months at 37°C (green triangles) and 45°C (red circles and blue diamonds). This figure is reprinted from Ref [70]. .....	28
Figure 1-3. Schematic representation of solution-state HDX reprinted from Ref. [78] .....	29
Figure 1-4. Correlation of deuterium uptake (% $D_{max}$ ) with high molecular weight species of mAb formulations stored at 5°C for 960 days (A), 25°C for 960 days (B), 40°C for 960 days (C), and 50°C for 180 days (D). The data were fit to a linear model to obtain the slope, intercept and $R^2$ values. Figure reprinted from Ref. [80] .....	33
Figure 2-1. Reaction pathways for the formation of pGlu through cyclization of N-terminal Gln or Glu (A). The reaction from Gln results in the loss of ammonia while the reaction from Glu results in the loss of a water molecule. Proposed mechanism of pGlu formation from Glu through a tetrahedral intermediate (B). .....	45
Figure 2-2. Kinetics of degradation of the EVQL peptide and formation of pGlu-VQL in solution (D-F; pH 4, 6 and 8) and in lyophilized solids prepared from these solutions (A-C). Concentrations of peptides EVQL peptide (black circle), pGlu-VQL peptide (dark gray square), summed side products (gray triangle), and total peptide concentration (light gray inverted triangle) after incubation at 50°C. n=9 (3 replicate measurements of 3 vials), mean $\pm$ S.D. ....	53
Figure 2-3. pGlu-VQL peptide concentration after 1 week (A), 5 weeks (B), and 10 weeks (C) of storage at 50°C in solution (gray) and lyophilized solid (black). n=9 (3 replicate measurements of 3 vials), mean $\pm$ S.D. ....	54
Figure 2-4. pGlu-VQL peptide concentration in formulations with 20 mM (black circle), 40 mM (gray square), and 60 mM (open triangle) buffer concentration over 10 weeks incubation at 50°C stored as lyophilized solid (A) and in solution (B). n=9 (3 replicate measurements of 3 vials), mean $\pm$ S.D. ....	56
Figure 2-5. ‘pH’-rate profile for pGlu formation in lyophilized solids (black circle) and in solution (gray square) at 50 °C. Error bars represent standard error of the first-order kinetic model regression fit (Equation 2.1). Rate constants have been adjusted to zero buffer concentration where applicable as described in the text. ....	57
Figure 3-1. Reaction pathway for the formation of pGlu through cyclization of N-terminal Glu via a tetrahedral intermediate. ....	65
Figure 3-2. Kinetics of degradation of the EVQL peptide and formation of pGlu-VQL in lyophilized solids (A-C) and solution controls (D-F) formulated at ‘pH’ 7 with trehalose (A,D), dextran (B,E), and hydroxyectoine (C,F). Concentrations of EVQL peptide (circles), pGlu-VQL	

peptide (squares), summed side products (triangles), and total peptide concentration (inverted triangles) after incubation at 50 °C, n=9 (3 replicate measurements of 3 vials), mean ± S.D..... 72

Figure 3-3. ‘pH’-rate profiles for pGlu formation in lyophilized solids (A) and solution controls (B) containing trehalose (circles), dextran (triangles), and hydroxyectoine (squares) at 50 °C. Error bars represent standard error of the first-order kinetic model regression fit (Equation 3.1). ..... 73

Figure 3-4. Deuterium incorporation in ssHDX-MS studies (11% RH, 25 °C) of EVQL peptide formulations containing: (A) trehalose, (B) dextran, (C) hydroxyectoine, and (D) all formulations; see Table 3-1 for formulation compositions. Lines represent fits to a biexponential model (Equation 3.2).  $n = 3$ , mean ± SD; error bars not shown when less than the height of the symbol. .... 75

Figure 3-5. ssHDX-MS kinetic parameters,  $D_{fast}$  (A),  $D_{slow}$  (B),  $k_{fast}$  (C), and  $k_{slow}$  (D), fit to the biexponential model in Eq. 3.2 for EVQL peptide formulations containing trehalose (red), dextran (blue), and hydroxyectoine (green). HDX was performed at 11% RH and 25 °C. See Table 3-1 for formulation compositions. Error bars represent standard error of regression..... 76

Figure 3-6. pGlu-VQL peptide concentration formed in lyophilized solids containing the EVQL peptide stored at 50 °C for 15 weeks as a function of (A)  $D_{fast}$  and (B) total deuterium incorporation,  $D_{fast} + D_{slow}$  (Equation 3.2) measured by ssHDX-MS. Samples were formulated with trehalose (circles), dextran (diamonds), and hydroxyectoine (squares) at ‘pH’ 6 (open markers), 7 (cross-haired markers) and 8 (solid markers). The solid lines indicate linear regression. .... 77

Figure 3-7. pGlu-VQL peptide concentration formed in lyophilized solids initially containing the EVQL peptide at 50 °C and: (A) formulated with trehalose or dextran and stored under desiccated conditions, at 6% RH or 11% RH, and (B) formulated with trehalose without glycerol, with 2.5% glycerol or with 5% glycerol. n=9 (3 replicate measurements of 3 vials), mean ± S.D. .... 79

Figure 3-8. pGlu-VQL peptide concentration in lyophilized solids containing the EVQL peptide after 8-weeks storage at 50 °C as a function of moisture content (A) and  $T_g$  (B). Samples were formulated with trehalose (circles) or dextran (squares). Varied moisture content and  $T_g$  were generated by storing samples under desiccated conditions, at 6% RH and 11% RH and by formulation with trehalose with glycerol added at 2.5% (cross-haired diamond) and 5% glycerol (open diamond) (w/w) of excipient content. pGlu concentration, n=9 (3 replicate measurements of 3 vials), mean ± S.D; moisture content, n=3, mean ± S.D.;  $T_g$  n=1..... 80

Figure 4-1. Moisture content (A) and  $T_g$  values (B) of lyophilized mAb formulations containing 0% (purple circles), 5% (blue triangles), or 10% (green squares) glycerol as a function of RH and temperature.  $T_0$  indicates values post-lyophilization before ssHDX incubation. (moisture content  $n = 3$ , mean ± SD;  $T_g$   $n = 1$ ; error bars not shown when less than the height of the symbol)..... 96

Figure 4-2. ssHDX-MS of trehalose-mAb formulations without glycerol (purple circle), and containing 5% glycerol (blue triangle), and 10% glycerol (green square) carried out at 5, 25 and 40 °C and 6, 23, and 43% RH.  $n=3$ , mean ±SD; error bars are not when less than the height of the symbol..... 98

Figure 4-3.  $D_{fast}$  values (Eq 4.2) as a function of temperature (A) and RH (B) for trehalose-mAb formulations containing 0% glycerol (purple circles), 5% glycerol (blue triangles), and 10% glycerol (green squares)..... 100

Figure 4-4.  $k_{fast}$  values (Eq 4.2) as a function of temperature (A) and RH (B) for trehalose-mAb formulations containing 0% glycerol (purple circles), 5% glycerol (blue triangles), and 10% glycerol (green squares). ..... 101

Figure 4-5  $D_{fast}$  (A,C) and  $k_{fast}$  (B,D) values (Eq. 4.2) as a function of moisture content (A,B) and T-Tg (C,D) for lyophilized mAb formulations containing 0% glycerol (purple circles), 5% glycerol (blue triangles), and 10% glycerol (green squares). Solid lines represent linear fit for all data points ..... 104

Figure 4-6. Apparent exchange rate constant ( $k_{app}$ ) as a function of  $aD \times T$  (A) and  $A0/D_{fast}$  as a function of  $1/(aD \times T)$  (B) for lyophilized mAb formulations at 5 °C (red), 25 °C (blue), and 40 °C (green) where  $aD = (\% RH/100)$  at equilibrium. Solid lines represent best fit lines for all data points. .... 109

Figure 4-7. The inverse of  $D_{fast}$  (A) and  $k_{fast}$  (B) values (Eq. 4.2) as a function of the inverse of the product of ssHDX RH and temperature and as the product of RH and temperature, respectively, for lyophilized mAb formulations containing 0% glycerol (purple circles), 5% glycerol (blue triangles), and 10% glycerol (green squares). Solid lines represent linear fit for all data points. .... 111

## LIST OF ABBREVIATIONS

$a_D$	D <sub>2</sub> O <sub>(g)</sub> activity
ANOVA	Analysis of variance
D <sub>fast</sub>	Number (or percent) of exchanging amides in the fast pool
DSC	Differential scanning calorimetry
D <sub>slow</sub>	Number (or percent) of exchanging amides in the slow pool
DVS	Dynamic vapor sorption
EVQL	Synthetic model peptide EVQLVESGGGLVQPGGSLR
FTIR	Fourier transform infrared spectroscopy
Gln	Glutamine
Glu	Glutamate
$k_{fast}$	Apparent first-order rate constant of the fast exchanging amide groups
$k_{slow}$	Apparent first-order rate constant of the slow exchanging amide groups
$k_{obs}$	Observed rate constant
LC-MS	Liquid chromatography mass spectrometry
mAb	Monoclonal antibody
'pH'	Effective pH
pGlu	Pyroglutamate
pGlu-VQL	Pyroglutamate peptide pGlu-VQLVESGGGLVQPGGSLR
PXRD	Powder X-ray diffraction
RH	Relative humidity
rp-HPLC	Reversed phase high performance liquid chromatography
ssHDX-MS	Solid-state hydrogen-deuterium exchange mass spectrometry
S/P	Sugar to protein weight ratio
SST	Treatment sum of squares
T0	Time zero
TFA	Trifluoroacetic acid
Tg	Glass transition temperature

## ABSTRACT

Therapeutic proteins are vital to global health, yet they are challenging to develop due to their large size and complexity. Much about their behavior is still to be understood. The research presented in this dissertation explores chemical reactions in peptides and proteins in the solid-state in order to understand formulation and matrix properties that affect reactions in solid-state therapeutic proteins. More specifically, the work applies two reactions to study reactivity: pyroglutamate (pGlu) formation and solid-state hydrogen-deuterium exchange (ssHDX). pGlu is a chemical degradant found in peptides and proteins with either glutamate (Glu) or glutamine (Gln) at the N-terminal that can occur non-enzymatically during storage. N-terminal Glu and Gln are prevalent in monoclonal antibodies (mAbs), a growing class of biologics, thus understanding this chemical modification is relevant to the development of therapeutic proteins. ssHDX with mass spectrometric analysis (ssHDX-MS) is used as an analytic tool to provide high resolution information on protein structure, stability, and matrix interactions in solid-state peptides and proteins. In this reaction deuterium donors compete for hydrogen bonding sites, which allows interrogation of the protein hydrogen bond network. While well studied when applied to the solution state, the mechanism of exchange in the solid state is not fully understood. The research and findings can be divided into three sections described below.

The first section explores the mechanism of pGlu formation in the solution and solid states using a model peptide. pGlu formation and parent peptide loss were monitored by high performance liquid chromatography under accelerated storage conditions in lyophilized solid and solution formulations with vary 'pH' levels. 'pH' dependence in the solid state differed markedly from that in solution. Moreover, at the 'pH' where mAbs are often formulated the rate of pGlu formation in the solid state was greater than in solution.

The second section aims to develop formulations that inhibit pGlu formation and to identify formulation characteristic and matrix properties that are indicative of pGlu formation. Again, a model peptide was used to monitor pGlu formation in lyophilized solid and solution formulations with varied 'pH' and excipients stored under accelerated conditions. The results indicate that pGlu can be inhibited by low molecular weight hydrogen bonding excipients and low moisture content.

The final section aims to identify solid-state properties that affect ssHDX-MS. The effects of temperature, relative humidity (RH), and mobility on ssHDX were probed using formulations

of lyophilized mAb plasticized with varying levels of glycerol. The results indicate that ssHDX kinetic parameters were influenced by RH and temperature, but not glycerol level. There was a clear linear correlation with molecular mobility ( $T - T_g$  (glass transition temperature)). A first-order kinetic model was proposed that suggests a linear dependence of deuterium incorporation kinetic parameters on the product of RH and temperature, which provides a better correlation than  $T - T_g$ .

The outcomes of this dissertation provide insight into solid-state reaction behavior in peptides and proteins. They have implications for the rational design of stable formulations of therapeutic proteins by expanding our understanding of a relevant chemical instability, pGlu formation, and of a high-resolution analytical technique, ssHDX-MS, that can be used to probe solid-state proteins.

# CHAPTER 1. INTRODUCTION

## 1.1 Therapeutic Proteins

Therapeutic proteins have had a widespread positive impact on global health. Since the approval of the first therapeutic protein, human insulin, in 1982 they have become one of the fastest growing classes of pharmaceuticals. In the three and a half year period from January 2015 to July 2018 the number of approved biopharmaceuticals in the United States more than doubled the typical five-year historical approval rate.<sup>1</sup> A surge of biosimilar approvals contributed to this growth, whose market share is projected to continue growing with the expiration of innovator patents in the coming years.<sup>2</sup> Although nucleic acid- and cell-based therapies are gaining traction, especially since the beginning of the COVID-19 pandemic, the profile of products in advanced clinical trials suggests that protein-based products will continue to dominate the market in the coming years.<sup>1</sup>

The high specificity and complex functionality of therapeutic proteins allows them to be used for a variety of therapies including cancer, autoimmune disease, allergies, and infectious diseases.<sup>3</sup> However the success of any biopharmaceutical product relies on maintenance of the native structure during production, transportation, storage and administration. Disruption of the native structure through either chemical or physical pathways risks loss of therapeutic function. This is challenging for formulation scientists due to a protein's immense size and complexity, which can consist of hundreds to thousands of bonds and interactions, each with the potential to compromise the native structure.

Monoclonal antibodies (mAbs), the leading therapeutic protein on the market both in novel molecules and biosimilars, are particularly challenging because they are large (i.e., ~150 kDa), highly complex, multi-domain molecules. They consist of four polypeptide chains (two heavy chains and two light chains) each containing a variable, at the amino-terminus and a constant region at the carboxyl-terminus. Functionality of the mAb comes from the specific antigen binding site located in the complementarity determining region (CDR) of the variable region. Chemical modification in the CDR has been shown to directly affect antigen binding, specificity, and affinity. In one case, *in vivo* asparagine (Asn) deamidation in the second CDR loop of the heavy chain resulted in a decrease in antigen binding.<sup>4</sup> In another, tryptophan oxidation in the third CDR loop

of the heavy chain of a humanized mAb resulted in a decrease in antigen binding and biologic function.<sup>5</sup> Maintaining both the chemical and physical structure of mAbs in this region is critical for their therapeutic function. But, for a pharmaceutical product to be deemed both safe *and* efficacious the native structure must be maintained here and throughout the entire molecule.

## 1.2 Mechanisms of Protein Stability in the Solid State

To prolong shelf life, proteins with persistent physicochemical instabilities are often stored as solid products, where molecular mobility and interactions are reduced. There are two main theories that govern the stability of proteins in the solid state: the vitrification theory, describing kinetic stabilization, and the water replacement theory, describing thermodynamic stability. Understanding these theories and how they contribute to protein stability is important for effective protein formulation and stability characterization.

Thermodynamic stability is achieved by shifting the equilibrium between the native and denatured states towards the native state. In the solution state, a protein's native structure is stabilized by a network hydrogen bonds within the protein and between the protein surface and the surrounding water molecules. When water is removed during the drying process the equilibrium is shifted towards the denatured state and the conformation of the protein is compromised. The water replacement theory assumes that in the solid state the hydrogen bonds to water are replaced by hydrogen bonds to hydroxyl-containing excipients, such as disaccharides and polyols. These bonds help maintain the native state and shift the equilibrium towards the folded state.<sup>6</sup> Protein-sugar interactions observed in lyophilized samples by Fourier transform infrared (FTIR) analysis appear similar to protein-water interactions in solution in support of the replacement theory.<sup>7</sup> Furthermore, conservation of the amide II band, indicative of protein secondary structure and hydrogen bonding, between solution and solid states has been shown to correlate with protein stability.<sup>7</sup>

Despite experimental support of this theory there are several shortcomings that warrant mention. First, during the drying process, the system is not likely at equilibrium between folding and unfolding due to the long time scales of molecular motion creating a conceptual inaccuracy to the theory.<sup>6</sup> Additionally, that the native structure is maintained in stable lyophilized formulations does not necessarily confirm the water replacement theory; there could be other mechanisms stabilizing the native structure. Lastly, thermodynamic stability may not imply pharmaceutical

stability. For example, in cases where the reactive sites are on the surface of the protein, reaction may still occur despite maintaining the native conformation.

The vitrification theory is based on kinetic stability. Accordingly, proteins are immobilized and diluted in a rigid, amorphous glassy matrix in the solid state. Coupling of the protein and glassy matrix reduce molecular mobility.<sup>6</sup> Glassification occurs when a solution is supercooled such that viscosity becomes high and molecular mobility slow so that conformational rearrangement cannot occur. The addition of a disaccharide or other glass formers, can increase the degree of supercooling and promote glassification.<sup>8</sup> The glass transition temperature ( $T_g$ ), where a solid transitions from a rubbery state to a glassy state and molecular motions are severely limited, often serves as a metric for kinetic stability. Several studies have shown a large increase in stability when proteins stored below their  $T_g$ .<sup>9-11</sup> For example, interleukin-2 showed good stability when formulated with carbohydrates at a  $T_g$  greater than storage temperature. But when formulated at a  $T_g$  below the storage temperature, degradation was faster despite a greater initial preservation of the native state in the solid.<sup>10</sup> While the addition of excipients, such as disaccharides and polymers, with high  $T_g$  has proven to be advantageous in maintaining protein stability, a formulation with the highest  $T_g$  does not necessarily imply the greatest stability.<sup>12-14</sup>

However, the relationship between glass dynamics and stability is more complex than the vitrification theory implies. There are two circumstances when the theory doesn't hold: when coupling between the glass matrix and protein is insufficient and when degradation motions fall outside of those captured by calorimetric structural relaxation (i.e.,  $T_g$  motions). The former can occur during phase separation or other instances of poor miscibility between excipient and protein.<sup>6</sup> To understand the latter requires a brief discussion of different mobility scales.

Glassification prevents the global, long-range motions ( $\alpha$ -relaxation) captured by  $T_g$  measurements. However, below  $T_g$  small-scale, local motions ( $\beta$ -relaxation), such as diffusion of small molecules or intramolecular interactions, can still occur and may cause instability. Chang and Pikal rationalize the importance of  $\beta$ -relaxation below  $T_g$  by describing two reaction pathways from a native state to a reacted or denatured state.<sup>6</sup> The first pathway is a highly cooperative process between several molecules requiring significant free volume. The process involves  $\alpha$ -relaxation and has a high activation energy, which is unlikely to be overcome at temperatures below  $T_g$ , when global mobility is low. The second pathway is the "fast dynamic process" ( $\beta$ -relaxation), which involves many small amplitude motions. It does not require cooperative motion

and therefore has a very low activation energy, which can easily be overcome below T<sub>g</sub>. Thus, through the second pathway, degradation can still occur despite glassification. In fact, recently, it was observed that  $\beta$ -relaxation correlated more strongly with protein stability than T<sub>g</sub> in cases including both chemical and physical degradation processes.<sup>15,16</sup>

Neither the water replacement theory nor the vitrification theory can describe the stability of lyophilized proteins on their own. As evidenced in the discussion above, there is often overlap between the excipients that contribute to each mechanism; good glass formers often contain hydroxyl groups which are good for hydrogen bonding. Stability in the solid state is likely achieved through a combination of the two theories. Interestingly, the relevant contributions from each mechanism are heavily dependent on the system of interest.<sup>17</sup> Yet it is clear that they do not encapsulate all mechanisms of protein degradation. Neither offer a universal or quantitative metric for predicting protein stability in lyophilized matrices, which necessitates the exploration of other predictive tools, mechanisms or factors to aid in protein formulation.

### **1.3 Formulating to Achieve Stability in Lyophilized Proteins**

Currently, freeze-drying, or lyophilization, is the most common method used for producing solid-state protein therapeutics and is the focus of this work.<sup>13</sup> It utilizes low pressure to sublime solvent from frozen protein solutions over three stages: freezing, primary drying, and secondary drying.

During freezing, water is separated from the sample solutes as ice and two phases are formed, an ice phase and an amorphous phase. The separation of water can cause interfacial surface denaturation and causes a concentration of solutes (“freeze concentrate”), which can cause protein stresses due to increased protein interaction and increased salt concentration or pH shift due to crystallization of buffer species.<sup>18</sup> Optimization of the freezing rate and temperature, as well as limiting the concentration of salts in the formulation, can help reduce these stresses.<sup>8</sup>

Primary drying is the longest step of the lyophilization process. The majority of water is removed via ice sublimation. Protein stress can occur here due to removal of the hydrogen bond network at the protein surface. The use of effective lyoprotectants, such as disaccharides, in the formulation can reduce the stresses of drying as described by the water replacement theory.

The final stage of lyophilization is secondary drying where the remaining “unfrozen water” is removed through diffusion. In amorphous material, nearly 20% of the water remains unfrozen

and amorphous and cannot be removed during primary drying.<sup>19</sup> During secondary drying the hydration layer most closely associated with the protein surface is removed, which can affect protein stability.

While the main purpose of lyophilization is improved storage stability, through elongated degradation time scales, the process itself introduces its own protein stresses. Moreover, lyophilized proteins still face countless instabilities. Formulation and process design must be considered meticulously in order to overcome these factors and create stable and efficacious products. The following sections describe formulation strategies and their stability mechanisms for lyophilized therapeutic proteins.

### **1.3.1 Sugars and Carbohydrates**

Sugars and carbohydrates stabilize by forming an amorphous glass with the protein to reduce molecular mobility and by helping to maintain the native structure of proteins. They provide protection during both freezing and drying. During freezing, the sugar concentration contributes to the degree of supercooling, which promotes glass formation. Here, the degree of protection from sugar is independent of the protein concentration. During drying, sugar stabilizes through hydrogen bonding interactions and reaches a saturation limit when all possible bonds have been formed. Protection depends on the sugar to protein weight ratio (S/P), where good stability is typically achieved at a S/P of 1:1.<sup>20</sup> Disaccharides, such as sucrose and trehalose, are typically the most effective protein stabilizers due to effective supercooling.<sup>8</sup> Compared to monosaccharides, they have a higher Tg' (i.e., glass transition temperature of the maximally freeze concentrated solution), and configurational flexibility, making them better stabilizers.<sup>21</sup> Reducing sugars should be avoided as they have the tendency to produce browning or discoloration via the Maillard reaction.<sup>12,20</sup>

Polymers, such as dextran, are also good glass formers and have been shown to provide stability to amorphous proteins.<sup>21,22</sup> In theory, polymers can provide enhanced stability compared to sugars due to their high Tg. Larger polymers are better glass formers as Tg typically increases with molecular weight. However, molecular size may also play a role in terms of conformational flexibility. Dextrans, for example, are often inferior to disaccharides in terms of maintaining a protein's native structure.<sup>22</sup> The balance of excipient size and Tg must be applied on a case by case basis and is not always easy to predict.

### **1.3.2 Buffer Salts and pH control**

Buffer salts are added to formulations for pH control. While pH is not defined in the solid state, the theory of ‘pH’ memory assumes that behavior in the solid-state mimics that of the solution state prior to lyophilization.<sup>23</sup> Accordingly, pre-lyophilization pH (‘pH’) has been shown to effect chemical and physical stability of protein products after lyophilization.<sup>23–27</sup> In addition, the effect of pH on solution stability must still be considered, albeit over shorter durations, to ensure product quality during manufacturing and after reconstitution.<sup>18</sup>

Formulation pH dictates the protonation state of protein functional groups based on pKa. This determines the overall charge state of the protein, which can influence its propensity to aggregate or denature.<sup>12</sup> On a local level, individual charges can also cause instabilities. Many chemical reactions are accelerated or inhibited based on a the protonation state of functional groups involved.<sup>24,28</sup> Moreover, ‘pH’ can also influence the extent of degradation caused by other factors, such as temperature and moisture content.<sup>28</sup>

Buffer type can also affect the stability of a lyophilized formulation. Some buffers, such as sodium phosphate, have the tendency to crystallize during freezing causing shifts in pH. Maintaining a low buffer concentration, in relation to other solutes, helps reduce this risk.<sup>29</sup> Volatile buffers, such as acetate, should be avoided as well for their risk of sublimation during freeze-drying.<sup>12</sup> This may result in a change in concentration after reconstitution that can be out of compliance or can cause instability. In some cases, buffers themselves may degrade and initiate instabilities in the protein, as has been shown for Tris buffer in lyophilized peptide formulations.<sup>30</sup>

### **1.3.3 Amino Acids and Osmolytes**

Protein stability by amino acids occurs by a variety of mechanisms including direct binding and preferential hydration. They can also serve as buffering agents and antioxidants.<sup>31,32</sup> The most commonly used amino acids are histidine, arginine, and glycine. However, methionine, lysine, proline, and Glu also can be used to stabilize proteins. These are common in both solid and solution states. Similar to sugars, amino acids can form hydrogen bonding interactions with proteins during drying to preserve the native structure.<sup>6,21</sup> Some amino acids have been utilized in high concentration antibody formulations without sugars to reduce aggregation and increase reconstitution time.<sup>33</sup> Many amino acids have a tendency to crystallize, with the exception of Arg,

which would render them ineffective stabilizers by the water replacement theory.<sup>34</sup> However, despite crystallization, some amino acids, such as glycine have still proven to be effective stabilizers, indicating a different mechanism is at play. The small size of amino acids may allow them to fill free void volume and stabilize through suppression of fast dynamics.<sup>35</sup> However, this mechanism is not fully understood. The use of amino acids to stabilize proteins in the solid state must be applied on a case-by-case basis.

Osmolytes are amino acid derivatives found in nature that stabilize microorganisms against dehydration, hypertonic states, and elevated temperatures.<sup>36-40</sup> They are low in molecular weight, polar, and either zwitterionic or uncharged molecules that have been shown to stabilize enzymes and therapeutic proteins in both the solid and solution states.<sup>36,38,41</sup> Like sugars, osmolytes are preferentially excluded and push thermodynamic equilibrium towards the native state.<sup>41</sup> The osmophobic protein backbone is hidden into the core of the folded protein in the presence of osmolytes and the hydroxyl groups of osmolytes are essential to stability on desiccation, which lends itself to the water replacement theory.<sup>40</sup> Many others have supported their stabilizing tendencies in the solid state.<sup>42-44</sup>

#### **1.3.4 Moisture Content**

Although not a formulation component, the moisture content of a solid matrix is highly relevant to protein stability. Moisture present in an amorphous solid can create regions of amorphous solution counteracting the benefit of the drying process on the local level. It can be residual from the drying process or can come from absorption of water vapor into the bulk structure, thus it is important to monitor moisture content during both production and storage.<sup>45</sup> Although extreme dehydration (i.e., below the monolayer water content) can also decrease stability, generally, degradation rates increase with increasing moisture content in amorphous solids.<sup>46,47</sup>

Water can affect chemical degradation in lyophilized solids in several ways: i) directly as a reactant or product, ii) indirectly as a medium (solvent), and iii) as a plasticizer.<sup>47-49</sup> First, if water is a reactant, as in hydrolysis, or product in the degradation reaction of interest it is clear that an increase in its concentration or activity would affect the equilibrium rate constant. As a medium, water changes the reactive environment which may alter the effective solvent dielectric or polarity. Such changes affect the Gibbs free energy of activation and thus can change reactivity.<sup>47</sup> Lastly, as a plasticizer water reduces viscosity and therefore increases molecular mobility and diffusivity.

In reactions under diffusion control this can directly impact the reaction rate constant.<sup>47</sup> To understand the impact of moisture content on a particular system, knowledge of the mechanisms of pertinent degradation reactions is required.

## 1.4 Pyroglutamate Formation

Proteins are susceptible to both physical and chemical degradation pathways, which can occur in the solution, frozen, and solid states. Physical degradation involves structural and conformational changes, including aggregation, surface adsorption, denaturation, and precipitation.<sup>50</sup> Chemical degradation involves the breaking and reforming of covalent bonds resulting in new chemical entities. This dissertation focuses on a chemical degradation, pyroglutamate (pGlu) formation which can occur in peptide and proteins.

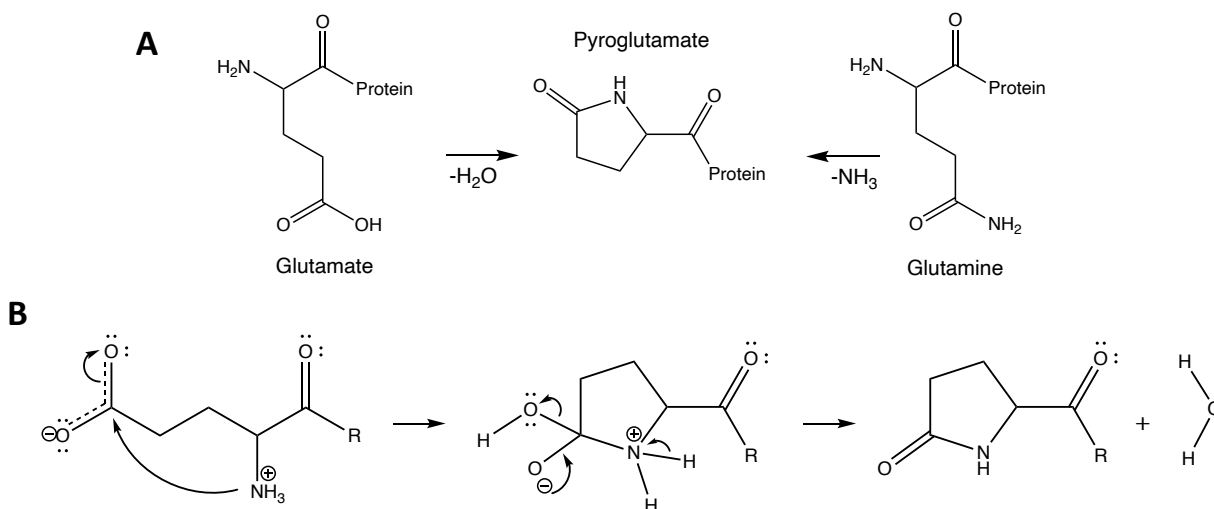


Figure 1-1. Reaction pathways for the formation of pGlu through cyclization of N-terminal Gln or Glu (A). The reaction from Gln results in the loss of ammonia while the reaction from Glu results in the loss of a water molecule. Proposed mechanism of pGlu formation from Glu through a tetrahedral intermediate (B).

pGlu formation is a chemically degraded form of Glu or Gln and can occur in peptides and proteins that have either of these amino acids at their N-terminals. pGlu formation is of interest due to the prevalence of N-terminal Glu and Gln in mAbs and the need to understand and control chemical modifications in this growing class of biologics.<sup>51,52</sup> pGlu formation is a condensation reaction that results from the nucleophilic attack of the N-terminal primary amine on the carbonyl

carbon of the side chain of Gln or Glu (Figure 1-1). In pGlu formation from Gln, N-terminal Gln cyclizes to form pGlu with the loss of ammonia, creating an acidic charge variant due to loss of the positive charge from the N-terminal amino group.<sup>53</sup> In pGlu formation from Glu, a water molecule is lost during cyclization of N-terminal Glu resulting in a basic charge variant, a higher isoelectric point (pI), and increased hydrophobicity.<sup>54</sup> Both reactions lead to the formation of a lactam ring and are generally considered irreversible.<sup>55-58</sup> In fact, pGlu has been reported to revert to Glu only under very harsh conditions: 2M HCl at 100°C for 2 hours.<sup>57</sup> The lactam ring does not serve as a proton acceptor, which contributes to the stability of pGlu.<sup>55</sup> Abraham et. al. hypothesized that the stability of the ring is due to the attraction of the Nitrogen-1 electron pair to the Carbon-5, which is double bonded to oxygen.<sup>58</sup>

*In vivo*, pGlu formation has been reported to increase aggregation and inter-fibril associations, decrease solubility, and influence the structure and activity of endogenous peptides and proteins.<sup>59,60</sup> pGlu formation occurs both enzymatically and spontaneously (i.e., chemically without enzyme catalysis).<sup>55,56,61-64</sup> Since non-enzymatic pGlu formation can occur in formulated drug products prior to administration, it is of primary interest to the biopharmaceutical industry. It is critical to have a complete understanding of pGlu formation from both Gln and Glu, as well as the effects that pGlu has on product safety and efficacy.

Of the two pathways, the reaction from Gln is better understood. A mechanism was first proposed by Dimarchi et al. whereby weak acids, but not strong acids, catalyze the cyclization of the N-terminal Gln.<sup>65</sup> More recently, Seifert et al. have explored the mechanism through kinetic isotope studies. They determined that a tetrahedral intermediate is formed, whose breakdown is the rate-limiting step of the reaction and proceeds through proton transfer between the N-terminal amide nitrogen and the oxygen of the  $\gamma$ -carbonyl carbon. Phosphate ions and glutaminyl cyclases increase the reaction rate. The authors hypothesized that both phosphate and glutaminyl cyclases act as acid-base catalysts by coordinating a dual proton transfer with the cyclic tetrahedral intermediate through a concerted mechanism.<sup>56</sup>

Much is known about the effects of buffer, pH and temperature on the Gln to pGlu reaction. There is a clear temperature effect. A study of pGlu formation in a model peptide saw a 5-fold increase in reaction rate when comparing room temperature with 37°C.<sup>66</sup> Similarly, during trypsin digestion, a significant decrease in pGlu formation was reported when the temperature was reduced

from 37°C to 0°C.<sup>67</sup> These results underscore the importance of process and storage temperature when manufacturing proteins susceptible to pGlu formation.

The influence of pH on the reaction from Gln has been investigated by several groups, but the overall conclusions are not entirely clear. Shih showed a significant increase in pGlu formed at the amino acid level over the range pH 3 to pH 10 in 0.1M sodium-phosphate buffer.<sup>57</sup> Similarly, Seifert et al. showed a slight increase in pGlu formation rate in short peptides from pH 5 to 7 in a 0.1M Tris, 0.05 M acetate, and 0.05 M MES buffer.<sup>55</sup> However, other studies have reported that the reaction is independent of pH from pH 4 to 10.<sup>55,56</sup> Dick et al. reported that low pH accelerates the reaction, but noted that the effects are small compared to other factors, such as buffer type and temperature.<sup>66</sup> These conflicting reports suggest that pH is not a primary determinant of pGlu formation rates in the reaction from Gln.

In contrast, buffer type and concentration have been shown to have significant effects on pGlu formation rate from Gln. Several groups have shown that phosphate buffer accelerates the reaction.<sup>56,66,67</sup> The catalytic effects of phosphate reported by Seifert et al. varied with buffer concentration and solution pH. pGlu formation was most proficiently catalyzed by phosphate at pH 7.<sup>56</sup> This observation may explain why Shih witnessed such a significant pH effect when analyzing Gln cyclization in sodium phosphate buffer while others reported a general pH independence for the reaction.<sup>57</sup> Ammonium carbonate and ammonium acetate buffers have also been shown to increase pGlu formation rates, but to a lesser extent than phosphate.<sup>67</sup> In contrast, Tris-HCl did not increase the amounts of pGlu formed in model peptides after 7 days at 37°C when compared to ammonium carbonate and sodium phosphate buffers.<sup>66</sup> These results support the conclusion by Dimarchi et al. that the reaction from Gln is susceptible to weak acid catalysis, and indicate that buffer selection is important when formulating molecules containing N-terminal Gln.

pGlu formation from Glu has been studied less than the reaction from Gln, perhaps because the cyclization reaction is slower in Glu than in Gln, making it less important in practical applications, or because the reaction was thought to be primarily enzymatic until recently.<sup>55,57,63</sup> A mechanism for pGlu formation from Glu has been proposed based on the work by Dimarchi et al. and involves catalysis by weak acids, similar to the Gln reaction.<sup>68</sup> This mechanism was proposed for the solid-state reaction; a solution state mechanism for pGlu formation from Glu has not been reported. Several groups have proposed that the protein structure and surrounding amino

acid microenvironment significantly influence the rate of pGlu formation from Glu.<sup>53,69</sup> For example, Liu et al. hypothesize that a negative charge on an amino acid near Glu may promote pGlu formation.<sup>53</sup> The theory is evidenced by the rates of pGlu formation in two mAbs where the reaction rates differ substantially despite significant sequence homology. The mAb not susceptible to pGlu formation was shown, through structural analysis, to have a neutral Pro near the N-terminal Glu, while the mAb which cyclized Glu rapidly had Asp near the N-terminal Glu creating a negatively charged environment.<sup>54</sup>

Several studies have reported formulation and process factors that may influence the rate of pGlu formation from Glu. Since Glu is thermodynamically less stable than the pGlu product, it is not surprising that elevated temperature increases the amount of pGlu formed.<sup>52,70</sup> Yu et al. reported a decrease in half-life from 4.8 to 2.4 years in an IgG1 mAb when the incubation temperature was increased from 37°C to 45°C. No pGlu was detected over the same time period at 4°C.<sup>70</sup>

Like the reaction from Gln, the mechanism of pGlu formation from Glu in the solid-state is thought to be catalyzed by weak acids and buffer species may have an effect on the reaction rate.<sup>65,68</sup> Beck et al. showed that pGlu formation from Glu in lyophilized solids was accelerated when the peptide was produced as an acetate or trifluoroacetate salt compared to a hydrochloride salt.<sup>71</sup> Theoretically, the reaction in solution may also be accelerated by weak acids, but there has been no conclusive evidence to support this hypothesis. Chelius et al. reported no difference in pGlu formation from Glu in solution mAb formulations in histidine and acetate buffer.<sup>52</sup> In contrast, Yu et al. reported greater pGlu formation in histidine buffer than acetate buffer. The effects of buffer species on pGlu formation from Glu in solution are thus unclear.<sup>70</sup>

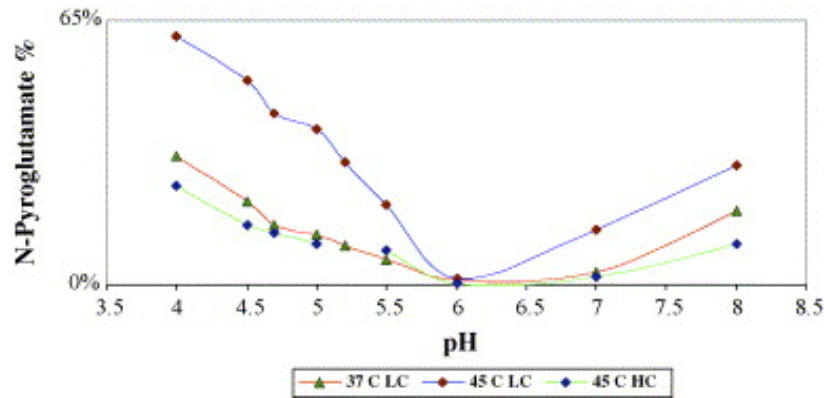


Figure 1-2. pH effects on pyroglutamate formation of the light chain (LC) and heavy chain (HC) of a mAb after storage as a lyophilized powder for 3 months at 37°C (green triangles) and 45°C (red circles and blue diamonds). This figure is reprinted from Ref [70].

There is, however, a clear influence of pH on Glu cyclization in solution. Several groups have reported a reaction minimum at pH 6-6.2 with greater rates of pGlu formation from Glu under acidic and basic conditions (Figure 1-2).<sup>52,55,70</sup> Seifert et al. hypothesized that the pH dependence may reflect the requirement for both a protonated  $\gamma$ -carboxyl group and a deprotonated  $\alpha$ -amino group for nucleophilic attack, which is unlikely at pH 6. Of all factors, pH has the greatest influence on Glu cyclization.

While it is clear that pGlu is formed in protein pharmaceuticals, evidence for an effect of pGlu on product safety and efficacy is inconclusive. It is noteworthy that pGlu is a naturally occurring modification of endogenous proteins, and has been detected in IgG2 mAbs at substantial levels *in vivo*.<sup>53</sup> Endogenous pGlu has been shown to have no effect on antibody clearance or turnover; Liu et al. therefore argue that pGlu poses little or no safety concern for pharmaceutical products.<sup>53</sup> Moreover, it has been suggested that pGlu formation could actually stabilize the molecule by making it more resistant to enzymatic and chemical degradation; pGlu is resistant to amino peptidases and prevents Edman degradation.<sup>57,72</sup> Additionally, several studies have shown that there is no loss in activity in mAbs due to pGlu formation, and assert that the transformation has no effect on structure, stability or function.<sup>52,73</sup>

Nevertheless, the N-terminals of both the light and heavy chains of mAbs are in the variable region, near the CDR. Therefore, it is reasonable to suspect that pGlu could affect target binding on a molecule-to-molecule basis. In fact, Beck et al. reported reduced activity in an N-terminal

Glu decapeptide when pGlu was present due to inferior binding to the target site.<sup>68,71</sup> Additionally, it has been hypothesized that the chemical change caused by pGlu formation could lead to changes in protein structure as has been shown for deamidation.<sup>74</sup> Despite some evidence that pGlu formation does not adversely affect structure, activity, or safety, further investigation is warranted in order to fully understand the reactions and their implications.

### 1.5 Solid-State Hydrogen-Deuterium Exchange Mass Spectrometry

Hydrogen-deuterium exchange (HDX) is a chemical reaction in which covalently bonded hydrogen atoms are replaced by deuterium atoms giving the molecule a heavier mass. Exchangeable hydrogens are those that are bonded to electronegative atoms (e.g., O, N, S), namely backbone amide hydrogens in proteins. Hydrogens bonded to carbon atoms do not exchange at a measurable rate.<sup>75</sup> Exchange occurs when a molecule is exposed to D<sub>2</sub>O either in solution or as a vapor.

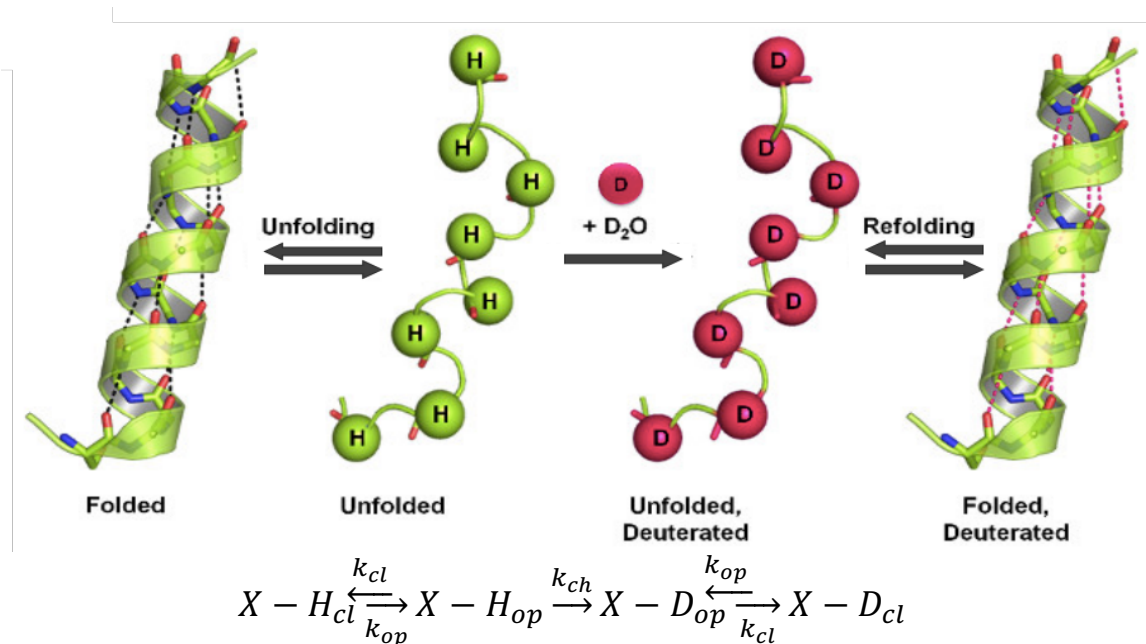


Figure 1-3. Schematic representation of solution-state HDX reprinted from Ref. [78]

In structured proteins, the process can be described by the Linderstrom-Lang model, in which exchange occurs due to reversible protein unfolding and irreversible hydrogen exchange as shown in Figure 1-3. The chemical exchange ( $k_{ch}$ ) is influenced by pH, temperature, protein

intramolecular hydrogen bonding, protein dynamics, and solvent accessibility.<sup>76</sup> Solvent accessible hydrogens, not involved in intramolecular hydrogen bonding exchange fast and most easily. Amide hydrogens that are involved in secondary and tertiary structure exchange more slowly during brief local unfolding events, referred to as “breathing motions”. These reversible motions intermittently break hydrogen amide bonds and allow for deuterium exchange as shown by the first step in the schematic of Figure 1-3. The technique can be used to study protein structure, protein-protein interactions, and protein ligand-interactions.<sup>77</sup>

Analysis of HDX can be performed using several techniques including, NMR, infrared, and mass spectrometry (MS). NMR is limited by its inability to analyse large molecules and its need for large samples. MS when paired with HDX, can monitor increases in molecular weight as a function of D<sub>2</sub>O exposure time. Current mass spectrometers can accurately detect changes in molecular mass as little as 1 Da, can measure very small samples (~picograms of protein), and can accommodate a wide range of protein sizes, including mAbs. Mass spectrometers also allow the analysis of both local and global dynamics. Through pepsin digestion of a deuterated sample before injection, peptide-level analysis can be performed.

In the solid state, HDX with MS analysis (ssHDX-MS) can be performed by exposing the sample to D<sub>2</sub>O at a controlled hydrogen activity, determined by relative humidity (RH), and temperature. In a typical ssHDX-MS experiment, once the desired exchange time is complete, the sample is reconstituted with quench buffer to stop the exchange reaction and prevent back exchange. The quench buffer is prepared ice-cold at pH 2.5, where HDX of amide hydrogens is at a minimum.<sup>78</sup> Reconstituted solution is then analyzed by MS to determine deuteration levels. Like solution, ssHDX-MS typically shows bi-exponential behavior (Eq. 1.1),

$$D(t) = D_{fast}(1 - e^{-k_{fast}t}) + D_{slow}(1 - e^{-k_{slow}t}) \quad 1.1$$

where  $D(t)$  is the deuterium uptake at labelling time  $t$ ,  $D_{fast}$  is the number of exchanging amides in the fast pool,  $D_{slow}$  is the number of exchanging amides in the slow pool, and  $k_{fast}$  and  $k_{slow}$  are the apparent first-order rate constants of the “fast” and “slow” exchanging amide groups, respectively.

Several additional aspects of HDX are notably different between solution and solid state experiments.<sup>79</sup> In the solid state, D<sub>2</sub>O is not in excess. Its distribution in the solid may be heterogenous due to the nature of the solid and mass transfer limitations. Second, a protein’s

structure in an amorphous solid is at least partially dictated by binding with the surrounding excipient. These factors obscure the distinction between fast and slow exchanging groups that are clearly delineated in solution HDX. Moreover, in solution, structure is predominately determined by intramolecular hydrogen bonds and hydrogen bonds with water. Lastly, molecular motions are severely limited in a solid. Thus, the “breathing motions” described by the mechanism proposed by Linderstrom-Lang may not be applicable in the solid state.

Unlike solution HDX, ssHDX-MS relies on both mass transport and chemical reactivity. At early timepoints, water vapor sorption and exchange may be occurring in tandem, which can complicate data interpretation and analysis. Several studies have shown that the timescale for water sorption is much shorter than ssHDX-MS kinetics.<sup>80,81</sup> Moreover, the confounding effects of water sorption was investigated through pre-hydration ssHDX-MS studies where lyophilized poly-D,L-alanine (PDLA) peptide samples were equilibrated in a controlled RH H<sub>2</sub>O environment prior to exposure to D<sub>2</sub>O in the ssHDX-MS experiment. Interestingly, there was not a significant difference between pre-hydrated and non-pre-hydrated amorphous samples. However, samples with evidence of recrystallization did show significant differences between the pre-hydrated and non-pre-hydrated samples.<sup>82</sup> The authors conclude that pre-hydration has little effect on ssHDX-MS kinetics in amorphous samples and they suggest that the potential for recrystallization be considered during the design of ssHDX-MS experiments.<sup>82</sup>

Recently, a mechanistic model (Eq. 1.2) has been proposed for ssHDX-MS that incorporates some of these factors and compensates for some of the shortcomings of the Linderstrom-Lang model when it is applied to the solid state.<sup>83</sup>



In Equation 1.2, A is the number or percent of exchangeable amides, B is the number or percent of deuterated amides,  $k_f$  and  $k_b$  are the forward and reverse rate constants for deuterium exchange, respectively. The forward and reverse reaction rates are assumed to be first-order in A and B, respectively. The forward reaction rate is assumed to be linearly dependent on the RH of D<sub>2</sub>O as described by Equation 1.3,

$$k_f = k_f^*(a_D) \quad 1.3$$

where  $k_f^*$  is the forward reaction rate in the absence of RH effects and  $a_D$  is the activity of D<sub>2</sub>O (i.e., the RH of D<sub>2</sub>O). This assumption is supported by the work of Kammari and Topp, where deuterium incorporation of lyophilized unstructured PDLA peptides was linearly dependent on the RH of D<sub>2</sub>O. The relationship was observed in the presence of a variety of excipients.<sup>83</sup> Considering Equations 1.2 and 1.3, the apparent deuterium incorporation rate constant ( $k_{ap}$ ) is dependent on  $a_D$  and the forward and reverse rate constants (Eq. 1.4).

$$k_{ap} = k_f^*(a_D) + k_b \quad 1.4$$

Kammari and Topp support the proposed model through extensive investigation of the reverse reaction in ssHDX-MS. In reversibility studies lyophilized PDLA peptides were first exposed to D<sub>2</sub>O for up to 15 days (the length of a typical ssHDX-MS experiment) and then transferred to a comparable H<sub>2</sub>O environment.  $k_f$  and  $k_b$  calculated from these experiments are on the same order or magnitude, and in some cases are not significantly different.<sup>82</sup> This suggests the reverse reaction cannot be neglected on the time scale of the ssHDX-MS experiments. It is reasonable that the reverse reaction takes prominence in the solid reaction as compared to solution ssHDX because the D<sub>2</sub>O activity is reduced in solid experiments. The local activity of a hydrogen atom that has undergone exchange is likely to be greater in solid than in solution increasing the likelihood of its participation in the reverse reaction. Therefore, the proposed model suggests that the exponential behavior of deuterium exchange in the solid state does not reflect the “opening” and “closing” events described by the Linderstrom-Lang model, but instead can be described by a series of deuterium incorporation and loss events that transmit the deuterium label throughout the exchangeable protein.<sup>82</sup> An intriguing segue to these findings would be the investigation of mobility on the effects of ssHDX-MS kinetics.

Despite the nascent mechanistic model describing ssHDX-MS, over the past ten years the technique has been used to evaluate conformational changes due to processing methods, formulation changes, and moisture content.<sup>80,81,84-86</sup> It has been evaluated as a long-term stability prediction tool for myoglobin (Mb) and an IgG1 mAb. In samples of Mb lyophilized with sucrose, deuterium uptake was lower and stability greater, than samples lyophilized with mannitol or sodium chloride. Increasing sucrose content also showed greater stability and reduced deuterium uptake.<sup>86</sup> In another example, deuterium uptake of four lyophilized mAb formulations was directly and strongly correlated with aggregation and chemical degradation rates during more than 2 years of

storage (Figure 1-4).<sup>80</sup> A negative correlation between stability and exchange parameters suggests that protection from deuterium exchange is indicative of more native conformation, or involvement in hydrogen bonding with excipients, which is reflected in lower degradation rates.

Most comparisons between ssHDX-MS and stability focus on physical stability, mainly defined by aggregation levels. Moorthy et al. has showed that ssHDX-MS parameters also correlated well with changes in charge heterogeneity in mAb formulations.<sup>80</sup> This suggests that the technique could also serve as a prediction tool for chemical degradation reactions dependent on proton transfer.

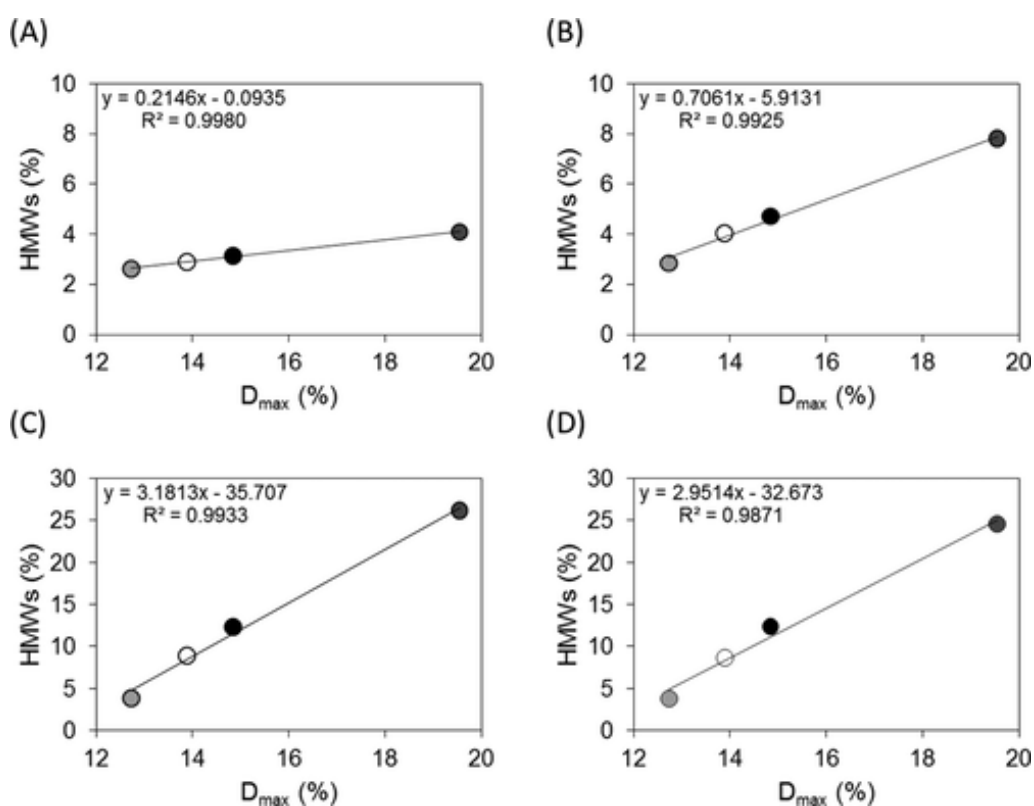


Figure 1-4. Correlation of deuterium uptake (%  $D_{max}$ ) with high molecular weight species of mAb formulations stored at 5°C for 960 days (A), 25°C for 960 days (B), 40°C for 960 days (C), and 50°C for 180 days (D). The data were fit to a linear model to obtain the slope, intercept and  $R^2$  values. Figure reprinted from Ref. [80]

## 1.6 Conclusions

Therapeutic proteins are particularly challenging for pharmaceutical development due to their large size and complexity. One approach to formulating unstable molecules is to develop a solid-state product via lyophilization or another means. The lyophilization process introduces new stresses despite the end goal of increasing stability. Pharmaceutical scientists must formulate accordingly. While much is known about the stability mechanisms in the solid state, there is still much to be discovered. Effective analytical techniques are key to further understanding solid-state protein stability mechanisms and to thorough characterization during pharmaceutical development. Continued exploration into stability mechanisms and solid-state analytical tools will facilitate a rational design approach to therapeutic protein development.

## 1.7 Research Scope

Broadly speaking, the research presented in this dissertation explores chemical reactions in the solid state. The work focuses on formulation and matrix properties that are descriptive of solid-state reactivity in pharmaceutically relevant systems with the objective to expand our knowledge of solid-state reaction behavior. More specifically, the work applies two reactions to study reactivity: pGlu formation, a chemical degradation reaction observed in peptides and proteins, and ssHDX, a reaction that is employed as an analytical tool to probe solid-state protein stability. On a practical level, the outcomes will have implications for the development of therapeutic proteins both in terms of formulation strategies and analytical techniques.

## 1.8 Dissertation Overview

This dissertation is organized into 5 chapters. **Chapter 1** provides an overview of therapeutic protein stability mechanisms and formulation strategies, followed by background on pyroglutamate formation and an overview of ssHDX-MS as an analytical tool for studying solid-state proteins.

**Chapter 2** aims to explore the mechanism of pGlu formation in the solid and solution states. It describes the results of an investigation of the effects of 'pH' on pGlu formation in a model peptide in lyophilized solids and in solution. The first 'pH'-rate profile for this reaction mechanism is presented.

**Chapter 3** follows from **Chapter 2** and aims to develop formulations that inhibit pGlu formation and to identify formulation characteristics and matrix properties that are indicative of pGlu formation. It describes the results of an investigation of the effect of excipient, moisture content and mobility on pGlu formation in lyophilized model peptide. The work includes an investigation of ssHDX-MS as an analytical screening tool for formulations susceptible to pGlu formation.

**Chapter 4** aims to identify solid-state properties that affect ssHDX-MS. It describes the results of an investigation of the effect of temperature, RH and mobility on ssHDX-MS in a lyophilized mAb. It presents a kinetic model for deuterium incorporation in ssHDX that incorporates both temperature and RH.

**Chapter 5** highlights the main findings and conclusions of the dissertation. It provides recommendations for future work in the field of chemical stability of proteins and peptides with a specific emphasis on pGlu formation and ssHDX-MS as an analysis tool.

Three appendices include supporting information to the results of Chapter 2 (**Appendix A**), Chapter 3 (**Appendix B**), and Chapter 4 (**Appendix C**).

## 1.9 References

1. Walsh, G. Biopharmaceutical benchmarks 2018. *Nat. Biotechnol.* 36, 1136–1145 (2018).
2. Trends in Biosimilars: Innovative Approaches to Expediting Development. <https://www.raps.org/news-and-articles/news-articles/2018/6/trends-in-biosimilars-innovative-approaches-to-ex>.
3. Nelson, A. L., Dhimolea, E. & Reichert, J. M. Development trends for human monoclonal antibody therapeutics. *Nat. Rev. Drug Discov.* 9, 767–774 (2010).
4. Huang, L., Lu, J., Wroblewski, V. J., Beals, J. M. & Riggin, R. M. In Vivo Deamidation Characterization of Monoclonal Antibody by LC/MS/MS. *Anal. Chem.* 77, 1432–1439 (2005).
5. Wei, Z. et al. Identification of a Single Tryptophan Residue as Critical for Binding Activity in a Humanized Monoclonal Antibody against Respiratory Syncytial Virus. *Anal. Chem.* 79, 2797–2805 (2007).
6. Chang, L. (Lucy) & Pikal, M. J. Mechanisms of protein stabilization in the solid state. *J. Pharm. Sci.* 98, 2886–2908 (2009).
7. Carpenter, J. F. & Crowe, J. H. An infrared spectroscopic study of the interactions of carbohydrates with dried proteins. *Biochemistry* 28, 3916–3922 (1989).
8. Kasper, J. C. & Friess, W. The freezing step in lyophilization: Physico-chemical fundamentals, freezing methods and consequences on process performance and quality attributes of biopharmaceuticals. *Eur. J. Pharm. Biopharm.* 78, 248–263 (2011).
9. Duddu, S. & Dal Monte, P. Effect of glass transition temperature on the stability of lyophilized formulations containing a chimeric therapeutic monoclonal antibody. *Pharm. Res.* 14, 591–595 (1997).
10. Prestrelski, S. J., Pikal, K. A. & Arakawa, T. Optimization of lyophilization conditions for recombinant human interleukin-2 by dried-state conformational analysis using fourier-transform infrared spectroscopy. *Pharm. Res.* 12, 1250–1259 (1995).
11. Streefland, L., Auffret, A. D. & Franks, F. Bond Cleavage Reactions in Solid Aqueous Carbohydrate Solutions. *Pharm. Res.* 15, 843–849 (1998).
12. Lai, M. C. & Topp, E. M. Solid-state chemical stability of proteins and peptides. *J. Pharm. Sci.* 88, 489–500 (1999).
13. Wang, W. Lyophilization and development of solid protein pharmaceuticals. *Int. J. Pharm.* 203, 1–60 (2000).

14. Chang, B. S., Beauvais, R. M., Dong, A. & Carpenter, J. F. Physical Factors Affecting the Storage Stability of Freeze-Dried Interleukin-1 Receptor Antagonist: Glass Transition and Protein Conformation. *Arch. Biochem. Biophys.* 331, 249–258 (1996).
15. Cicerone, M. T. & Soles, C. L. Fast Dynamics and Stabilization of Proteins: Binary Glasses of Trehalose and Glycerol. *Biophys. J.* 86, 3836–3845 (2004).
16. Cicerone, M. T. & Douglas, J. F. Beta-relaxation governs protein stability in sugar-glass matrices. *Soft Matter* 8, 2983–2991 (2012).
17. Mensink, M. A., Frijlink, H. W., van der Voort Maarschalk, K. & Hinrichs, W. L. J. How sugars protect proteins in the solid state and during drying (review): Mechanisms of stabilization in relation to stress conditions. *Eur. J. Pharm. Biopharm.* 114, 288–295 (2017).
18. L. Remmele, R., Krishnan, S. & J. Callahan, W. Development of Stable Lyophilized Protein Drug Products. *Curr. Pharm. Biotechnol.* 13, 471–496 (2012).
19. Nail, S. L., Jiang, S., Chongprasert, S. & Knopp, S. A. Fundamentals of Freeze-Drying. in *Development and manufacture of protein pharmaceuticals* 281–360 (Springer, 2002).
20. Carpenter, J., Pikal, M., Chang, B. & Randolph, T. Rational Design of Stable Lyophilized Protein Formulations: Some Practical Advice. *Pharm. Res.* 14, 969–975 (1997).
21. Ohtake, S., Kita, Y. & Arakawa, T. Interactions of formulation excipients with proteins in solution and in the dried state. *Adv. Drug Deliv. Rev.* 63, 1053–1073 (2011).
22. Allison, S. D. Optimization of Storage Stability of Lyophilized Actin Using Combinations of Disaccharides and Dextran. *J. Pharm. Sci.* 89, 16 (2000).
23. Costantino, H. R., Griebenow, K., Langer, R. & Klibanov, A. M. On the pH memory of lyophilized compounds containing protein functional groups. *Biotechnol. Bioeng.* 53, 345–348 (1997).
24. Song, Y., Schowen, R. L., Borchardt, R. T. & Topp, E. M. Effect of ‘pH’ on the rate of asparagine deamidation in polymeric formulations: ‘pH’–rate profile. *J. Pharm. Sci.* 90, 141–156 (2001).
25. Townsend, M. W. & DeLuca, P. P. Stability of Ribonuclease A in Solution and the Freeze-Dried State. *J. Pharm. Sci.* 79, 1083–1086 (1990).
26. Roy, M. L., Pikal, M. J., Rickard, E. C. & Maloney, A. M. The effects of formulation and moisture on the stability of a freeze-dried monoclonal antibody-vinca conjugate: a test of the WLF glass transition theory. *Dev. Biol. Stand.* 74, 323–339 (1992).
27. Chang, L. (Lucy) et al. Mechanism of protein stabilization by sugars during freeze-drying and storage: Native structure preservation, specific interaction, and/or immobilization in a glassy matrix? *J. Pharm. Sci.* 94, 1427–1444 (2005).

28. Oliyai, C., Patel, J. P., Carr, L. & Borchardt, R. T. Chemical pathways of peptide degradation. VII. Solid state chemical instability of an aspartyl residue in a model hexapeptide. *Pharm. Res.* 11, 901–908 (1994).
29. Wang, B. & Pikal, M. Rational Design of Solid Protein Formulations. in *Pharmaceutical Formulation Development of Peptides and Proteins, Second Edition* 239–268 (CRC Press, 2012). doi:10.1201/b12951-11.
30. Song, Y., Schowen, R. L., Borchardt, R. T. & Topp, E. M. Formaldehyde production by Tris buffer in peptide formulations at elevated temperature. *J. Pharm. Sci.* 90, 1198–1203 (2001).
31. Arakawa, T. et al. Suppression of protein interactions by arginine: a proposed mechanism of the arginine effects. *Biophys. Chem.* 127, 1–8 (2006).
32. Arakawa, T., Tsumoto, K., Kita, Y., Chang, B. & Ejima, D. Biotechnology applications of amino acids in protein purification and formulations. *Amino Acids* 33, 587–605 (2007).
33. Patel, S. & Choudhary, S. Use of Amino Acids as Stabilizing Compounds in Pharmaceutical Compositions Containing High Concentrations of Protein-Based Therapeutic Agents. (2019).
34. Mattern, M., Winter, G., Kohnert, U. & Lee, G. Formulation of Proteins in Vacuum-Dried Glasses. II. Process and Storage Stability in Sugar-Free Amino Acid Systems. *Pharm. Dev. Technol.* 4, 199–208 (1999).
35. Forney-Stevens, K. M., Bogner, R. H. & Pikal, M. J. Addition of Amino Acids to Further Stabilize Lyophilized Sucrose-Based Protein Formulations: I. Screening of 15 Amino Acids in Two Model Proteins. *J. Pharm. Sci.* 105, 697–704 (2016).
36. Kumar, R. Role of naturally occurring osmolytes in protein folding and stability. *Arch. Biochem. Biophys.* 491, 1–6 (2009).
37. Yancey, P. H. Water Stress, Osmolytes and Proteins. *Am. Zool.* 41, 699–7009 (2001).
38. Liu, Y. & Bolen, D. W. The Peptide Backbone Plays a Dominant Role in Protein Stabilization by Naturally Occurring Osmolytes. *Biochemistry* 34, 12884–12891 (1995).
39. Wang, A. & Bolen, D. W. A Naturally Occurring Protective System in Urea-Rich Cells: Mechanism of Osmolyte Protection of Proteins against Urea Denaturation †. *Biochemistry* 36, 9101–9108 (1997).
40. Lentzen, G. & Schwarz, T. Extremolytes: natural compounds from extremophiles for versatile applications. *Appl. Microbiol. Biotechnol.* 72, 623–634 (2006).
41. Arakawa, T. & Timasheff, S. N. The stabilization of proteins by osmolytes. *Biophys. J.* 47, 411–414 (1985).

42. Lippert, K. & Galinski, Erwin A. Enzyme stabilization by ectoine-type compatible solutes: protection against heating, freezing and drying. *Appl. Microbiol. Biotechnol.* 37, 61–65 (1992).
43. Ramos, A. et al. Stabilization of Enzymes against Thermal Stress and Freeze-Drying by Mannosylglycerate. *Appl. Environ. Microbiol.* 63, 4020–4025 (1997).
44. Barth, S. et al. Compatible-Solute-Supported Periplasmic Expression of Functional Recombinant Proteins under Stress Conditions. *Appl. Environ. Microbiol.* 66, 1572–1579 (2000).
45. Hancock, B. C. & Zografi, G. The Use of Solution Theories for Predicting Water Vapor Absorption by Amorphous Pharmaceutical Solids: A Test of the Flory–Huggins and Vrentas Models. *Pharm. Res.* 10, 1262–1267 (1993).
46. Hsu, C. C. et al. Determining the optimum residual moisture in lyophilized protein pharmaceuticals. *Dev. Biol. Stand.* 74, 255–70; discussion 271 (1992).
47. Shalaev, E. Y. & Zografi, G. How Does Residual Water Affect the Solid-state Degradation of Drugs in the Amorphous State? *J. Pharm. Sci.* 85, 1137–1141 (1996).
48. Lai, M. C. et al. Chemical stability of peptides in polymers. 2. Discriminating between solvent and plasticizing effects of water on peptide deamidation in poly(vinylpyrrolidone). *J. Pharm. Sci.* 88, 1081–1089 (1999).
49. Hageman, M. Water Sorption and Solid-State Stability of Proteins. in *Stability of Protein Pharmaceuticals: Part A, Chemical and Physical Pathways of Protein Degradation* 273–309 (Plenum, 1992).
50. Manning, M. C., Chou, D. K., Murphy, B. M., Payne, R. W. & Katayama, D. S. Stability of Protein Pharmaceuticals: An Update. *Pharm. Res.* 27, 544–575 (2010).
51. Ionescu, R. & Vlasak, J. Kinetics of Chemical Degradation in Monoclonal Antibodies: Relationship between Rates at the Molecular and Peptide Levels. *Anal. Chem.* 82, 3198–3206 (2010).
52. Chelius, D. et al. Formation of Pyroglutamic Acid from N-Terminal Glutamic Acid in Immunoglobulin Gamma Antibodies. *Anal. Chem.* 78, 2370–2376 (2006).
53. Liu, Y. D., Goetze, A. M., Bass, R. B. & Flynn, G. C. N-terminal Glutamate to Pyroglutamate Conversion in Vivo for Human IgG2 Antibodies. *J. Biol. Chem.* 286, 11211–11217 (2011).
54. Liu, Z. et al. Cyclization of N-Terminal Glutamic Acid to pyro-Glutamic Acid Impacts Monoclonal Antibody Charge Heterogeneity Despite Its Appearance as a Neutral Transformation. *J. Pharm. Sci.* (2019) doi:10.1016/j.xphs.2019.05.023.
55. Seifert, F. et al. Glutaminyl Cyclases Display Significant Catalytic Proficiency for Glutamyl Substrates. *Biochemistry* 48, 11831–11833 (2009).

56. Seifert, F. et al. Phosphate ions and glutaminyl cyclases catalyze the cyclization of glutaminyl residues by facilitating synchronized proton transfers. *Bioorganic Chem.* 60, 98–101 (2015).
57. Shih, F. F. Analysis of glutamine, glutamic acid and pyroglutamic acid in protein hydrolysates by high-performance liquid chromatography. *J. Chromatogr. A* 322, 248–256 (1985).
58. Abraham, G. N. & Podell, D. N. Pyroglutamic acid. in *The Biological Effects of Glutamic Acid and Its Derivatives* (ed. Najjar, V. A.) 181–190 (Springer Netherlands, 1981). doi:10.1007/978-94-009-8027-3\_11.
59. Kumar, A. & Bachhawat, A. K. Pyroglutamic acid: throwing light on a lightly studied metabolite. *Curr. Sci.* 102, 288–297 (2012).
60. Lai, Z. W., Petrera, A. & Schilling, O. Protein amino-terminal modifications and proteomic approaches for N-terminal profiling. *Curr. Opin. Chem. Biol.* 24, 71–79 (2015).
61. Huang, K.-F., Liu, Y.-L., Cheng, W.-J., Ko, T.-P. & Wang, A. H.-J. Crystal structures of human glutaminyl cyclase, an enzyme responsible for protein N-terminal pyroglutamate formation. *Proc. Natl. Acad. Sci.* 102, 13117–13122 (2005).
62. Twardzik, D. R. & Peterkofsky, A. Glutamic Acid as a Precursor to N-Terminal Pyroglutamic Acid in Mouse Plasmacytoma Protein. *Proc. Natl. Acad. Sci.* 69, 274–277 (1972).
63. Park, C. B., Lee, S. B. & Ryu, D. D. Y. L-Pyroglutamate spontaneously formed from L-glutamate inhibits growth of the hyperthermophilic archaeon *Sulfolobus solfataricus*. *Appl. Environ. Microbiol.* 67, 3650–3654 (2001).
64. Liu, H., Gaza-Bulseco, G. & Sun, J. Characterization of the stability of a fully human monoclonal IgG after prolonged incubation at elevated temperature. *J. Chromatogr. B* 837, 35–43 (2006).
65. Dimarchi, R. D., Tam, J. P., Kent, S. B. H. & Merrifield, R. B. Weak acid-catalyzed pyrrolidone carboxylic acid formation from glutamine during solid phase peptide synthesis: Minimization by rapid coupling. *Int. J. Pept. Protein Res.* 19, 88–93 (2009).
66. Dick, L. W., Kim, C., Qiu, D. & Cheng, K.-C. Determination of the origin of the N-terminal pyro-glutamate variation in monoclonal antibodies using model peptides. *Biotechnol. Bioeng.* 97, 544–553 (2007).
67. Khandke, K. M., Fairwell, T., Chait, B. T. & Manjula, B. N. Influence of ions on cyclization of the amino terminal glutamine residues of tryptic peptides of streptococcal PepM49 protein: Resolution of cyclized peptides by HPLC and characterization by mass spectrometry. *Int. J. Pept. Protein Res.* 34, 118–123 (2009).

68. Beck, A. et al. Stability and CTL activity of N-terminal glutamic acid containing peptides. *J. Pept. Res.* 57, 528–538 (2001).
69. Brorson, K. & Jia, A. Y. Therapeutic monoclonal antibodies and consistent ends: terminal heterogeneity, detection, and impact on quality. *Curr. Opin. Biotechnol.* 30, 140–146 (2014).
70. Yu, L. et al. Investigation of N-terminal glutamate cyclization of recombinant monoclonal antibody in formulation development. *J. Pharm. Biomed. Anal.* 42, 455–463 (2006).
71. Beck, A. et al. Stability and CTL-activity of P40/ELA melanoma vaccine candidate. *Biologicals* 29, 293–298 (2001).
72. Suzuki, Y., Motoi, H. & Sato, K. Quantitative analysis of pyroglutamic acid in peptides. *J. Agric. Food Chem.* 47, 3248–3251 (1999).
73. Lyubarskaya, Y., Houde, D., Woodard, J., Murphy, D. & Mhatre, R. Analysis of recombinant monoclonal antibody isoforms by electrospray ionization mass spectrometry as a strategy for streamlining characterization of recombinant monoclonal antibody charge heterogeneity. *Anal. Biochem.* 348, 24–39 (2006).
74. Alam, M. E. et al. Deamidation can compromise antibody colloidal stability and enhance aggregation in a pH-dependent manner. *Mol. Pharm.* 16, 1939–1949 (2019).
75. Jensen, P. F. & Rand, K. D. Hydrogen exchange: a sensitive analytical window into protein conformation and dynamics. in *Hydrogen exchange mass spectrometry of proteins: Fundamentals, methods and applications* 1–15 (John Wiley & Sons, Ltd, 2016).
76. Moorthy, B. S., Iyer, L. K. & Topp, E. M. Mass Spectrometric Approaches to Study Protein Structure and Interactions in Lyophilized Powders. *J. Vis. Exp.* 52503 (2015) doi:10.3791/52503.
77. Moorthy, B., Iyer, L. & Topp, E. Characterizing Protein Structure, Dynamics and Conformation in Lyophilized Solids. *Curr. Pharm. Des.* 21, 5845–5853 (2015).
78. Houde, D. & Engen, J. R. Conformational Analysis of Recombinant Monoclonal Antibodies with Hydrogen/Deuterium Exchange Mass Spectrometry. in *Glycosylation Engineering of Biopharmaceuticals* (ed. Beck, A.) vol. 988 269–289 (Humana Press, 2013).
79. Moorthy, B., Xie, B., Panchal, J. P. & Topp, E. M. Hydrogen exchange mass spectrometry for proteins adsorbed to solid surfaces, in frozen solutions, and in amorphous solids. in *Hydrogen exchange mass spectrometry of proteins: Fundamentals, methods and applications* 265–274 (John Wiley & Sons, Ltd, 2016).
80. Moorthy, B. S. et al. Solid-State Hydrogen–Deuterium Exchange Mass Spectrometry: Correlation of Deuterium Uptake and Long-Term Stability of Lyophilized Monoclonal Antibody Formulations. *Mol. Pharm.* 15, 1–11 (2018).

81. Sophocleous, A. M. & Topp, E. M. Localized Hydration in Lyophilized Myoglobin by Hydrogen–Deuterium Exchange Mass Spectrometry. 2. Exchange Kinetics. *Mol. Pharm.* 9, 727–733 (2012).
82. Kammari, R. & Topp, E. M. Prehydration and the Reversibility of Solid-State Hydrogen–Deuterium Exchange. *Mol. Pharm.* 17, 3541–3552 (2020).
83. Kammari, R. & Topp, E. M. Solid-State Hydrogen–Deuterium Exchange Mass Spectrometry (ssHDX-MS) of Lyophilized Poly- D , L -Alanine. *Mol. Pharm.* 16, 2935–2946 (2019).
84. Moussa, E. M. et al. Effects of Drying Process on an IgG1 Monoclonal Antibody Using Solid-State Hydrogen Deuterium Exchange with Mass Spectrometric Analysis (ssHDX-MS). *Pharm. Res.* 35, (2018).
85. Iyer, L. K., Sacha, G. A., Moorthy, B. S., Nail, S. L. & Topp, E. M. Process and Formulation Effects on Protein Structure in Lyophilized Solids Using Mass Spectrometric Methods. *J. Pharm. Sci.* 105, 1684–1692 (2016).
86. Moorthy, B. S., Schultz, S. G., Kim, S. G. & Topp, E. M. Predicting Protein Aggregation during Storage in Lyophilized Solids Using Solid State Amide Hydrogen/Deuterium Exchange with Mass Spectrometric Analysis (ssHDX-MS). *Mol Pharm.* 11, 1869–1879 (2014).

## CHAPTER 2. EFFECT OF 'pH' ON RATE OF PYROGLUTAMATE FORMATION IN SOLUTION AND LYOPHILIZED SOLIDS

*Adapted with permission from: Bersin, L. M., Patel, S. M. & Topp, E. M. Effect of 'pH' on the Rate of Pyroglutamate Formation in Solution and Lyophilized Solids. Mol. Pharmaceutics 18, 3116–3124 (2021).*

### 2.1 Abstract

N-terminal glutamate can cyclize to form pyroglutamate (pGlu) in pharmaceutically relevant peptides and proteins. The reaction occurs non-enzymatically during storage for monoclonal antibodies and shows a strong 'pH' dependence in solution, but the solid-state reaction has not been studied in detail.<sup>1-3</sup> This work investigates the effect of 'pH' and buffer species on pGlu formation for a model peptide (EVQLVESGGGLVQPGGSLR) in lyophilized solids and in solution. The model peptide was formulated from 'pH' 4 to 'pH' 9 in citrate, citrate-phosphate, phosphate, and carbonate buffers and stored at 50°C for at least 10 weeks. pGlu formation and loss of the parent peptide were monitored by reversed-phase high performance liquid chromatography. The apparent 'pH' dependence of the reaction rate in the solid state differed markedly from that in solution. Interestingly, in the 'pH' range often used to formulate mAbs ('pH' 5.5-6), the rate of pGlu formation in the solid state was greater than in solution. The results have implications for the rational design of stable formulations of peptides and proteins, and for the transition from solid to solution formulations during development

### 2.2 Introduction

Pyroglutamate (pGlu) is a chemically degraded form of glutamate (Glu) or glutamine (Gln) found in peptides and proteins with either of these amino acids at the N-terminus. The reaction can occur chemically or enzymatically, and pGlu-containing proteins have been detected both *in vivo* and in protein drug products.<sup>2,4-11</sup> In the body, pGlu formation occurs in endogenous proteins and appreciable levels of pGlu have been detected in IgG2 monoclonal antibodies (mAbs) *in vivo*.<sup>12</sup> While some reports suggest that pGlu formation *in vivo* has no effect on antibody clearance or turnover, others have associated pGlu with increased aggregation and inter-fibril association, decreased solubility, and altered structure and activity.<sup>12-14</sup> In protein drug products, non-

enzymatic pGlu formation is of interest due to the prevalence of N-terminal Glu and Gln in mAbs and the need to understand and control chemical modifications in this growing class of biologics.<sup>1,15</sup> pGlu formation contributes to the heterogeneity of protein drug products, complicating analytical characterization. Several studies have shown that there is no loss in the activity of therapeutic mAbs due to pGlu formation, and some have asserted that the transformation has no effect on structure, stability or function.<sup>1,12,16</sup> Others have suggested that pGlu formation may affect target binding because the N-termini of both the light and heavy chains of mAbs are in the variable region, near the complementarity determining region.<sup>17-19</sup> At present, the evidence for an effect of pGlu on product safety and efficacy is inconclusive and monitoring degradation of N-terminal Gln and Glu is likely to continue for the foreseeable future, at least until the reactions and their implications are fully understood.

Non-enzymatic pGlu formation in solution and solid protein formulations is the focus of the work reported here. In solution, non-enzymatic pGlu formation is initiated by nucleophilic attack of the N-terminal primary amine on the carbonyl carbon of the side chain of Gln or Glu (Figure 2-1A). When pGlu is formed from Gln, N-terminal Gln cyclizes to form pGlu with the loss of ammonia, creating an acidic charge variant due to loss of the positive charge from the N-terminal amino group.<sup>12</sup> When pGlu is formed from Glu, water is removed during cyclization of N-terminal Glu resulting in a basic charge variant with higher pI.<sup>20</sup> Both reactions produce a lactam-containing product that is more hydrophobic than the reactant.<sup>5,20</sup> The lactam ring is a poor proton acceptor, contributing to the stability of pGlu.<sup>4</sup> In fact, pGlu has been reported to revert to Glu only under very harsh conditions (e.g., 2M HCl, 100°C, 2 h).<sup>21</sup> Both the Gln and Glu reactions are temperature dependent and are generally considered irreversible.<sup>4,5,21-24</sup>

Of the two pathways, the reaction from Gln is better understood. The reaction proceeds through a tetrahedral intermediate.<sup>5</sup> Breakdown of this intermediate is the rate-limiting step and involves proton transfer between the N-terminal amide nitrogen and the oxygen of the  $\gamma$ -carbonyl carbon.<sup>5</sup> Weak acids, but not strong acids, catalyze the cyclization of the N-terminal Gln.<sup>25</sup> Phosphate buffer catalysis has been observed and phosphate ions are thought to act as acid-base catalysts by coordinating dual proton transfer with the cyclic tetrahedral intermediate, accelerating its breakdown through a concerted mechanism.<sup>5</sup> The catalytic effects of phosphate have been shown to vary with buffer concentration and solution pH and were greatest at pH 7.<sup>5</sup> Buffer

catalysis has also been reported for ammonium carbonate and ammonium acetate buffers, but to lesser extents, while Tris-HCl did not catalyze pGlu formation.<sup>23,24</sup> The influence of pH on the reaction from Gln has been investigated by several groups, but the overall conclusions are not clear. Some reports show pGlu formation rates increasing from pH 3 to 10, while others have shown pH independence over a similar pH range.<sup>4,5,21</sup> Another report shows that low pH accelerates the reaction moderately.<sup>23</sup> These conflicting reports suggest that pH is not a primary determinant of pGlu formation rates from Gln and that other factors, such as buffer type and temperature may be more important.<sup>23</sup>

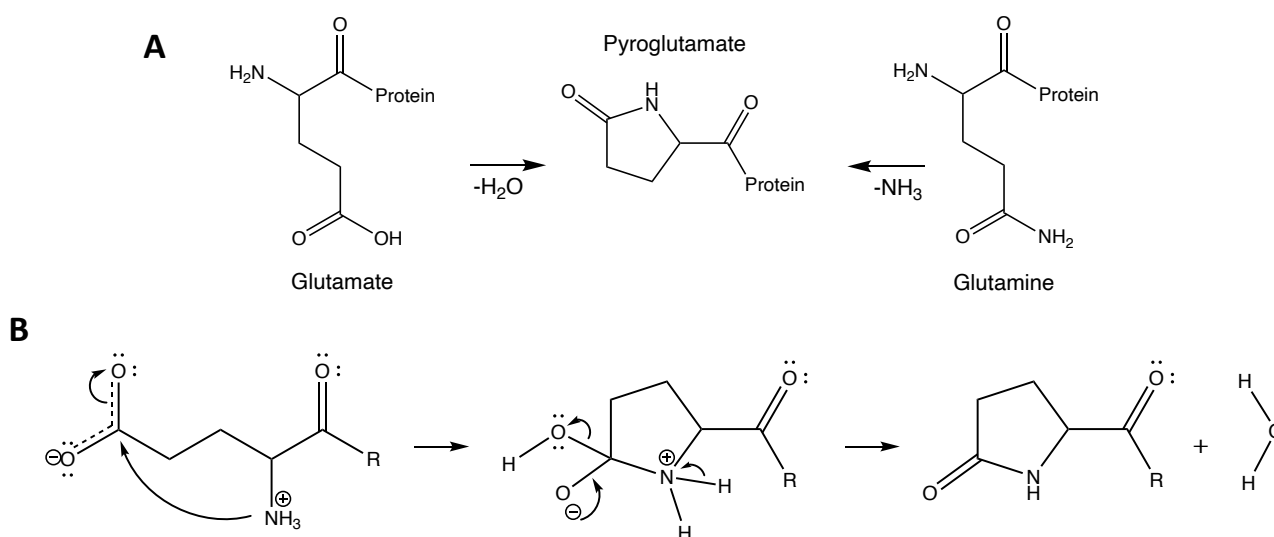


Figure 2-1. Reaction pathways for the formation of pGlu through cyclization of N-terminal Gln or Glu (A). The reaction from Gln results in the loss of ammonia while the reaction from Glu results in the loss of a water molecule. Proposed mechanism of pGlu formation from Glu through a tetrahedral intermediate (B).

The focus of this work is pGlu formation from Glu, which has been studied less than the reaction from Gln, perhaps because the Glu cyclization reaction is slower or because the Glu reaction was thought to be primarily enzymatic until recently.<sup>4,10,21,26</sup> A solution-state mechanism for pGlu formation from Glu has not been reported. However, a mechanism for solid-state pGlu formation from Glu has been proposed and involves catalysis by weak acids, as in the Gln reaction.<sup>17</sup> Accordingly, buffer species may have an effect on the reaction rate.<sup>17,25</sup> In lyophilized solids, pGlu formation from Glu was accelerated when the peptide was produced as an acetate or trifluoroacetate salt compared to a hydrochloride salt.<sup>17</sup> In solution, there is conflicting evidence as to whether pGlu formation is greater in histidine buffer or acetate buffer.<sup>1,2</sup> The effects of buffer

species on pGlu formation from Glu in solution thus are unclear, and further investigation is warranted. There is, however, a clear influence of pH on Glu cyclization in solution. Several groups have reported a reaction rate minimum at pH 6-6.2 with faster rates under acidic or basic conditions.<sup>1,2,4,27</sup> The pH dependence is thought to reflect the requirement for both a protonated  $\gamma$ -carboxyl group and a deprotonated  $\alpha$ -amino group for nucleophilic attack (i.e., charge neutral forms of both functional groups), which is unlikely at pH 6.

The studies reported here address the mechanism of pGlu formation from Glu, with a focus on lyophilized solids and the effects of pre-lyophilization pH. To date, there have been no mechanistic studies of pGlu formation from either Gln or Glu in solid samples, nor has the effect of ‘pH’ on the solid-state reaction been addressed in detail. A model “EVQL” peptide (EVQLVESGGGLVQPGGSLR) was formulated from ‘pH’ 4 to ‘pH’ 9 in citrate, citrate-phosphate, phosphate, and carbonate buffers and stored at 50°C for at least 10 weeks. Through the generation of ‘pH’-rate profiles, the results demonstrate that the ‘pH’ dependence of pGlu formation in the solid state is markedly different from that in solution. Interestingly, in the ‘pH’ range where mAbs are most often formulated, ‘pH’ 5.5-6, pGlu formation from Glu is faster in the solid state than in solution.

## 2.3 Experimental Section

### 2.3.1 Materials

The model “EVQL” peptide (EVQLVESGGGLVQPGGSLR) and its pGlu degradation product “pGlu-VQL” (pGlu-VQLVESGGGLVQPGGSLR) were custom synthesized by GenScript (Piscataway, NJ). The peptide content of the materials as received was ~95% of the total weight. The peptides were subjected to dialysis to remove residual salts remaining from synthesis as described below. Anhydrous methanol (99.8%), sucrose, citric acid, potassium citrate tribasic, potassium phosphate monobasic, potassium phosphate dibasic, potassium carbonate, and potassium bicarbonate were obtained from Sigma-Aldrich (St. Louis, MO). HPLC-grade acetonitrile, HPLC-grade trifluoroacetic acid (TFA), MS-grade water, MS-grade formic acid and MS-grade acetonitrile were obtained from Fischer Scientific (Fair Lawn, NJ).

### 2.3.2 Preparation of Model Peptide Solutions

Prior to its use in formulations and method development, the EVQL peptide was dissolved in deionized water to an approximate concentration of 10 mg/mL and dialyzed using a cellulose ester membrane (MWCO 100-500 Da) (Spectrum Laboratories, Inc., Rancho Dominguez, CA) for 24 h to remove any residual salts remaining from the synthesis process. After dialysis, the peptide solution was filtered using a 0.2  $\mu$ M PVDF syringe filter (Pall Corporation, Port Washington, NY) and lyophilized (LyoStar 3, SP Scientific, Stone Ridge, NY). The same procedure was used to purify the pGlu-VQL peptide, which was used as a standard for analytical method development.

### 2.3.3 Preparation of Buffer Solutions

Preliminary studies were conducted to evaluate and select buffers that could maintain 'pH' in both solution and lyophilized solid samples. An acceptable buffer for these studies must: (i) be stable at the storage temperature (50°C), (ii) not contain volatile species, such as acetate, that may be lost during lyophilization or storage at elevated temperature, (iii) maintain the target pH after lyophilization, storage and reconstitution, (iv) not be subject to differential salt precipitation during lyophilization and (v) be pharmaceutically relevant and generally regarded as safe (GRAS).

Formulations were prepared using a variety of buffers over a range of concentrations and evaluated against the criteria above. Tris buffer (tris-(hydroxy methyl) aminomethane) has previously been shown to degrade to formaldehyde at elevated temperatures and therefore was not included in buffer screening studies.<sup>28</sup> Since formulations prepared with histidine exhibited hydrolysis (clipping) products upon initial storage, histidine was also omitted. The buffer species selected for each 'pH' were: citrate for 'pH' 4 and 5, citrate-phosphate for 'pH' 5.5 and 6, phosphate for 'pH' 6.5, 7 and 8, and carbonate for 'pH' 9. Potassium phosphate has a reduced risk of differential precipitation and crystallization during lyophilization over other salt forms, therefore the potassium salt was used. A concentration of 20 mM was selected as it was the lowest concentration that gave sufficient 'pH' control throughout sample processing and storage. Each buffer was prepared by titrating 20 mM stock solutions of the conjugate acid/base pairs to the target pH. After titration, 0.185% (w/v) sucrose was added to each buffer and the pH was confirmed. Sucrose was added at a protein to sugar ratio of 2 (w/w).

Possible buffer catalysis was evaluated for each buffer type. The following conditions were selected for the buffer catalysis study: citrate at 'pH' 4, citrate-phosphate at 'pH' 5.5, phosphate at 'pH' 7, and carbonate at 'pH' 9. Buffer solutions were prepared according to the above procedure. Stock concentrations were set at the target buffer concentrations for this study: 20, 40 and 60 mM.

### **2.3.4 Preparation of Formulations in the Solid and Solution States**

Purified and lyophilized EVQL peptide was dissolved in deionized water to prepare a concentrated stock solution. The stock solution was then added to each of the eight formulation buffers to the target peptide concentration, 200  $\mu$ M. Peptide concentration was verified by reversed-phase high performance liquid chromatography (rp-HPLC) and further dilutions were made as needed. Each formulation was then filled into clear glass vials (2 mL, Wheaton, Millville, NJ) at a volume of 250  $\mu$ L. Half the samples were designated as solution state samples and were stored at 5°C during lyophilization of the solid-state samples. The remaining samples were lyophilized according to a fixed lyophilization cycle, in which (i) the starting shelf temperature was set at 10 °C and kept for 5 min, followed by (ii) freezing over three steps with a temperature ramp rate of 0.75 °C/min (hold at 5 °C for 10 min, -5 °C for 15 min, -45 °C for 120 min), (iii) primary drying under 70 mTorr at -50 °C for 24 h, (iv) increased to 25 °C at 0.2 °C/min, and (v) secondary drying under 70 mTorr at 25 °C for 6 h. The lyophilized samples were sealed under vacuum using Daikyo FluroTec stoppers (West Pharmaceutical Services Inc., Exton, PA). Both solution and solid samples were crimped with aluminum seals (13 mm, Wheaton, Millville, NJ) and immediately transferred to 50°C for stability storage.

### **2.3.5 Accelerated Stability Studies**

Stability studies were carried out at 50°C to investigate the effect of 'pH' on pGlu formation in lyophilized solids and solution controls. For lyophilized samples, 'pH' here refers to that of the solution prior to lyophilization, while for solution samples, 'pH' indicates the solution pH. The storage temperature was selected to maximize pGlu formation in the solid state, such that rate constants could be calculated accurately. The effects of buffer concentration on pGlu formation were also evaluated for each buffer system. At designated time intervals over at least

ten weeks, triplicate samples of each solid and solution formulation were removed from 50°C for analysis. Solid samples were reconstituted using 250 µL of deionized water. Solution and reconstituted lyophilized solid samples were analyzed in triplicate by rp-HPLC as described below. The pH values of all solutions and reconstituted lyophilized solids were measured with a pH-meter (Fisherbrand Accumet model AB15) equipped with a Mettler Toledo InLab Micro pH probe to verify that the pH did not shift over the study duration.

### 2.3.6 Sample Analysis

The EVQL peptide and its pGlu product (pGlu-VQL) were quantified using rp-HPLC with UV detection and calibration curves generated for both peptides. Solutions with a range of peptide concentrations (~5–315 µM) were prepared in potassium phosphate buffer (5 mM, pH 7.5) to construct the calibration curves. All samples used for quantitation were prepared in triplicate. The above samples were analyzed using rp-HPLC (1200 Series HPLC; ZORBAX Eclipse Plus C18 column, 4.6 × 250 mm, particle size 5 µm; Agilent Technologies). The injection volume for each sample was 40 µL, and the detection wavelength was 215 nm. The solvents and the gradient method were: filtered deionized water with 0.1% TFA (solvent A), HPLC-grade acetonitrile with 0.1% TFA (solvent B); a gradient flow from 15% solvent B to 60% solvent B in 21 min. The peptide concentrations and their corresponding chromatographic peak areas were recorded.

The parent peptide and pGlu product peptide identities were confirmed by mass spectrometry. The peptide sample was diluted with MS grade water (containing 0.1% formic acid) to 300 nM for LC–MS analysis (1260 Infinity Series HPLC; 6230 TOF LC–MS; ZORBAX 300SB-C18 column, 1.0 × 50 mm, particle size 3.5 µm; Agilent Technologies, Santa Clara, CA). The solvents and the gradient method were: MS-grade water with 0.1% formic acid (solvent A), MS-grade acetonitrile with 0.1% formic acid (solvent B); a constant 10% solvent B flow from 0 to 2 min, followed by a gradient flow from 10% B to 75% B in 11 min.

### 2.3.7 Kinetic Analysis

In solid and solution formulations, the observed rate constant ( $k_{obs}$ ) for the formation of pGlu was determined from linear regression of the mole fraction of pGlu peptide formed versus time according to a first-order kinetic model:

$$\ln(1 - X_{pGlu}) = k_{obs}t \quad 2.1$$

where  $X_{pGlu}$  is the mole fraction of pGlu-VQL peptide in each sample at time  $t$ . Previous studies have shown that the reaction of Glu to pGlu follows first order kinetics in solution.<sup>1,2</sup> Initial analysis also indicated that the solution data best fits to a first-order kinetic model (data not shown). In glassy solids, degradation often follows “stretched time kinetics”, in which degradation products increase linearly with the square root of time.<sup>29,30</sup> pGlu formation in this study did in fact fit slightly better to square root of time kinetics than to first order kinetics (not shown). However, to allow quantitative comparison of solid and solution rate constants, a first order model was used for the solid-state data. A comparison of the square root of time and first order kinetic models for the solid samples is presented in Appendix A (Figure A.1 Table A.1).

Using the first order model (Equation **Error! Reference source not found.** 2.1), values of  $k_{obs}$  were calculated for each formulation by linear regression using GraphPad Prism (GraphPad Software Inc., San Diego, CA). A ‘pH’-rate profile was generated from the  $k_{obs}$  values. In cases where buffer catalysis had a significant effect on pGlu formation kinetics, as determined in the buffer catalysis study,  $k_{obs}$  was extrapolated to zero buffer concentration (see Results) and reported as  $k_0$ .

### 2.3.8 Moisture Content of Lyophilized Solids

An 831 KF Coulometer (Metrohm, Riverview, FL) was used to measure the moisture content of the lyophilized samples in each formulation by Karl Fisher titration. Anhydrous methanol was used to reconstitute the lyophilized samples. The moisture content (in ppm) of the anhydrous methanol and the reconstituted samples was recorded. The moisture content was calculated accordingly and reported as a weight percentage (%w/w).

## 2.4 Results

### 2.4.1 EVQL and pGlu-VQL Peptide Analysis

EVQL and pGlu-VQL standard peptides in separate stock solutions appeared as single peaks on the rp-HPLC chromatogram eluting at ~13 min and ~14.5 min, respectively. When injected as a mixture, the peptides were baseline resolved, and retention times were unchanged from those of the standards injected separately. A calibration curve was generated for each peptide relating concentration to the corresponding chromatographic peak area. Upon repeated generation of the calibration curves, statistical analysis showed that the regression lines for the two peptides were not significantly different from one another. Thus, a single calibration curve, that of the EVQL peptide, was used for all subsequent analyses. Representative chromatograms for both peptides and their calibration curves are presented in Appendix A (Figure A.2).

Select samples were analyzed by LC/MS to confirm pGlu-VQL product identity. The pGlu-VQL product exhibited a mass change of -18 Da compared to the EVQL peptide and its retention time coincided with that of the synthetic pGlu-VQL standard. Extracted ion spectra of the parent EVQL peptide and the pGlu-VQL product are presented in Appendix A (Figure A.3). The pH of solution and reconstituted solid samples was monitored throughout the study. A pH shift less than 0.2 pH units was observed for all formulations.

### 2.4.2 pH Effect on Accelerated Stability

The effect of 'pH' on the formation of pGlu-VQL was investigated under accelerated conditions at 50°C. The EVQL peptide was formulated from 'pH' 4-9 at 200 µM and stored in sealed and crimped 2 mL glass vials as either a solution or a lyophilized powder. The concentrations of EVQL, pGlu-VQL, any side products, and the total peptide concentration were monitored over time. Several different side products were formed at low concentrations, as indicated by chromatographic peaks distinct from those of EVQL and pGlu-VQL. In order to maintain focus on the pGlu reaction (i.e., EVQL to pGlu-VQL), the areas of these peaks were summed and a single value was reported as the side product. In cases where side product formation became large and pGlu-VQL was no longer the main product, data sets were truncated for use in the rate calculation, as described below. Figure 2-2 **Error! Reference source not found.** shows the peptide concentration versus time profiles for a representative set of formulations at 'pH' 4,

'pH' 6, and 'pH' 8; similar curves for all formulations studied are presented in Appendix A, Figure A.4.

In solid samples, pGlu-VQL concentrations were relatively low, but continued to increase throughout the study (Figure 2-2A-C, Figure 2-3). The amounts of pGlu-VQL detected were slightly greater in the acidic region with a maximum at 'pH' 5 (Figure 2-3). However, differences in pGlu-VQL concentration were small across the 'pH' range with the exception of 'pH' 8 and 9, where very little pGlu-VQL was formed. At 'pH' 9, the concentration of pGlu-VQL peptide was below the working range of the calibration curve.

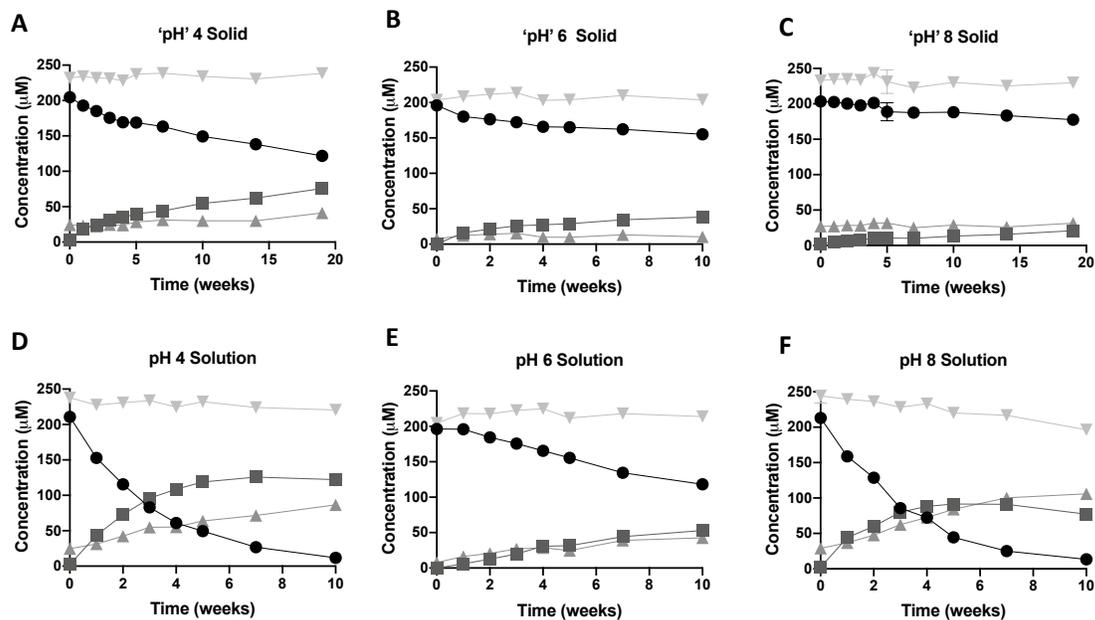


Figure 2-2. Kinetics of degradation of the EVQL peptide and formation of pGlu-VQL in solution (D-F; pH 4, 6 and 8) and in lyophilized solids prepared from these solutions (A-C). Concentrations of peptides EVQL peptide (black circle), pGlu-VQL peptide (dark gray square), summed side products (gray triangle), and total peptide concentration (light gray inverted triangle) after incubation at 50°C. n=9 (3 replicate measurements of 3 vials), mean  $\pm$  S.D.

In solution, the concentration of pGlu-VQL detected showed a clear dependence on pH across the pH range investigated (Figure 2-2D-F, Figure 2-3), with greater pGlu-VQL concentrations detected at pH 4 and pH 8 than at pH 6 (Figure 2-2D-F, Figure 2-3). pGlu-VQL concentrations in solution samples were greatest at pH 4, decreased as pH approached neutral, and then increased again from pH 6.5 to 8 (Figure 2-3). pGlu-VQL concentration then decreased again at pH 9. This trend was consistent at all timepoints.

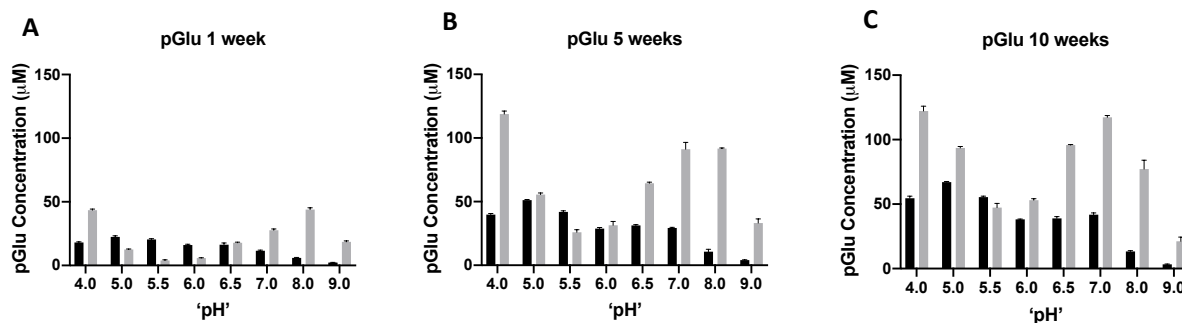


Figure 2-3. pGlu-VQL peptide concentration after 1 week (A), 5 weeks (B), and 10 weeks (C) of storage at 50°C in solution (gray) and lyophilized solid (black). n=9 (3 replicate measurements of 3 vials), mean  $\pm$  S.D.

As expected, the amount of pGlu-VQL formed was greater in solution than in lyophilized solids for most formulations. Interestingly, at ‘pH’ 5.5 and ‘pH’ 6, pGlu-VQL concentrations were similar in solid and solution states for most time points. After one week of storage, the pGlu-VQL concentration was greater in solid samples for ‘pH’ 5, ‘pH’ 5.5, and ‘pH’ 6 (Figure 2-3). Moreover, at ‘pH’ 5.5, the amount of pGlu-VQL formed remained greater in the solid samples than in solution at all timepoints. These observations are particularly relevant for the biopharmaceutical industry because many mAbs are formulated in the ‘pH’ 5 to ‘pH’ 6 range.

Several side products were detected over the duration of the study. The species formed were also present in the starting material as received from the supplier at  $\sim$ 10% by weight. Solid samples showed little increase in the concentrations of side products with time (Figure 2-2A-C), while solution samples showed a steady increase in side product concentrations throughout the study (Figure 2-2D-F). At higher pH in solution, the concentrations of side products became greater than the pGlu-VQL concentration with time. For example, side products dominated at pH 9 in solution after just 3 weeks (Figure A.4). This indicates that the EVQL peptide undergoes a variety of degradation processes, particularly at high pH in solution. Once side reactions dominate, the system no longer serves as an appropriate means to investigate pGlu formation. The low levels of pGlu-VQL at high ‘pH’ detected in solution samples at later times (Figure 2-3C) reflect these side reactions, which may include degradation of the pGlu-VQL product itself and should not be taken as an accurate measure of its rate of formation.

Total peptide concentration was monitored throughout the study to ensure that mass balance was maintained. Total peptide concentration was estimated by summing chromatographic peak areas and assuming that the extinction coefficients for all products were identical to that of

the EVQL parent at 215 nm. A loss of mass balance was observed in solution formulations at pH 8 and pH 9, in which total peptide concentration decreased throughout the study. This is probably the result of peptide bond hydrolysis at the relatively high storage temperature (50°C) and pH (pH 8, 9) of these formulations. The resulting peptide bond fragments may not be detected or may have a lower molar absorptivity than EVQL during rp-HPLC analysis. The loss of mass balance corresponds to an increase in side products (Figure 2-2F, Figure A.4O,P), further emphasizing that reactions other than pGlu formation dominate under these conditions.

A decrease in pGlu-VQL concentration was also observed in solution pH 4 and pH 7 samples after 7 weeks and 10 weeks of storage, respectively (Figure 2-2D, Figure A.4E,N). In all other formulations the amount of pGlu-VQL continually increased throughout the study. pGlu-VQL loss corresponds to a substantial formation of side products; the total concentration of side products was nearly equal to or greater than the concentration of pGlu-VQL (Figure 2-2D,F, Figure A.4E,N-P). The decrease also corresponds to a loss of EVQL peptide to less than ~10% of the initial concentration. These observations suggest that pGlu-VQL is itself degraded by one or more of the side reactions. This possibility will be further addressed in the kinetic analysis.

### **2.4.3 Buffer Catalysis**

The effect of buffer concentration was investigated in solution and solid samples representing each of the four buffer systems used in the ‘pH’ study: citrate at ‘pH’ 4, citrate-phosphate at ‘pH’ 5.5, phosphate at ‘pH’ 7, and carbonate at ‘pH’ 9. In solid samples, the amount of pGlu-VQL formed over 10 weeks did not differ significantly among the three buffer concentrations for any of the buffer systems (Figure 2-4A, Figure A.5A-D), indicating that buffer catalysis is not observed. Similarly, buffer catalysis was not observed in solution samples containing citrate, phosphate or carbonate buffers (Figure A.5E,G,H). However, in solutions containing citrate-phosphate buffer, after 5 weeks, pGlu-VQL concentrations increased with increasing buffer concentration (Figure 2-4B), indicating buffer catalysis. Accordingly, rates of pGlu-VQL formation in solutions containing citrate phosphate buffer (i.e., pH 5.5, 6) were extrapolated to zero buffer concentration when constructing the pH-rate profile (see below).

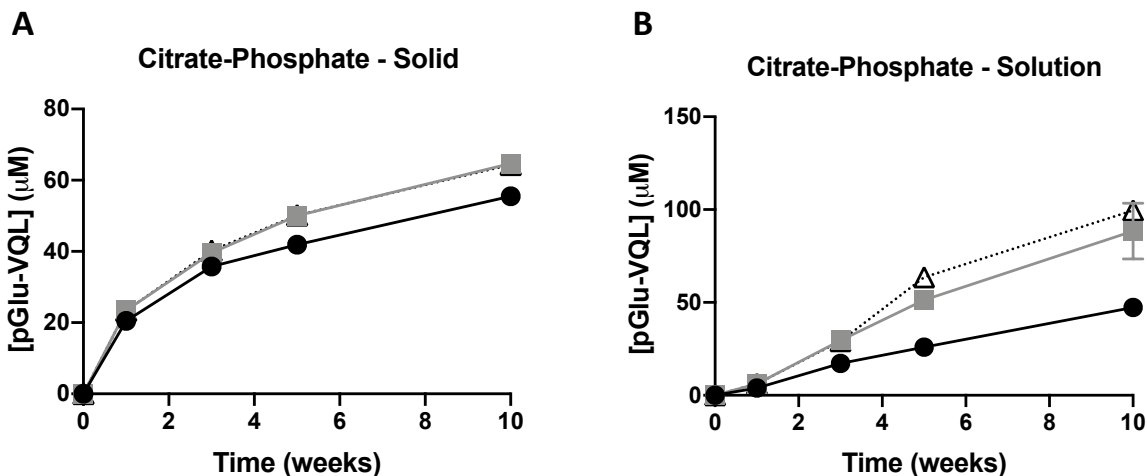


Figure 2-4. pGlu-VQL peptide concentration in formulations with 20 mM (black circle), 40 mM (gray square), and 60 mM (open triangle) buffer concentration over 10 weeks incubation at 50°C stored as lyophilized solid (A) and in solution (B).  $n=9$  (3 replicate measurements of 3 vials), mean  $\pm$  S.D.

#### 2.4.4 Rate Constants

Apparent first-order rate constants for pGlu formation were calculated for each formulation using linear regression according to Equation 2.1; see Appendix A Table A.3 for tabulated rate constants. The dependence of the rate constants on 'pH' in solution and solid samples is summarized in the 'pH'-rate profile (Figure 2-5). Several adjustments have been made to the rate constants for specific formulations in order to isolate the pGlu formation reaction and minimize confounding effects. First, in some formulations, the pGlu concentration began to decrease at later time points, suggesting that pGlu-VQL was degrading as well as being formed. To minimize effects of pGlu degradation on estimated formation rate constants, these data sets were truncated: pH 4 solution at 7 weeks, pH 7 solution at 10 weeks, pH 8 solution at 5 weeks, 'pH' 9 solution and solid at 4 weeks and 5 weeks, respectively.

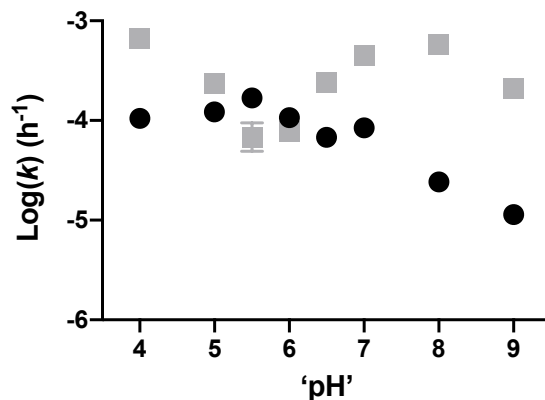


Figure 2-5. ‘pH’-rate profile for pGlu formation in lyophilized solids (black circle) and in solution (gray square) at 50 °C. Error bars represent standard error of the first-order kinetic model regression fit (Equation 2.1). Rate constants have been adjusted to zero buffer concentration where applicable as described in the text.

In addition, rate constants for pGlu-VQL formation in solutions containing citrate-phosphate buffer were extrapolated to zero buffer concentration based on the results of the buffer catalysis study (Figure A.6, Table A.2). As a reference, ‘pH’-rate profiles without these modifications are presented in Figure A.8. Regardless of these modifications the observed trends between solid and solutions state ‘pH’ dependence, described below, are the same.

Several features of the ‘pH’-rate profile (Figure 2-5) are noteworthy. Overall, the curve is U-shaped for solution samples suggesting a degree of catalysis in both the acidic and basic regions, as reported previously.<sup>1,2</sup> In solution, the pH of maximum stability occurs at pH 5.5 to 6. Although the rate constant for pH 5.5 in solution is slightly less than that at pH 6, a t-test indicates the two values are not significantly different. In the acidic solutions (pH 4 to pH 6), the pH-rate profile is linear with a slope of  $-0.52 \pm 0.13$ . This value is less than that expected for specific acid catalysis (i.e., -1), suggesting that catalysis by hydronium ions does not control the rate-determining step in this region. In neutral solutions (pH 6 to pH 7), the pH-rate profile has a positive slope of  $0.77 \pm 0.13$ . This value approaches +1, suggesting specific base catalysis. The rate constant decreases at pH 9 likely due to degradation of the pGlu-VQL peptide and/or the formation of side products. Kinetic analysis of EVQL loss, rather than pGlu-VQL formation, shows an increase in rate constant from pH 8 to pH 9 (data not shown), consistent with degradation via multiple pathways at pH 9.

The shape of the ‘pH’-rate profile for pGlu formation in lyophilized samples is notably different from that for solutions (Figure 2-5). In solids, the dependence of rate constant on ‘pH’ is nearly flat from ‘pH’ 4 to 7, with a weak maximum at ‘pH’ 5.5 (Figure 2-5). The rate constant at ‘pH’ 5.5 is significantly different from rate constants in solid samples lyophilized at all other ‘pH’ values. The slope of the ‘pH’-rate profile for solid samples in the ‘pH’ 4 to 7 range is  $0.06 \pm 0.05$ , a value not significantly different from zero, indicating that the reaction rate is independent of ‘pH’ in this region. In the neutral to basic region (‘pH’ 7 to 9), the ‘pH’-rate profile is approximately linear with a slope of  $-0.73 \pm 0.11$ . The rate of pGlu-VQL formation is least in solids at ‘pH’ 9; the rate of EVQL degradation is also at a minimum at this ‘pH’. Thus, with regard to pGlu formation in solid samples, the apparent ‘pH’ of maximum stability is highly basic and differs considerably from the optimal pH in solution (Figure 2-5).

## 2.5 Discussion

In this work, pGlu was formed in the model peptide EVQL in both solid and solution samples from ‘pH’ 4-9. Overall, the ‘pH’ dependence of the reaction rate was weaker than for other chemical degradation reactions of peptides and proteins such as deamidation, diketopiperazine formation, and peptide bond hydrolysis.<sup>28,31,32</sup> The ‘pH’-rate profile (Figure 2-5) has two notable features that challenge the conventional understanding of solid and solution-state reactions. First, the ‘pH’-rate profile shows markedly different shapes for the solid and solution-state reactions. ‘pH’-rate profiles are often thought to be roughly parallel in solid and solution states, with the solid-state profile expected to show the same general ‘pH’ dependence as the solution-state profile, but at slower rates. In solution, pGlu formation was accelerated by acidic and basic conditions with greater pH sensitivity (i.e., the slope of the pH-rate profile) in the basic region and maximum stability at pH 5.5-6 (Figure 2-5). In contrast, the ‘pH’-rate profile in the solid state is independent of ‘pH’ for ‘pH’ 4-7 and shows a sharp decrease in reaction rate from ‘pH’ 7-9 (Figure 2-5). The apparent ‘pH’ of maximum stability in the solid state is highly basic and differs considerably from the optimal pH in solution (Figure 2-5). Second, the pGlu reaction rate is slower in solution than in solid samples near the ‘pH’ of maximum solution stability (‘pH’ 5.5-6), a range used for many mAb formulations. At ‘pH’ 5.5 the difference between solution and solid reaction rates is significant, while at ‘pH’ 6 the difference is not (p-value 0.0759). Protein drug products are often formulated as solids in an attempt to reduce degradation rates and improve

shelf stability, exploiting the typically lower reactivity in the solid state. The results suggest that this strategy may not be successful in reducing pGlu formation under weakly acidic conditions (Figure 2-3, Figure 2-5). There were no catalytic effects of buffer species at the levels investigated here, with the exception of citrate-phosphate buffer in solution samples. It is reasonable to expect buffer catalysis since the Gln to pGlu reaction is catalyzed by phosphate ions and the mechanism for the reaction from Glu is likely to be similar.<sup>5</sup> The low buffer concentrations used in this study may explain the absence of buffer catalysis.

There are several possible explanations for the differences in the ‘pH’-rate profiles in solution and solid samples. At a broad level, the differences may suggest that ‘pH’ does not indicate the propensity of the peptide to form pGlu in the solid state. This in turn may be the result of: (i) differences in the pKa of the reacting  $\gamma$ -carboxyl and  $\alpha$ -amino groups in solutions and solids, e.g., due to differences in dielectric constant as suggested previously for deamidation,<sup>33</sup> (ii) more fundamental differences in the ionization states of these groups in solution and solid samples, (iii) ‘pH’ shifts during freezing, and/or (iv) differences in acid-base catalytic effects. In solution at pH 5.5-6, both the carboxylic acid and the primary amine are ionized, which is unfavorable for nucleophilic attack and pGlu ring formation (Figure 2-1B). In the solid state, charges on these groups are less likely to be stabilized by interactions with water, and they may not be ionized in the conventional sense (e.g., water shielded, charge separated). This muting of charge may create  $\gamma$ -carboxyl and  $\alpha$ -amino groups that are more nearly neutral, lowering the barrier for reaction and resulting in faster rates in solids than in solution (i,ii). With regard to ‘pH’ shifts on freezing (iii), the formulations studied here were examined for ‘pH’ shifts using a low temperature pH probe (data not shown); only formulations at ‘pH’ 6.5 and ‘pH’ 9 showed a shift greater than 0.5 ‘pH’ units upon freezing at -30°C, an observation that does not fully explain the differences in the ‘pH’-rate profiles. Regarding catalytic effects (iv), the ‘pH’-rate profiles suggest that acid-base catalytic effects may differ in solution and solid samples, as evidenced by the opposite dependences on ‘pH’ in solution and solid samples in the basic region (Figure 2-5). Like options (i-iii), this may suggest differences in ionization states of reactants and/or buffers for the reaction in the solid state vs. solution.

In addition to these ‘pH’ and ionization related effects, other factors may contribute to the faster pGlu formation rates in solid samples under weakly acidic conditions. Fundamentally, pGlu formation is a condensation reaction that produces water as a product. The low water content in

solid samples thus may help to drive the forward reaction and increase the reaction rate in the solid state relative to that in solution. Crystallization of excipients during freezing may lead to phase separated domains in the lyophilized solid, which may have different reaction rates than more homogenous amorphous materials. Here, formulations were examined for signs of crystallization upon freezing at -30°C by polarized light microscopy; only formulations at ‘pH’ 6.5 and ‘pH’ 9 showed signs of crystallization (data not shown). Macroscopic phase separation thus may affect reaction rates under these conditions, though the magnitude and direction of any changes are not known. Finally, it is possible that the reaction mechanism or rate determining step may differ in solution and solid samples, though the low levels of side products in solid samples (Figure A.4) suggest that this is unlikely.

Several limitations in the experimental approach and data interpretation should be noted. First, a model peptide was used to study pGlu formation rather than a larger protein or mAb. While larger proteins are arguably more relevant to the industry, the use of a model peptide allowed focus on the mechanistic aspects of the pGlu formation reaction without the possible confounding effects of higher order structure. In addition, the use of a model peptide allowed the parent peptide and the pGlu product to be quantified against known synthetic standards. Second, these studies were performed under stressed conditions to allow pGlu formation to be assessed in practical experiment times. In the strictest sense, the results apply only under these stressed conditions. Third, the formation of pGlu containing side products may have led to an underestimation of degradation rates in some samples. Rates of pGlu formation were calculated assuming that pGlu-VQL is the only pGlu-containing species. However, it is possible that the pool of side products also includes some pGlu-containing species, so that the overall pGlu formation rate is underestimated. This error is likely to be small when the concentration of side products is low, as in most samples studied here. However, the error may be important for samples with higher side product concentrations, a condition that applies in particular to solution samples at pH 9. Undetected pGlu side products may have contributed to the slow apparent pGlu formation rate under these conditions (Figure 2-5). Lastly, as in many studies on amorphous materials, a complete characterization of the samples at the molecular scale is lacking here. X-ray diffraction or nuclear magnetic resonance could provide insight into formulation homogeneity and any phase separation in solid formulations. Due to material limitations, those analyses were not possible in the current study.

The results reported here have implications for developing pGlu-prone pharmaceuticals. Formulating a dry product may not reduce the rate and extent of pGlu formation relative to solution, particularly in the weakly acidic 'pH' range, and changing between solid and solution formulations during development may not have predictable effects on stability. The weak 'pH' dependence, especially for the solid-state reaction, suggests that changing formulation 'pH' may also have little effect in controlling the rate and extent of pyroglutamate formation from Glu. In previous reports, formulation and process factors have been shown to influence the rate of the reaction, including temperature, buffer type, protein higher order structure, and surrounding amino acid environment in the solution state.<sup>1-3,12,17,20,25</sup> Further investigation of the effects of excipients, moisture, and mobility on pGlu formation in the solid state is warranted and would help to support the development of stable solid-state protein drug products.

## 2.6 Conclusions

The effects of 'pH' and buffer species on rates of pGlu formation in a model peptide (EVQLVESGGGLVQPGGSLR) were investigated in lyophilized solids and in solution at 50 °C. The apparent 'pH' dependence of the reaction rate in the solid state differed markedly from that in solution. In solution, weak pH dependence and a U-shaped pH-rate profile with a minimum near pH 5.5 to 6 were observed. In solid samples, pGlu formation rates were independent of 'pH' under acidic and neutral conditions ('pH' 4-7) and decreased with increasing 'pH' in the basic region ('pH' 7-9). Interestingly, in the 'pH' range often used to formulate mAbs ('pH' 5.5-6), the rate of pGlu formation in the solid state was greater than in solution.

## 2.7 References

1. Chelius, D. *et al.* Formation of Pyroglutamic Acid from N-Terminal Glutamic Acid in Immunoglobulin Gamma Antibodies. *Anal. Chem.* **78**, 2370–2376 (2006).
2. Yu, L. *et al.* Investigation of N-terminal glutamate cyclization of recombinant monoclonal antibody in formulation development. *J. Pharm. Biomed. Anal.* **42**, 455–463 (2006).
3. Yu, L., Remmele, R. L. & He, B. Identification of N-terminal modification for recombinant monoclonal antibody light chain using partial reduction and quadrupole time-of-flight mass spectrometry. *Rapid Commun. Mass Spectrom.* **20**, 3674–3680 (2006).
4. Seifert, F. *et al.* Glutaminyl Cyclases Display Significant Catalytic Proficiency for Glutamyl Substrates. *Biochemistry* **48**, 11831–11833 (2009).
5. Seifert, F. *et al.* Phosphate ions and glutaminyl cyclases catalyze the cyclization of glutaminyl residues by facilitating synchronized proton transfers. *Bioorganic Chem.* **60**, 98–101 (2015).
6. Schilling, S., Hoffmann, T., Manhart, S., Hoffmann, M. & Demuth, H.-U. Glutaminyl cyclases unfold glutamyl cyclase activity under mild acid conditions. *FEBS Lett.* **563**, 191–196 (2004).
7. Huang, K.-F., Liu, Y.-L., Cheng, W.-J., Ko, T.-P. & Wang, A. H.-J. Crystal structures of human glutaminyl cyclase, an enzyme responsible for protein N-terminal pyroglutamate formation. *Proc. Natl. Acad. Sci.* **102**, 13117–13122 (2005).
8. Xu, Y. *et al.* Structure, heterogeneity and developability assessment of therapeutic antibodies. *mAbs* **11**, 239–264 (2019).
9. Twardzik, D. R. & Peterkofsky, A. Glutamic Acid as a Precursor to N-Terminal Pyroglutamic Acid in Mouse Plasmacytoma Protein. *Proc. Natl. Acad. Sci.* **69**, 274–277 (1972).
10. Park, C. B., Lee, S. B. & Ryu, D. D. Y. L-Pyroglutamate spontaneously formed from L-glutamate inhibits growth of the hyperthermophilic archaeon *Sulfolobus solfataricus*. *Appl. Environ. Microbiol.* **67**, 3650–3654 (2001).
11. Liu, H., Gaza-Bulseco, G. & Sun, J. Characterization of the stability of a fully human monoclonal IgG after prolonged incubation at elevated temperature. *J. Chromatogr. B* **837**, 35–43 (2006).
12. Liu, Y. D., Goetze, A. M., Bass, R. B. & Flynn, G. C. N-terminal Glutamate to Pyroglutamate Conversion *in Vivo* for Human IgG2 Antibodies. *J. Biol. Chem.* **286**, 11211–11217 (2011).
13. Kumar, A. & Bachhawat, A. K. Pyroglutamic acid: throwing light on a lightly studied metabolite. *Curr. Sci.* **102**, 288–297 (2012).
14. Lai, Z. W., Petrera, A. & Schilling, O. Protein amino-terminal modifications and proteomic approaches for N-terminal profiling. *Curr. Opin. Chem. Biol.* **24**, 71–79 (2015).

15. Ionescu, R. & Vlasak, J. Kinetics of Chemical Degradation in Monoclonal Antibodies: Relationship between Rates at the Molecular and Peptide Levels. *Anal. Chem.* **82**, 3198–3206 (2010).
16. Lyubarskaya, Y., Houde, D., Woodard, J., Murphy, D. & Mhatre, R. Analysis of recombinant monoclonal antibody isoforms by electrospray ionization mass spectrometry as a strategy for streamlining characterization of recombinant monoclonal antibody charge heterogeneity. *Anal. Biochem.* **348**, 24–39 (2006).
17. Beck, A. *et al.* Stability and CTL activity of N-terminal glutamic acid containing peptides. *J. Pept. Res.* **57**, 528–538 (2001).
18. Beck, A. *et al.* Stability and CTL-activity of P40/ELA melanoma vaccine candidate. *Biologicals* **29**, 293–298 (2001).
19. Alam, M. E. *et al.* Deamidation can compromise antibody colloidal stability and enhance aggregation in a pH-dependent manner. *Mol. Pharm.* **16**, 1939–1949 (2019).
20. Liu, Z. *et al.* Cyclization of N-Terminal Glutamic Acid to pyro-Glutamic Acid Impacts Monoclonal Antibody Charge Heterogeneity Despite Its Appearance as a Neutral Transformation. *J. Pharm. Sci.* (2019) doi:10.1016/j.xphs.2019.05.023.
21. Shih, F. F. Analysis of glutamine, glutamic acid and pyroglutamic acid in protein hydrolysates by high-performance liquid chromatography. *J. Chromatogr. A* **322**, 248–256 (1985).
22. Abraham, G. N. & Podell, D. N. Pyroglutamic acid. in *The Biological Effects of Glutamic Acid and Its Derivatives* (ed. Najjar, V. A.) 181–190 (Springer Netherlands, 1981). doi:10.1007/978-94-009-8027-3\_11.
23. Dick, L. W., Kim, C., Qiu, D. & Cheng, K.-C. Determination of the origin of the N-terminal pyro-glutamate variation in monoclonal antibodies using model peptides. *Biotechnol. Bioeng.* **97**, 544–553 (2007).
24. Khandke, K. M., Fairwell, T., Chait, B. T. & Manjula, B. N. Influence of ions on cyclization of the amino terminal glutamine residues of tryptic peptides of streptococcal PepM49 protein: Resolution of cyclized peptides by HPLC and characterization by mass spectrometry. *Int. J. Pept. Protein Res.* **34**, 118–123 (2009).

## CHAPTER 3. FORMULATION APPROACH TO INHIBIT PYROGLUTAMATE FORMATION IN A MODEL PEPTIDE

### 3.1 Abstract

Pyroglutamate (pGlu) is a chemical degradant formed by cyclization of N-terminal glutamate (Glu) in therapeutic peptides and proteins. The reaction occurs for monoclonal antibodies (mAbs) on storage in both the solid and solution states, but the solid-state reaction has not been studied in detail. This work investigates the effect of excipient, 'pH', moisture content and glass transition temperature (T<sub>g</sub>) on pGlu formation for a model peptide (EVQLVESGGGLVQPGGSLR) in lyophilized solids and solution. The model peptide was formulated from 'pH' 4 to 8 with either trehalose, dextran or hydroxyectoine excipients. Moisture content was controlled through storage at varied relative humidity (RH) and T<sub>g</sub> was varied through moisture content and by the addition of glycerol. Formulations were stored at 50 °C for up to 15 weeks, and pGlu formation and loss of the parent peptide were monitored by reversed-phase high performance liquid chromatography. Excipient type, 'pH', moisture content and T<sub>g</sub> all affected pGlu formation in the solid state. In solution, there was no effect of excipient type. The extent of deuterium incorporation in solid-state hydrogen deuterium exchange-mass spectrometry (ssHDX-MS) showed some correlation with solid-state stability. The results suggest strategies for formulating pGlu-prone peptides and proteins in the solid state and use of ssHDX-MS as a broad screening tool for such formulations.

### 3.2 Introduction

Pyroglutamate (pGlu) is a chemical degradant found in peptides and proteins with either glutamate (Glu) or glutamine (Gln) at the N-terminus. pGlu-containing proteins have been detected *in vivo* and in protein drug products and are formed through both chemical and enzymatic pathways.<sup>1-9</sup> N-terminal Glu and Gln are prevalent in monoclonal antibodies (mAbs), a growing class of biologics, thus understanding this chemical modification is relevant to their development.<sup>10,11</sup> Currently, the effects of pGlu formation on safety and efficacy are unclear. Several studies have shown that there is no loss of activity, structure or function.<sup>11-13</sup> However, pGlu formation may affect target binding due to the proximity of the N-termini of both mAb light

and heavy chains to the complementarity determining region.<sup>14-16</sup> pGlu formation also contributes to the heterogeneity of protein drug products, complicating analytical characterization.

Of the two reactions, pGlu from Glu has been studied less, and is the focus of this work. Non-enzymatic pGlu formation occurs via nucleophilic attack of the N-terminal primary amine on the carbonyl carbon of the Glu side chain with the loss of water (Figure 3-1). This dehydration step is rate-limiting and involves proton transfer from the N-terminal amide nitrogen to the oxygen of the  $\gamma$ -carbonyl carbon.<sup>17</sup> The lactam-containing product is a more hydrophobic, basic charge variant with a higher pI than the Glu-containing precursor.<sup>3,18</sup> Formation of pGlu is generally considered irreversible because the lactam ring is a poor proton acceptor and has been shown to revert to Glu only under very harsh conditions (e.g., 2M HCl, 100°C, 2 h).<sup>2,19</sup>

A mechanism for pGlu formation from Glu in the solid state has been proposed and involves catalysis by weak acids.<sup>14</sup> Previous work from our group examined the effects of ‘pH’ on the solid and solution-state reactions, where ‘pH’ refers to that of the solution prior to lyophilization.<sup>20</sup> The resulting ‘pH’-rate profiles were markedly different in the solid and solution states. In solution, a U-shaped dependence of the log of the observed reaction rate constant ( $k_{obs}$ ) on ‘pH’ was observed with a minimum at pH 5.5-6, in agreement with previous reports.<sup>1,2,11,21</sup> In the solid state, the reaction was essentially independent of ‘pH’ from ‘pH’ 4 to 7 and decreased with increasing ‘pH’ from 7 to 9. The effects of excipients on pGlu formation have been reported for a spray-dried antibody fragment (Fab).<sup>22</sup> Trehalose and hydroxyectoine, an amino-acid derived excipient, showed equal protection against pGlu formation that was superior to excipient-free and ectoine-containing samples.<sup>22</sup>

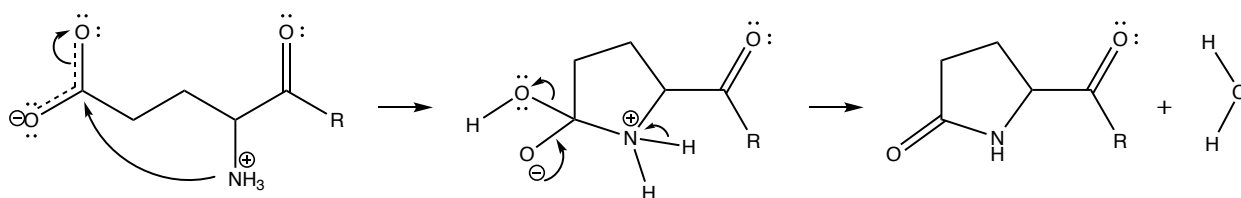


Figure 3-1. Reaction pathway for the formation of pGlu through cyclization of N-terminal Glu via a tetrahedral intermediate.

The studies reported here investigate various formulation strategies for inhibiting pGlu formation by examining the effect of excipients, ‘pH’, moisture content, and mobility as measured by the glass transition temperature (T<sub>g</sub>). To date, the effects of excipients, moisture content, or T<sub>g</sub>

on pGlu formation from Glu in lyophilized solids have not been reported. A model peptide, “EVQL” (EVQLVESGGGLVQPGGSLR) was formulated from ‘pH’ 4 to 8 with the excipients trehalose, dextran (6 kDa), or hydroxyectoine and stored at 50 °C for up to 15 weeks in open vials. Moisture content was varied in trehalose and dextran-containing samples by storing them at different relative humidities (RH). Tg was manipulated through both moisture content and by the addition of glycerol in trehalose-containing samples. Hydroxyectoine was excluded from the moisture content and Tg investigation due to its low Tg in relation to storage conditions. The results demonstrate that pGlu formation can be reduced by low molecular weight hydrogen bonding excipients and low moisture content.

Select formulations were also analyzed by solid-state hydrogen deuterium exchange-mass spectrometry (ssHDX-MS) to assess the technique’s ability to identify pGlu-prone formulations. ssHDX-MS has been used to quantify conformational changes and matrix interactions in lyophilized proteins and to predict long-term stability outcomes in proteins, including mAbs, as measured by aggregation behavior.<sup>23–26</sup> Previous work from our lab suggests that deuterium incorporation by ssHDX-MS may also be related to the rates of reactions that depend on proton transfer, such as pGlu formation.<sup>23</sup> The results reported herein suggest that ssHDX-MS can be useful as a broad screening tool for this reaction.

### **3.3 Experimental Section**

#### **3.3.1 Materials**

The model “EVQL” peptide (EVQLVESGGGLVQPGGSLR) and its pGlu degradation product “pGlu-VQL” (pGlu-VQLVESGGGLVQPGGSLR) were custom synthesized by GenScript (Piscataway, NJ). The peptide content of the materials as received was ~95% of the total weight. The peptides were subjected to dialysis to remove residual salts remaining from synthesis as described below. Anhydrous methanol (99.8%), hydroxyectoine, lithium bromide, and buffer salts (citric acid, potassium citrate tribasic, potassium phosphate monobasic, and potassium phosphate dibasic) were obtained from Sigma-Aldrich (St. Louis, MO). Trehalose, glycerol, lithium chloride, lyophilization vials (Wheaton type I clear glass 2 mL serum vials), stoppers (Daikyo FluroTec stoppers, West Pharmaceutical Services Inc., Exton, PA), all liquid chromatography mass spectrometry (LC-MS) grade solvents (water, acetonitrile, formic acid, and

methanol) and high-performance liquid chromatography (HPLC) grade solvents (acetonitrile, trifluoroacetic acid) were purchased from Fisher Scientific (Hanover Park, IL). Dextran (6 kDa) was purchased from Alfa Aesar (Haverhill, MA). Deuterium oxide (D<sub>2</sub>O, 99.9%) was purchased from Cambridge Isotope Laboratories (Andover, MA). Float-A-Lyzer dialysis devices (molecular weight cutoff 100-500 Da) were purchased from Spectrum Laboratories, Inc. (Rancho Dominguez, CA). Syringe filters (0.2 μM PVDF) were purchased from Pall Corporation (Port Washington, NY).

### 3.3.2 Sample Preparation

Prior to its use in formulations, the EVQL peptide was dissolved in deionized water to an approximate concentration of 15 mg/mL and dialyzed using a cellulose ester membrane (MWCO 100-500 Da) for 24 h and then filtered using a 0.2 μM PVDF syringe filter. Purified, concentrated stock solutions of EVQL peptide were then added to each of the 14 formulation buffers to the target peptide concentration of 200 μM. Formulation buffers were prepared by titrating 12 mM stock solutions of the conjugate acid/base pairs to the target pH. The buffer species selected for each 'pH' were: citrate for 'pH' 4 and 5; citrate-phosphate for 'pH' 5, 5.5 and 6; and phosphate for 'pH' 6, 6.5, 7 and 8. Excipient was added to each buffer at a target sugar to protein ratio (S/P) of 15 (w/w). Concentrated glycerol was spiked into formulations to the desired concentration where applicable. Glycerol concentrations are reported as a percentage of the excipient concentration. Table 3-1 and Table 3-2 present the detailed study designs for investigating excipient and 'pH' effects (Table 3-1) and moisture content and T<sub>g</sub> effects (Table 3-2).

Table 3-1. Composition of EVQL peptide formulations for study of excipient and 'pH' effects.

<b>Formulation ID</b>	<b>Excipient</b>	<b>'pH'</b>	<b>Buffer Species</b>
F1	Trehalose	4	Citrate
F2		5	
F3		5	Citrate-Phosphate
F4		5.5	
F5		6	
F6		6	Phosphate
F7		7	
F8		8	
F9	Dextran (6 kDa)	6	
F10		7	
F11		8	
F12	Hydroxy-ectoine	6	
F13		7	
F14		8	

Each formulation was filled into 2 mL clear glass vials at a volume of 250  $\mu$ L. For the studies in Table 3-1, solution controls were stored at 5  $^{\circ}$ C during lyophilization of the solid-state samples. The lyophilization cycle consisted of freezing at -45  $^{\circ}$ C with a 2 h hold; primary drying at -50  $^{\circ}$ C and 70 mTorr for 24 h; a 0.2  $^{\circ}$ C/min ramp to 25  $^{\circ}$ C; and secondary drying at 25  $^{\circ}$ C and 70 mTorr for 6 hours. The lyophilization cycle for the moisture content and Tg investigation was modified to accommodate the lower Tg of glycerol-containing samples; freezing was carried out at -50  $^{\circ}$ C and the vacuum setpoint for both drying steps was 40 mTorr. The lyophilized samples were stoppered under vacuum.

Table 3-2. Composition of EVQL peptide formulations for moisture content and mobility investigation.

Excipient	Glycerol Content <sup>1</sup>	Storage RH
Trehalose	0	0% <sup>2</sup>
		6%
		11%
Dextran	0	0% <sup>2</sup>
		6%
		11%
Trehalose	2.5	0% <sup>2</sup>
	5	

<sup>1</sup>Reported as percent (w/w) of trehalose content (i.e., 5% indicates 5% of 5.65%)

<sup>2</sup>Samples stored under desiccant

### 3.3.3 Accelerated Stability Studies

Stability studies were carried out at 50 °C to investigate pGlu formation in lyophilized solids and solution controls. To vary moisture content, samples were stored uncapped in desiccators containing desiccant or saturated salt solutions of LiBr or LiCl to control RH at 6% and 11%, respectively (Table 3-2). Sealed desiccators were placed at 50 °C for the study duration. Samples used to investigate the effect of excipient and ‘pH’ were stored stoppered and crimped without RH control (Table 3-1). At designated time intervals, triplicate samples of each solid and solution formulation were removed from 50°C for analysis. Solid samples were reconstituted using 250 µL of deionized water. Solution and reconstituted lyophilized solid samples were analyzed in triplicate by reversed phase HPLC (rp-HPLC) and select samples were analyzed by LC/MS to confirm pGlu-VQL product identity, as described previously.<sup>20</sup> The pH values of all solutions and reconstituted lyophilized solids were measured with a pH-meter (Fisherbrand Accumet model AB15) equipped with a Mettler Toledo InLab Micro pH probe to verify that the pH did not shift during the study. The moisture content of all samples was measured at each timepoint by Karl Fischer (KF) titration.

### 3.3.4 Kinetic Analysis

To further investigate excipient and ‘pH’ effects, the observed rate constant ( $k_{obs}$ ) for the formation of pGlu was determined for each formulation (Table 3-1) from linear regression of the

mole fraction of pGlu peptide formed versus time according to a first-order kinetic model using GraphPad Prism (GraphPad Software Inc., San Diego, CA):

$$\ln(1 - X_{pGlu}) = k_{obs}t \quad 3.1$$

where  $X_{pGlu}$  is the mole fraction of pGlu-VQL peptide in each sample at time  $t$ . Previous studies have shown that the reaction of Glu to pGlu follows first order kinetics in solution.<sup>1,11</sup> Buffer catalysis was not observed in previous reports in the range of buffer concentration used here.<sup>20</sup>

### 3.3.5 Solid-State HDX-MS

In ssHDX-MS studies, deuterium labelling was carried out by placing uncapped vials of lyophilized EVQL peptide into a sealed desiccator containing a saturated solution of LiCl, which at equilibrium produces 11% RH in the headspace, and storing at 25 °C.<sup>27</sup> The vials were removed at designated time intervals (3h, 6h, 12h, 24h, 48h, 5 days and 10 days), capped, quenched by flash freezing in liquid N<sub>2</sub> and stored at -80 °C. Deuterium uptake of the quenched samples was measured by LC-MS (Agilent 6230 TOF; ZORBAX 300SB-C18 column, 1.0 × 50 mm, particle size 3.5 μm; Agilent Technologies, Santa Clara, CA) equipped with a custom refrigeration unit capable of maintaining low temperatures to minimize deuterium back exchange. Prior to injection, quenched samples were reconstituted with 250 μL of ice-cold quench buffer (0.2% formic acid and 5% methanol in water, pH 2.5) and diluted. Injected samples were held on a peptide micro trap (Michrom Biosources, Inc., Auburn, CA) and desalted for 1.8 min with 0.1% formic acid in water at a flow rate of 0.2 mL/min (isocratic) before elution onto the LC column. Elution was by gradient flow over 7 minutes using 0.1% formic acid in MS-grade water and 0.1% formic acid in MS-grade acetonitrile. Mass spectra were obtained over a 100-1700  $m/z$  range.

An undeuterated control was used to obtain the peptide mass list using the MassHunter Workstation software (Agilent Technologies). The peptide mass list was used as a reference to calculate the percent deuterium uptake in deuterium labeled samples using HDExaminer (Version 2.0 Sierra Analytics, Modesto, CA). The percent deuterium uptake data were fit to a biexponential equation (Eq. 3.2), and the kinetic parameters calculated using GraphPad Prism (GraphPad Software, Inc., San Diego, CA):

$$D(t) = D_{fast}(1 - e^{-k_{fast}t}) + D_{slow}(1 - e^{-k_{slow}t}) \quad 3.2$$

where  $D(t)$  is the deuterium uptake at labelling time  $t$ ,  $D_{fast}$  is the percent of exchanging amides in the rapidly exchanging pool,  $D_{slow}$  is the percent of exchanging amides in the slowly exchanging pool, and  $k_{fast}$  and  $k_{slow}$  are the apparent first-order rate constants of the two groups.

### 3.3.6 Moisture Content of Lyophilized Solids

An 831 KF Coulometer (Metrohm, Riverview, FL) was used to measure the moisture content of the lyophilized samples in each formulation after reconstitution in anhydrous methanol. The moisture content (in ppm) of the anhydrous methanol and the reconstituted samples was recorded and sample moisture content reported as a weight percentage (%w/w).

### 3.3.7 Modulated Differential Scanning Calorimetry (DSC)

Thermal analysis of lyophilized samples was performed using a differential scanning calorimeter (DSC 25, TA Instruments, New Castle, DE). The resulting data were analyzed using Trios software (Version 4.2.1, TA Instruments). Lyophilized powder from 3 vials was pooled for each measurement. Approximately 5 mg of sample was hermetically sealed in a Tzero pan using a Tzero hermetic lid. Samples were cooled to -5 °C, held for 5 min, and then heated from -5 °C to 150 °C at a ramp rate of 2 °C/min under nitrogen gas flow. A sinusoidal temperature modulation of ±0.5 °C every 60 s was applied. An empty, crimped aluminum pan was used as a reference. Only samples used to investigate moisture and mobility effects were analyzed by DSC due to material limitations.

## 3.4 Results

### 3.4.1 Excipient and 'pH' Effects

The effects of 'pH' and excipient type on the formation of pGlu-VQL were investigated under accelerated conditions at 50 °C. Several different side products were formed at low concentrations as indicated by chromatographic peaks distinct from those of EVQL and pGlu-VQL. To maintain focus on the pGlu reaction, the areas of these peaks were summed and a single

value reported as the side product. Significant levels of side product were only detected in solution samples. Figure 3-2 shows the peptide concentration versus time for representative formulations containing trehalose, dextran, and hydroxyectoine; similar curves for all formulations studied are presented in SI (Figure B-1, Figure B-2). pGlu-VQL concentrations increased throughout the study in all formulations and corresponded to a decrease in the parent EVQL peptide (Figure 3-2, Figure B-1, Figure B-2). Notable differences in pGlu concentration were found among solid samples and were least in hydroxyectoine samples. In solution, pGlu concentrations were similar across all excipient types throughout the study.

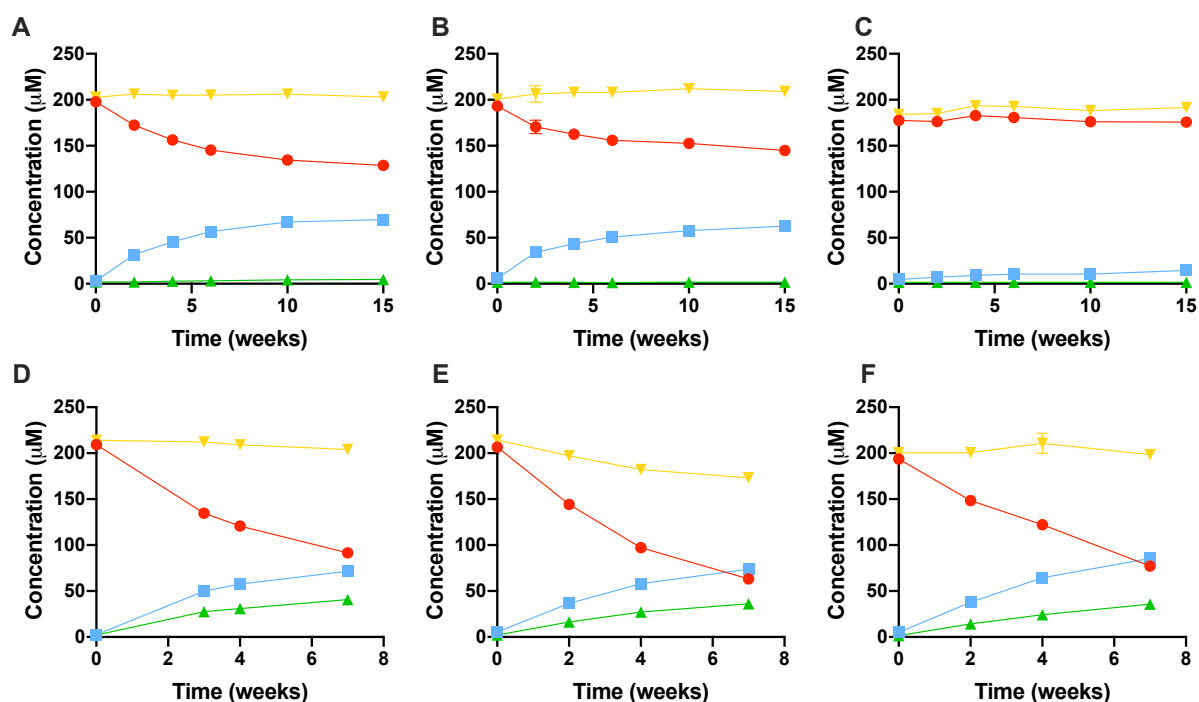


Figure 3-2. Kinetics of degradation of the EVQL peptide and formation of pGlu-VQL in lyophilized solids (A-C) and solution controls (D-F) formulated at ‘pH’ 7 with trehalose (A,D), dextran (B,E), and hydroxyectoine (C,F). Concentrations of EVQL peptide (circles), pGlu-VQL peptide (squares), summed side products (triangles), and total peptide concentration (inverted triangles) after incubation at 50 °C, n=9 (3 replicate measurements of 3 vials), mean ± S.D.

Apparent first-order rate constants for pGlu formation were calculated for each formulation using linear regression (Equation 3.1); see Table B-1 for tabulated rate constants. The dependence of the rate constants on ‘pH’ in lyophilized solids and solution controls is summarized in the ‘pH’-rate profiles (Figure 3-3A,B).

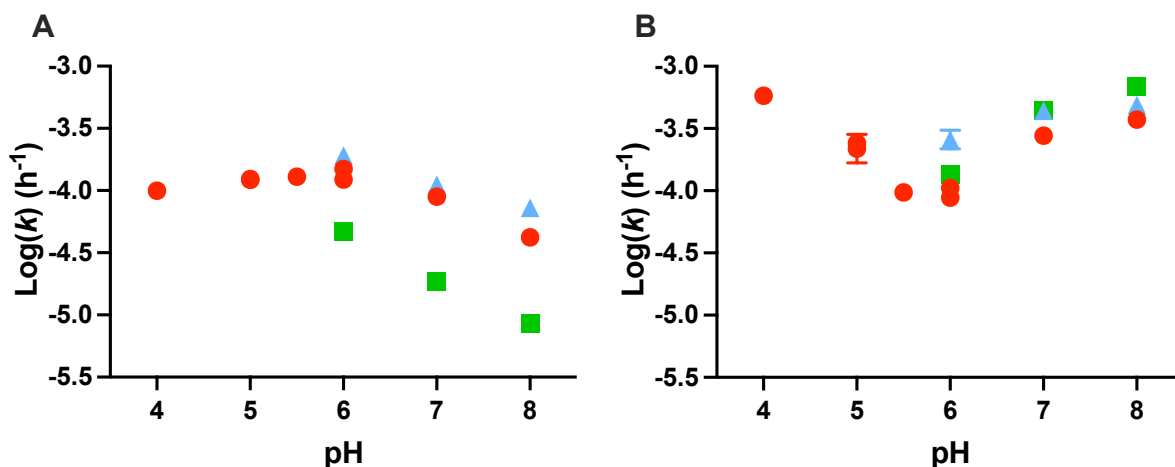


Figure 3-3. ‘pH’-rate profiles for pGlu formation in lyophilized solids (A) and solution controls (B) containing trehalose (circles), dextran (triangles), and hydroxyectoine (squares) at 50 °C. Error bars represent standard error of the first-order kinetic model regression fit (Equation 3.1).

In solid samples containing trehalose (F1-F8), differences in rates were small across the ‘pH’ range with the exception of ‘pH’ 8, where very little pGlu-VQL was formed (Figure 3-3A). From ‘pH’ 5-6 there was a slight maximum in pGlu formation rates. Solid samples containing dextran (F9-11) and hydroxyectoine (F12-F14) showed a similar trend with pGlu formation rates decreasing from ‘pH’ 6 to ‘pH’ 8.

In solution samples containing trehalose (F1-F8), the concentration of pGlu-VQL showed a clear dependence on pH (Figure 3-2D-F, Figure 3-3B, Figure B-2). The U-shaped curve suggests a degree of catalysis in both the acidic and basic regions, as reported previously.<sup>1,11,20</sup> Rate constants were greatest at pH 4 and 8, with the pH of maximum stability at pH 5.5-6. In samples containing dextran (F9-11) and hydroxyectoine (F12-14) the degradation rate also increased from pH 6 to 8. Notably, the rate of pGlu formation was greater at ‘pH’ 5.5-6 in solution samples containing trehalose (F4-6) or dextran (F9) (Figure 3-3B). Similar trends have previously been reported in a sucrose matrix.

Distinct excipient dependences of pGlu-VQL concentration and corresponding rate constants were observed in solid samples (Figure 3-2A-C, Figure 3-3A). Rate constants were lowest in hydroxyectoine samples (F12-F14), where pGlu-VQL levels were minimal. In fact, at ‘pH’ 7 and 8 (F13, F14), pGlu-VQL levels were below the working range of the calibration curve throughout the study. pGlu formation was similar in lyophilized trehalose and dextran formulations (F6-8 and F9-11, respectively), with slightly higher rates in dextran-containing formulations. In

lyophilized samples, all formulations showed a similar dependence of pGlu formation rate on ‘pH’, regardless of excipient type.

Excipient effects were not observed in solution samples (Figure 3-2D-F, Figure 3-3B). At each pH, rate constants were similar among all excipients, with the exception of dextran-containing samples at pH 6 (F9). In this formulation precipitation was observed at later timepoints, which may have influenced the pGlu-VQL concentrations and corresponding rate constant as evidenced by a decrease in total peptide concentration during the study (Figure B-2)

### **3.4.2 ssHDX-MS Analysis of Excipient and ‘pH’ Effects**

ssHDX-MS data were acquired for up to 240 h of deuterium exposure for the 14 lyophilized formulations with varied excipient and ‘pH’ (Table 3-1). Exchange was carried out at constant temperature and RH (25 °C, 11% RH). Formulations containing dextran showed the greatest deuterium incorporation (Figure 3-4B,D). Trehalose formulations showed greater deuterium uptake than hydroxyectoine formulations with the exception of trehalose at ‘pH’ 8 (F8) (Figure 3-4A,C,D). Overall, hydroxyectoine provided the greatest protection from exchange followed by trehalose and then dextran. For all excipients, formulations at ‘pH’ 8 showed the least deuterium incorporation after 10 d, though the difference between ‘pH’ 8 and ‘pH’ 6 and 7 was not significant for dextran formulations (p-value 0.245 and 0.054, respectively). Deuterium incorporation was similar for all ‘pH’ values with the exception of ‘pH’ 8. Overall, formulations containing trehalose and hydroxyectoine at ‘pH’ 8 (F8 and F14, respectively) had the lowest deuterium incorporation at 10 d and the greatest protection from exchange.

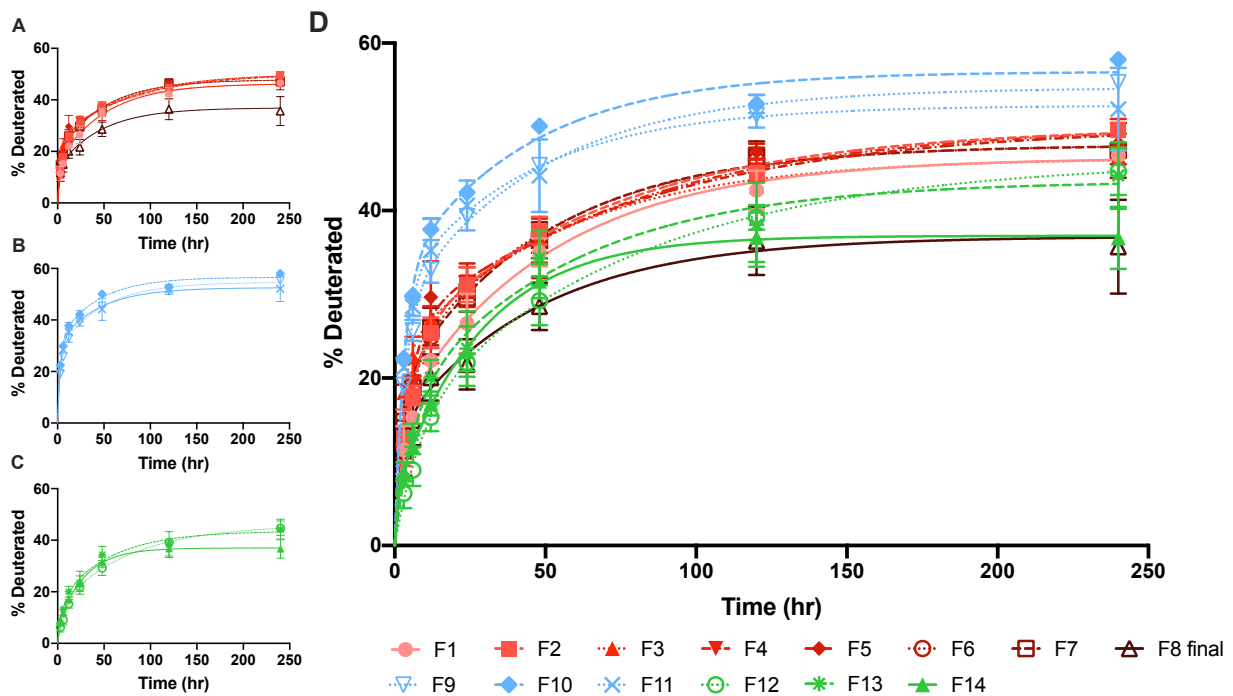


Figure 3-4. Deuterium incorporation in ssHDX-MS studies (11% RH, 25 °C) of EVQL peptide formulations containing: (A) trehalose, (B) dextran, (C) hydroxyectoine, and (D) all formulations; see Table 3-1 for formulation compositions. Lines represent fits to a biexponential model (Equation 3.2).  $n = 3$ , mean  $\pm$  SD; error bars not shown when less than the height of the symbol.

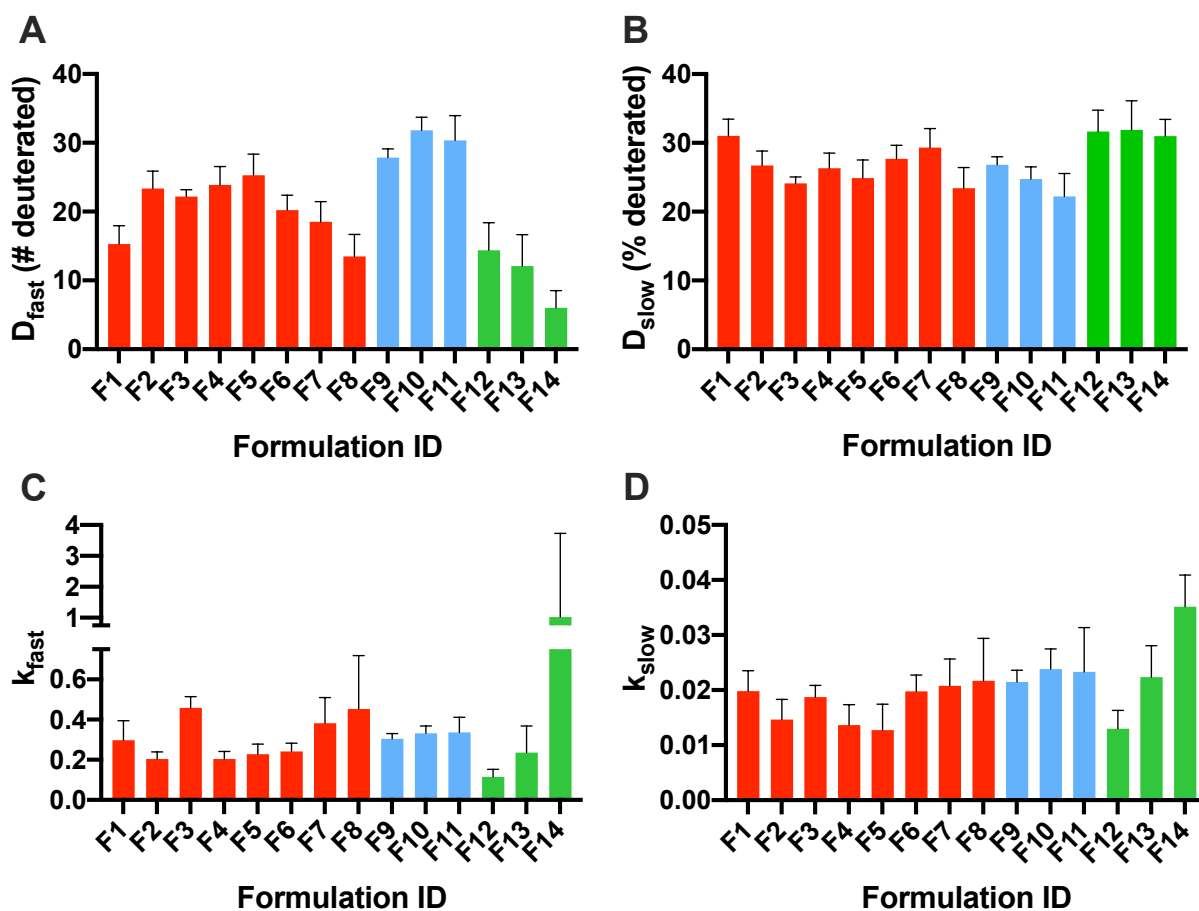


Figure 3-5. ssHDX-MS kinetic parameters,  $D_{fast}$  (A),  $D_{slow}$  (B),  $k_{fast}$  (C), and  $k_{slow}$  (D), fit to the biexponential model in Eq. 3.2 for EVQL peptide formulations containing trehalose (red), dextran (blue), and hydroxyectoine (green). HDX was performed at 11% RH and 25 °C. See Table 3-1 for formulation compositions. Error bars represent standard error of regression.

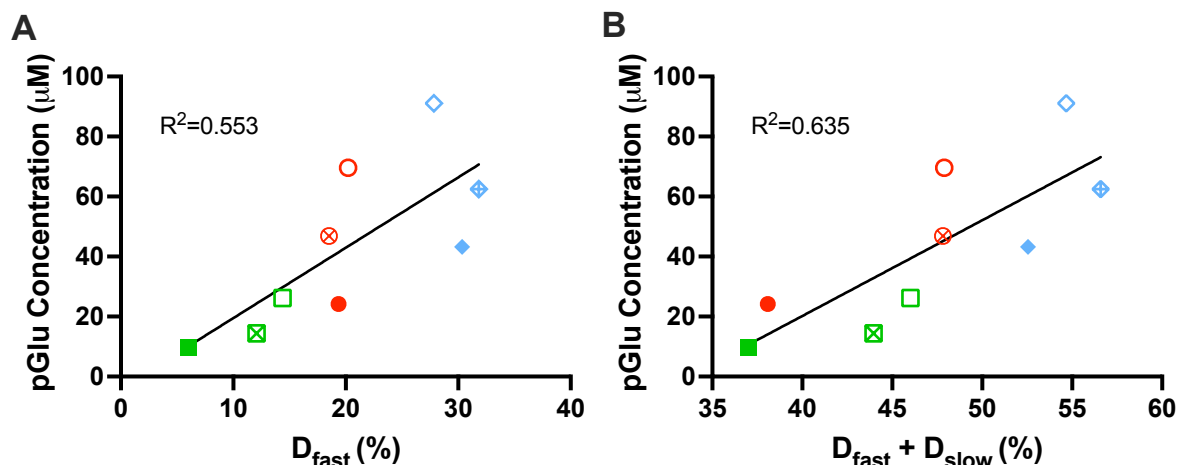


Figure 3-6. pGlu-VQL peptide concentration formed in lyophilized solids containing the EVQL peptide stored at 50 °C for 15 weeks as a function of (A)  $D_{fast}$  and (B) total deuterium incorporation,  $D_{fast} + D_{slow}$  (Equation 3.2) measured by ssHDX-MS. Samples were formulated with trehalose (circles), dextran (diamonds), and hydroxyectoine (squares) at ‘pH’ 6 (open markers), 7 (cross-haired markers) and 8 (solid markers). The solid lines indicate linear regression.

Deuterium incorporation kinetics were fit to a biexponential model (Equation 3.2) and regression parameters determined. Among the formulations, differences in  $D_{fast}$  were greater than differences for all other parameters (Figure 3-5). Overall,  $D_{fast}$  was greatest in dextran-containing formulations (F9-11), followed by trehalose (F1-8) and then hydroxyectoine (F12-14) (Figure 3-5A). For both trehalose and hydroxyectoine-containing samples,  $D_{fast}$  decreased from ‘pH’ 6 to 8. Across all formulations,  $D_{fast}$  was least for hydroxyectoine at ‘pH’ 8 (F14). The extent of pGlu formation showed good agreement with  $D_{fast}$  and total deuterium incorporation,  $D_{fast} + D_{slow}$  (Figure 3-6) (i.e., formulations with low pGlu formation also had low  $D_{fast}$ ,  $D_{fast} + D_{slow}$ ). This indicates that ssHDX-MS may be useful as a broad screening tool for solid formulations containing pGlu-prone molecules.

For all formulations, there were no notable differences in  $D_{slow}$ , suggesting that the maximum number of deuterated amides in the slowly exchanging pool is not affected appreciably by excipient type or ‘pH’ (Figure 3-5B). On average, there were no notable differences in the rate constants ( $k_{slow}$  and  $k_{fast}$ ) across excipients (Figure 3-5C-D). However, both  $k_{fast}$  and  $k_{slow}$  increased with ‘pH’ for hydroxyectoine formulations. Overall, hydroxyectoine samples at ‘pH’ 8 (F14) had the greatest exchange rate constants ( $k_{fast}$ ,  $k_{slow}$ ) for both the fast and slow exchanging groups, although the differences among  $k_{fast}$  values for formulations F12-F14 are not significant.

Increasing 'pH' in samples containing hydroxyectoine was associated with an increase in exchange rate, but a decrease in the extent of exchange ( $D_{fast}$ ).

### 3.4.3 Moisture Content and Tg Effects

The effects of moisture content and Tg on pGlu formation were investigated under accelerated conditions at 50 °C. Peptide concentrations were measured and analyzed as described above; pGlu-VQL concentrations are shown in Figure 3-7 and complete concentration profiles containing EVQL and side product concentrations are presented in SI (Figure B-3). At all timepoints, pGlu-VQL concentrations increased with increasing storage RH regardless of excipient (Figure 3-7A). As expected, dextran-containing samples had higher pGlu-VQL levels than those containing trehalose, overall, and the addition of glycerol did not have an appreciable effect on pGlu-VQL concentrations (Figure 3-7B). At early timepoints there was a slight decrease in pGlu-VQL concentration with increasing glycerol concentration. However, at 8 weeks the difference in pGlu-VQL concentration for 2.5% glycerol and 5% glycerol samples was not significant (paired t-test;  $p = 0.885$ ).

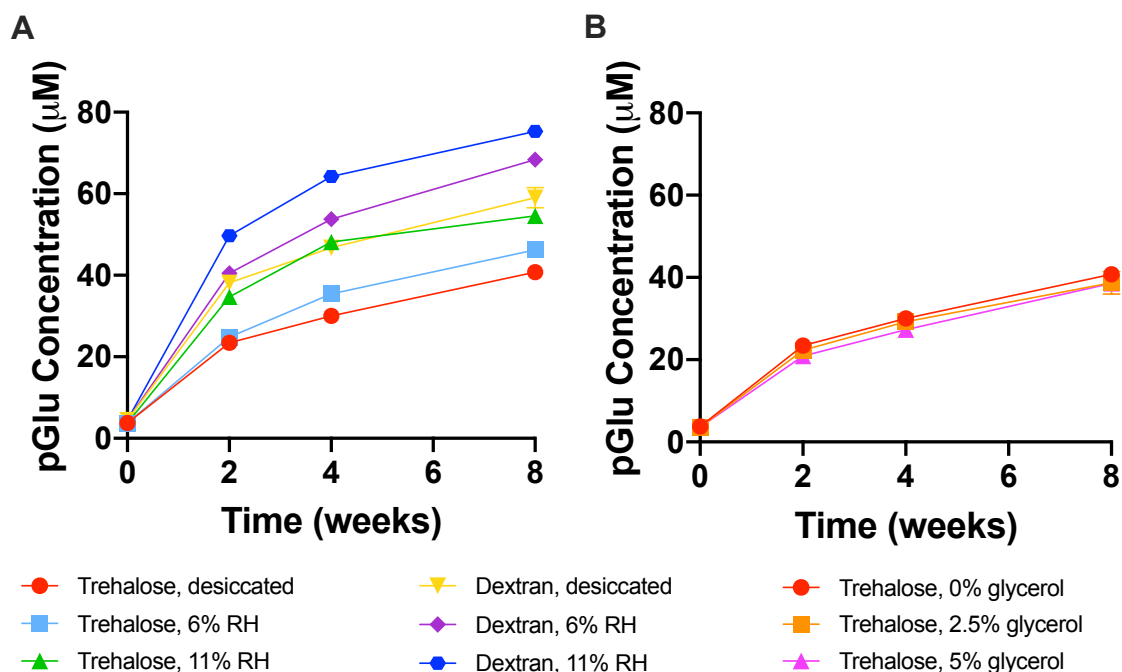


Figure 3-7. pGlu-VQL peptide concentration formed in lyophilized solids initially containing the EVQL peptide at 50 °C and: (A) formulated with trehalose or dextran and stored under desiccated conditions, at 6% RH or 11% RH, and (B) formulated with trehalose without glycerol, with 2.5% glycerol or with 5% glycerol. n=9 (3 replicate measurements of 3 vials), mean  $\pm$  S.D.

Moisture content was measured by KF at each timepoint and was consistent throughout the study, ranging from  $\sim$ 2% w/w (desiccated conditions) to  $\sim$ 6% w/w (11% RH storage) (Table B-2). An increase in moisture content was linearly related to an increase in pGlu-VQL concentration for both dextran and trehalose formulations ( $R^2=0.914$  and  $0.970$ , respectively) (Figure 3-8A). The slopes of the best fit lines in Figure 3-8A are not significantly different from one another (p-value 0.305), suggesting that the rate of increase in the extent of exchange with increasing moisture content is independent of excipient molecular weight and structure.

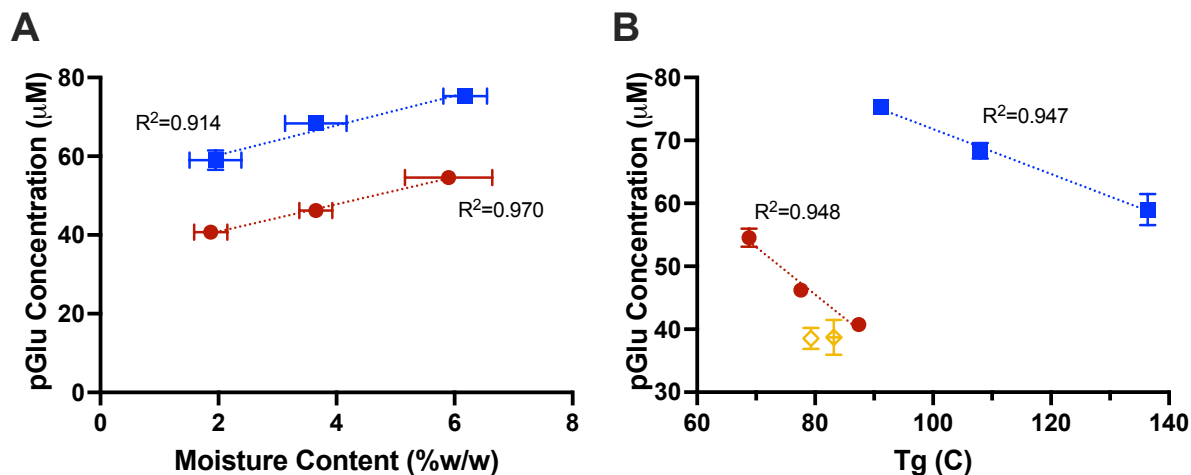


Figure 3-8. pGlu-VQL peptide concentration in lyophilized solids containing the EVQL peptide after 8-weeks storage at 50 °C as a function of moisture content (A) and Tg (B). Samples were formulated with trehalose (circles) or dextran (squares). Varied moisture content and Tg were generated by storing samples under desiccated conditions, at 6% RH and 11% RH and by formulation with trehalose with glycerol added at 2.5% (cross-haired diamond) and 5% glycerol (open diamond) (w/w) of excipient content. pGlu concentration, n=9 (3 replicate measurements of 3 vials), mean  $\pm$  S.D; moisture content, n=3, mean  $\pm$  S.D.; Tg n=1.

Tg was measured by DSC to assess the effect of mobility on pGlu formation. In this study, Tg was manipulated by varying storage RH and by the addition of glycerol. When Tg was manipulated by storage RH (i.e., varied moisture content), pGlu concentration was inversely proportional to Tg for both dextran and trehalose formulations ( $R^2=0.914$  and  $0.948$ , respectively) (Figure 3-8B). However, when Tg was reduced by the addition of glycerol in trehalose-containing samples (Figure 3-8B), pGlu concentration did not increase. The dependence of moisture content and Tg on pGlu concentration was explored by analysis of variance (ANOVA). An effect test revealed that moisture content (p-value = 0.0008) contributed more to the variation in pGlu concentration than Tg (p-value = 0.2467) (Table B-3).

### 3.5 Discussion

The effects of excipient, 'pH', moisture content, and mobility on pGlu formation were investigated in a lyophilized model peptide, EVQL. 'pH'-rate profiles confirmed that the 'pH' dependence in the solid state differs from that of solution controls (Figure 3-3) as we reported previously.<sup>20</sup> In solution, pGlu formation was accelerated by acidic and basic conditions, while in

solids pGlu formation was generally ‘pH’ independent in the acidic to neutral region, with pGlu formation rate decreasing with increasing ‘pH’ in the basic region. The ‘pH’ dependence in the solid state was similar for all excipients tested, although a somewhat greater ‘pH’ sensitivity was observed in solid hydroxyectoine samples as indicated by the slope of the ‘pH’-rate profile from ‘pH’ 6 to 8 (Figure 3-3).

pGlu formation also depended on excipient type. Overall, hydroxyectoine (MW 158) showed the least pGlu formation in lyophilized solids followed by trehalose (MW 342) and then dextran (MW 6,000) (Figure 3-3A). In solution controls, pGlu formation rates were similar for all three excipients (Figure 3-3B). The lower molecular weight of hydroxyectoine may contribute to its effectiveness, better enabling it to form hydrogen bonds with the EVQL peptide than the other excipients tested, perhaps due to a lack of steric hinderance.<sup>28,29</sup> Molecular size, however, does not explain the similar performances of trehalose and dextran, which is nearly 20 times larger than trehalose. Unlike trehalose and dextran, hydroxyectoine is ionizable and zwitterionic in the pH range used here, which may contribute to its superior ability to protect against pGlu formation. Protection through ionization interactions, rather than hydrogen bonding interactions, by hydroxyectoine may also explain why these formulations only showed a modest difference in deuterium incorporation by ssHDX, compared to trehalose and dextran, but a larger difference in pGlu formation.

Increasing moisture content was associated with increased pGlu formation for both trehalose and dextran formulations (Figure 3-8A). Water can affect chemical degradation in lyophilized solids in several ways: i) directly as a reactant or product, ii) indirectly as a medium (solvent) by changing the reaction environment, and iii) as a plasticizer to increase reactant mobility.<sup>30-32</sup> pGlu formation is not hydrolytic and water is a product of the reaction. Increasing moisture content then might be expected to decrease pGlu formation according to Le Chatlier’s principle. That this was not observed suggests that direct participation of water as a reaction product does not dominate the kinetics of pGlu formation in solid samples.

Water may increase reactivity through solvent effects by decreasing the Gibbs free energy of activation for reactions under kinetic control. For pGlu formation, this may occur through facilitating proton transfer or by changing the polarity of the reaction environment.<sup>31</sup> The mechanism of pGlu formation from Glu has been explored using density functional theory. The simulations showed that at least two water molecules are necessary to overcome steric hindrance

and assist in proton transfer, but that the activation energy barrier is not further reduced when more than two water molecules are present.<sup>17</sup> Here, in the formulations with the lowest moisture content (~2%), the bulk material has ~100 water molecules per peptide molecule based on the overall composition. The hydrophilicity of the EVQL N-terminus suggests that local water concentration is at least as high as in the bulk near the reacting Glu residue. Thus, the increase in pGlu formation with water content probably is not a result of solvent facilitated proton transfer. Alternatively, solvent polarity may be important. The protonation states of N-terminal Glu and the tetrahedral intermediate integral to pGlu formation (Figure 3-1) may be affected by a change in local polarity due to water content and may reduce the Gibbs free energy of activation.<sup>2</sup> Thus, it is possible that water acts as a solvent and affects pGlu formation kinetics through changes in polarity.

Water may also increase reactivity by acting as a plasticizer, increasing the free volume and decreasing viscosity.<sup>31</sup> The linear relationship between pGlu concentration and Tg (Figure 3-8B) when Tg was manipulated by moisture content suggests that plasticization may be important. However, this interpretation is confounded by the inherent coupling of Tg and moisture content (Figure 3-8A,B). Plasticizing the trehalose formulations with glycerol allowed a degree of decoupling of these effects. If the reaction rate is strongly coupled to Tg, pGlu concentrations for the glycerol-plasticized formulations (Figure 3-8B, diamonds) would be expected to fall on the line of best fit for moisture-plasticized formulations (Figure 3-8B, circles). Instead, in formulations plasticized by glycerol, pGlu concentration was less than predicted by this best fit line, suggesting that Tg alone does not determine reactivity (Figure 3-8B). Given that pGlu formation occurs intramolecularly, limited coupling to Tg might be expected.<sup>31</sup> Thus, it is reasonable to conclude that water influences reactivity as a reaction medium under the conditions studied here. However, the apparent lack of coupling to Tg (i.e.,  $\alpha$ -relaxation) does not rule out mobility effects associated with  $\beta$ -relaxation since Tg does not measure  $\beta$ -relaxation.<sup>33-35</sup>

Peptide formulations containing trehalose, dextran (6 kDa) and hydroxyectoine at various 'pH' values were subjected to ssHDX-MS to test the relationship between the kinetics of deuterium exchange and the kinetics of pGlu formation. ssHDX-MS interrogates the hydrogen bond network in the solid matrix by introducing a deuterium donor that competes for hydrogen bonding sites. Thus, it is reasonable to hypothesize that rates of ssHDX-MS may correlate with rates of chemical reactions that depend on proton transfer, such as pGlu formation. Analysis of ssHDX kinetics provided the regression parameters  $D_{fast}$ ,  $D_{slow}$ ,  $k_{fast}$  and  $k_{slow}$  (Eq. 3.2). Of the four parameters  $D_{fast}$ ,

and total deuterium incorporation,  $D_{\text{fast}}+D_{\text{slow}}$  showed the closest relationship to the extent of pGlu formation (Figure 3-6). The trend is most notable when comparing excipient effects; overall, deuterium incorporation and pGlu formation are greatest for dextran formulations (Figure 3-6, diamonds) and least for hydroxyectoine formulations (Figure 3-6, squares).

This suggests that greater deuterium incorporation ( $D_{\text{fast}}$ ,  $D_{\text{fast}}+D_{\text{slow}}$ ) is associated with more facile proton transfer and greater susceptibility to pGlu formation. pGlu formation relies on both the availability of the amide nitrogen for nucleophilic attack and flexibility of the peptide backbone for cyclization.<sup>2,17</sup> While exchange of the N-terminal amide hydrogen involved in pGlu formation is not captured by ssHDX kinetics,  $D_{\text{fast}}$  and  $D_{\text{fast}}+D_{\text{slow}}$  serve as indicators of overall amide accessibility. A greater proportion of unprotected amide hydrogens ( $D_{\text{fast}}$ ,  $D_{\text{fast}}+D_{\text{slow}}$ ) may suggest the N-terminal amide nitrogen is less likely to be involved in hydrogen bonds with the matrix and available for nucleophilic attack. Alternatively, greater  $D_{\text{fast}}$  or  $D_{\text{fast}}+D_{\text{slow}}$  values may indicate a peptide backbone that is highly hydrogen bonded to the amorphous matrix and therefore may be flexible enough for cyclization to occur.

### 3.6 Conclusions

The effects of excipient, 'pH', moisture content and Tg on pGlu formation in a model peptide (EVQLVESGGGLVQPGGSLR) were investigated in lyophilized solids and in solution. The apparent 'pH' dependence of the reaction rate in the solid state differed from that of the solution state; solution formulations showed maximum stability near pH 5.5 to 6 while solid formulations showed the lowest pGlu formation rate in the basic region. In the solid state, formulations containing hydroxyectoine showed less pGlu formation than those containing trehalose or dextran. pGlu formation increased with increasing moisture content and with decreasing Tg when formulations were plasticized by water. However, when formulations were plasticized by glycerol, pGlu formation was independent of Tg. In ssHDX-MS studies, a moderate correlation between the extent of deuterium incorporation and the extent of pGlu formation was observed, suggesting that the technique may serve as a broad screening tool for pGlu-prone formulations.

### 3.7 References

1. Yu, L. et al. Investigation of N-terminal glutamate cyclization of recombinant monoclonal antibody in formulation development. *Journal of Pharmaceutical and Biomedical Analysis* 42, 455–463 (2006).
2. Seifert, F. et al. Glutaminyl Cyclases Display Significant Catalytic Proficiency for Glutamyl Substrates. *Biochemistry* 48, 11831–11833 (2009).
3. Seifert, F. et al. Phosphate ions and glutaminyl cyclases catalyze the cyclization of glutaminyl residues by facilitating synchronized proton transfers. *Bioorganic Chemistry* 60, 98–101 (2015).
4. Schilling, S., Hoffmann, T., Manhart, S., Hoffmann, M. & Demuth, H.-U. Glutaminyl cyclases unfold glutamyl cyclase activity under mild acid conditions. *FEBS Letters* 563, 191–196 (2004).
5. Huang, K.-F., Liu, Y.-L., Cheng, W.-J., Ko, T.-P. & Wang, A. H.-J. Crystal structures of human glutaminyl cyclase, an enzyme responsible for protein N-terminal pyroglutamate formation. *Proceedings of the National Academy of Sciences* 102, 13117–13122 (2005).
6. Xu, Y. et al. Structure, heterogeneity and developability assessment of therapeutic antibodies. *mAbs* 11, 239–264 (2019).
7. Twardzik, D. R. & Peterkofsky, A. Glutamic Acid as a Precursor to N-Terminal Pyroglutamic Acid in Mouse Plasmacytoma Protein. *Proceedings of the National Academy of Sciences* 69, 274–277 (1972).
8. Park, C. B., Lee, S. B. & Ryu, D. D. Y. L-Pyroglutamate spontaneously formed from L-glutamate inhibits growth of the hyperthermophilic archaeon *Sulfolobus solfataricus*. *Applied and Environmental Microbiology* 67, 3650–3654 (2001).
9. Liu, H., Gaza-Bulseco, G. & Sun, J. Characterization of the stability of a fully human monoclonal IgG after prolonged incubation at elevated temperature. *Journal of Chromatography B* 837, 35–43 (2006).
10. Ionescu, R. & Vlasak, J. Kinetics of Chemical Degradation in Monoclonal Antibodies: Relationship between Rates at the Molecular and Peptide Levels. *Analytical Chemistry* 82, 3198–3206 (2010).
11. Chelius, D. et al. Formation of Pyroglutamic Acid from N-Terminal Glutamic Acid in Immunoglobulin Gamma Antibodies. *Analytical Chemistry* 78, 2370–2376 (2006).
12. Liu, Y. D., Goetze, A. M., Bass, R. B. & Flynn, G. C. N-terminal Glutamate to Pyroglutamate Conversion in Vivo for Human IgG2 Antibodies. *Journal of Biological Chemistry* 286, 11211–11217 (2011).

13. Lyubarskaya, Y., Houde, D., Woodard, J., Murphy, D. & Mhatre, R. Analysis of recombinant monoclonal antibody isoforms by electrospray ionization mass spectrometry as a strategy for streamlining characterization of recombinant monoclonal antibody charge heterogeneity. *Analytical Biochemistry* 348, 24–39 (2006).
14. Beck, A. et al. Stability and CTL activity of N-terminal glutamic acid containing peptides. *Journal of Peptide Research* 57, 528–538 (2001).
15. Beck, A. et al. Stability and CTL-activity of P40/ELA melanoma vaccine candidate. *Biologicals* 29, 293–298 (2001).
16. Alam, M. E. et al. Deamidation can compromise antibody colloidal stability and enhance aggregation in a pH-dependent manner. *Mol. Pharmaceutics* 16, 1939–1949 (2019).
17. Nakayoshi, T., Kato, K., Kurimoto, E. & Oda, A. Computational studies on nonenzymatic pyroglutamylation mechanism of N-terminal glutamic acid residues in aqueous conditions\*. *Molecular Physics* 118, e1702727 (2020).
18. Liu, Z. et al. Cyclization of N-Terminal Glutamic Acid to pyro-Glutamic Acid Impacts Monoclonal Antibody Charge Heterogeneity Despite Its Appearance as a Neutral Transformation. *Journal of Pharmaceutical Sciences* (2019) doi:10.1016/j.xphs.2019.05.023.
19. Shih, F. F. Analysis of glutamine, glutamic acid and pyroglutamic acid in protein hydrolysates by high-performance liquid chromatography. *Journal of Chromatography A* 322, 248–256 (1985).
20. Bersin, L. M., Patel, S. M. & Topp, E. M. Effect of ‘pH’ on the Rate of Pyroglutamate Formation in Solution and Lyophilized Solids. *Mol. Pharmaceutics* acs.molpharmaceut.1c00338 (2021) doi:10.1021/acs.molpharmaceut.1c00338.
21. Wilson, H. & Cannan, R. K. The glutamic acid-pyrrolidonecarboxylic acid system. *Journal of Biological Chemistry* 119, 309–331 (1937).
22. Nayak, P. K., Goode, M., Chang, D. P. & Rajagopal, K. Ectoine and Hydroxyectoine Stabilize Antibodies in Spray-Dried Formulations at Elevated Temperature and during a Freeze/Thaw Process. *Molecular Pharmaceutics* 17, 3291–3297 (2020).
23. Moorthy, B. S. et al. Solid-State Hydrogen–Deuterium Exchange Mass Spectrometry: Correlation of Deuterium Uptake and Long-Term Stability of Lyophilized Monoclonal Antibody Formulations. *Mol. Pharmaceutics* 15, 1–11 (2018).
24. Iyer, L. K., Sacha, G. A., Moorthy, B. S., Nail, S. L. & Topp, E. M. Process and Formulation Effects on Protein Structure in Lyophilized Solids Using Mass Spectrometric Methods. *Journal of Pharmaceutical Sciences* 105, 1684–1692 (2016).
25. Moussa, E. M. et al. Effects of Drying Process on an IgG1 Monoclonal Antibody Using Solid-State Hydrogen Deuterium Exchange with Mass Spectrometric Analysis (ssHDX-MS). *Pharmaceutical Research* 35, (2018).

26. Sophocleous, A. M. & Topp, E. M. Localized Hydration in Lyophilized Myoglobin by Hydrogen–Deuterium Exchange Mass Spectrometry. 2. Exchange Kinetics. *Molecular Pharmaceutics* 9, 727–733 (2012).
27. Greenspan, L. Humidity fixed points of binary saturated aqueous solutions. *J. Res. Natl. Bur. Stan. Sect. A.* 81A, 89 (1977).
28. Allison, S. D., Chang, B., Randolph, T. W. & Carpenter, J. F. Hydrogen bonding between sugar and protein is responsible for inhibition of dehydration-induced protein unfolding. *Archives of Biochemistry and Biophysics* 365, 289–298 (1999).
29. Tanaka, K., Takeda, T. & Miyajima, K. Cryoprotectant effect of saccharides on denaturation of catalase by freeze-drying. *Chem. Pharm. Bull.* 39, 1091–1094 (1991).
30. Lai, M. C. et al. Chemical stability of peptides in polymers. 2. Discriminating between solvent and plasticizing effects of water on peptide deamidation in poly(vinylpyrrolidone). *Journal of Pharmaceutical Sciences* 88, 1081–1089 (1999).
31. Shalaev, E. Y. & Zografi, G. How Does Residual Water Affect the Solid-state Degradation of Drugs in the Amorphous State? *Journal of Pharmaceutical Sciences* 85, 1137–1141 (1996).
32. Hageman, M. Water Sorption and Solid-State Stability of Proteins. in *Stability of Protein Pharmaceuticals: Part A, Chemical and Physical Pathways of Protein Degradation* 273–309 (Plenum, 1992).
33. Cicerone, M. T., Tellington, A., Trost, L. & Sokolov, A. Substantially improved stability of biological agents in dried form. *BioProcess International* 1–9 (2003).
34. Cicerone, M. T. & Soles, C. L. Fast Dynamics and Stabilization of Proteins: Binary Glasses of Trehalose and Glycerol. *Biophysical Journal* 86, 3836–3845 (2004).
35. Cicerone, M. T. & Douglas, J. F. Beta-relaxation governs protein stability in sugar-glass matrices. *Soft Matter* 8, 2983–2991 (2012).

## **CHAPTER 4. EFFECTS OF TEMPERATURE AND RELATIVE HUMIDITY ON SOLID-STATE HYDROGEN DEUTERIUM EXCHANGE (SSHDX-MS) OF A MONOCLONAL ANTIBODY**

### **4.1 Abstract**

Solid-state hydrogen-deuterium exchange mass spectrometry (ssHDX-MS) has been used to assess protein structure, stability, and matrix interactions in amorphous solids, but the mechanism of exchange in the solid state is not fully understood. This work addresses the effects of temperature, mobility, and RH on ssHDX-MS. An IgG monoclonal antibody (mAb) was lyophilized with varying levels of glycerol as a plasticizer and formulations were exposed to D<sub>2</sub>O vapor at different RH and temperature. Deuterium exchange was monitored over time and the rate and extent of deuterium incorporation were calculated using a biexponential model. Kinetic parameters were influenced by RH and temperature, but not glycerol content, and there was a clear correlation between kinetic parameters and molecular mobility as measured by (T-T<sub>g</sub>). A reversible first-order model for deuterium uptake in ssHDX is proposed that incorporates both RH and temperature. The model suggests a linear dependence of deuterium incorporation kinetic parameters on the product of RH and temperature, which provides a better correlation than T-T<sub>g</sub>.

### **4.2 Introduction**

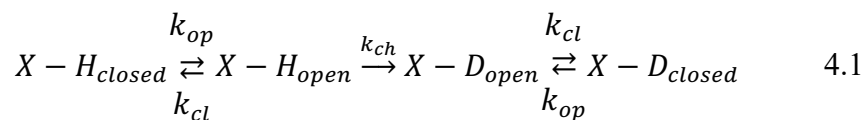
Therapeutic proteins that exhibit inadequate stability in solution are often lyophilized to produce solid powders, with the goal of improving their chemical and physical stability for distribution and storage. To assess drug product candidates, stability studies are carried out over months to years. Physicochemical analyses, including moisture content, glass transition temperature (T<sub>g</sub>), and protein secondary structure are commonly measured to supplement stability assessments. These measurements are valuable for understanding the solid-state properties but are often poorly correlated with storage stability. There is a need for a stability-indicating analytical method for proteins in the amorphous solid state that can reduce the burden of time-consuming and costly stability studies.

Over the past decade, our group has developed solid-state hydrogen-deuterium exchange with mass spectrometric analysis (ssHDX-MS) to provide high resolution information on protein

structure and matrix interactions in lyophilized solids.<sup>1-12</sup> In ssHDX-MS experiments, a lyophilized peptide or protein is exposed to D<sub>2</sub>O vapor in a sealed desiccator at controlled temperature and D<sub>2</sub>O activity (i.e., relative humidity (RH) in D<sub>2</sub>O). Over the time course of the experiment, samples are removed, and the reaction is quenched (pH 2.5, ~0 °C). The number of deuterons incorporated during exchange then can be determined by liquid chromatography-mass spectrometry (LC-MS), for both the intact protein and peptic digest, as the difference between the undeuterated mass and the mass at each time point.<sup>1-4</sup> The kinetics of deuterium incorporation can be fit to either a mono- or biexponential model.

The technique has been used to evaluate changes in protein conformation and matrix interactions due to processing methods, formulation, and moisture content.<sup>3-8</sup> Recently, exchange kinetics have been shown to be highly correlated with aggregation on extended stability for lyophilized myoglobin and a monoclonal antibody (mAb) and on accelerated stability of lyophilized and spray-dried proteins.<sup>5,6,13</sup> These results suggest that ssHDX-MS may be useful for ranking formulations or processing methods during product development. However, the mechanism of exchange in the solid state is still unclear. There is an unmet need to establish a molecular basis for interpreting the rate and extent of deuteration in ssHDX-MS, which could allow a better interpretation of ssHDX-MS data and an improved understanding of the amorphous solid state.

For HDX studies in solution, the results are often interpreted using the Linderstrom-Lang model in which exchange is attributed to reversible protein unfolding, described as “opening” and “closing” events, with rate constants  $k_{op}$  and  $k_{cl}$ , and irreversible chemical exchange of the available amide groups with rate constant  $k_{ch}$ .<sup>14,15</sup> The model (Eq. 4.1) assumes that exchange only occurs while the protein is in the open state, when the amide hydrogen bonds involved in secondary and tertiary structure have broken and the amides are available for exchange. It is well established that the rate of exchange in solution,  $k_{ch}$ , is dependent on intramolecular hydrogen bonds, solvent accessibility, temperature and pH.<sup>16-21</sup>



Several observations suggest that the Linderstrom-Lang does not adequately describe HDX in the solid state. First, unstructured peptides in lyophilized solids have shown protection from exchange during ssHDX that varies with excipient type;<sup>8</sup> according to the Linderstrom-Lang model, these unstructured peptides should not be protected at all, since protein-excipient interactions are not described by the Linderstrom-Lang model and protection would not be expected in solution state HDX. The rate and extent of exchange in ssHDX are also affected by D<sub>2</sub>O activity, while the Linderstrom-Lang model assumes a large and invariant D<sub>2</sub>O activity in the donor solution. A reversible first-order kinetic model has been proposed for ssHDX-MS that predicts a linear relationship between D<sub>2</sub>O activity and the forward exchange rate constant.<sup>4,8,22</sup> This model accurately describes ssHDX of unstructured PDLA peptides and challenges the Linderstrom-Lang assumption that exchange is irreversible.<sup>8</sup> The mechanism is attributed to rapid absorption of D<sub>2</sub>O into the solid until equilibrium with the vapor phase is reached, followed by initial exchange of amide protons that are not involved, or are weakly involved, in intra- or intermolecular hydrogen bonds. There are abundant sources of protons for the reverse reaction in ssHDX, including excipient and buffer species, residual H<sub>2</sub>O in the matrix, and the peptide or protein itself. Over the long ssHDX experimental time course (hours to days), deuterium labels can be removed from a deuterated amide group via the reverse reaction, and then shuttled through the matrix to more protected regions by a series of forward and reverse exchange steps.

In solution HDX, there is a clear effect of temperature on the rate of exchange,  $k_{ch}$ , which has been shown to decrease 14-fold from 25 to 0 °C.<sup>16,17</sup> A temperature dependence has also been observed in ssHDX of lyophilized myoglobin and was thought to reflect the temperature dependence of water vapor sorption and forward exchange processes.<sup>23</sup> However, the extent of this dependence and the underlying mechanisms are not fully understood. In some cases, reactivity in amorphous solids is coupled to T<sub>g</sub> and to molecular mobility, often defined as T-T<sub>g</sub>, where T is the experimental temperature.<sup>24-26</sup> The inherent coupling of temperature and T<sub>g</sub>, which is not a concern in the solution state, complicates the interpretation of any observed temperature dependence in the solid state.

The aim of this work is to evaluate the contributions of temperature, mobility, and RH to the kinetics of ssHDX-MS. Elucidating these effects will contribute to an improved mechanistic understanding of ssHDX-MS and will help to support experiment design and data interpretation. Here, an IgG mAb was lyophilized with trehalose and varying levels of glycerol added as a

plasticizer. Formulations were exposed to D<sub>2</sub>O at different RH and temperature conditions, and deuterium exchange was monitored over time. The kinetics of deuterium incorporation were fit to a biexponential model. Statistical analysis showed that the model parameters were influenced by RH and temperature, but not glycerol content. There was a clear correlation between kinetic parameters and the product of RH and temperature, and between these parameters and molecular mobility (T-T<sub>g</sub>). A reversible first-order model for deuterium uptake in ssHDX is proposed that incorporates both RH and temperature and provides an alternative mechanistic explanation for the observed dependence on (T -T<sub>g</sub>).

### **4.3 Experimental Section**

#### **4.3.1 Materials**

The IgG1 mAb was provided by AstraZeneca as a frozen buffered solution, 50 mg/mL mAb. Lithium bromide, potassium acetate, and potassium phosphate salts (monobasic, and dibasic) and Amicon Ultra-15 Centrifugal Filter Units (UFC9010, MWCO 10 kDa) were obtained from Sigma-Aldrich (St. Louis, MO). Trehalose, glycerol, lyophilization vials (Wheaton type I clear glass 2 mL serum vials), stoppers (Duran Wheaton Kimble, part W224100-093), and all liquid chromatography mass spectrometry (LC-MS) grade solvents (water, acetonitrile, formic acid, and methanol) were purchased from Fisher Scientific (Hanover Park, IL). Deuterium oxide (D<sub>2</sub>O, 99.9%) was purchased from Cambridge Isotope Laboratories (Andover, MA).

#### **4.3.2 Experimental Design**

Lyophilized mAb formulations with different T<sub>g</sub> values were stored at varying RH and temperature conditions and deuterium incorporation measured over time by ssHDX-MS. A 3 × 3 × 3 full factorial design was implemented to generate conditions with a wide range of mobility, as defined by T-T<sub>g</sub>. The experimental factors were glycerol content (0, 5, 10%), temperature (5, 25, 40 °C) and RH (6, 23, 43%). The resulting study design contains nine storage conditions (3 temperatures × 3 RH levels) and three formulations, for 27 total combinations.

### 4.3.3 Statistical Analysis

The results of the full factorial ssHDX-MS experiments were evaluated using the JMP® Pro 16.0 software. Means were compared using analysis of variance (ANOVA) for each of the ssHDX kinetic parameters. A statistically significant ANOVA p-value, determined by the F-statistic, indicates that the mean of at least one experimental factor, or “treatment”, is significantly different from the others, i.e., that at least one treatment significantly contributes to the variability in the output parameter (i.e., ssHDX kinetic parameter). p-values < 0.01 from ANOVA were considered statistically significant. Effect tests were then performed to determine which factors have significant effects on the output parameter using the F-statistic. p-values from the effect tests will be referred to as “treatment” p-values and were considered statistically significant when < 0.05. Experimental factors with treatment p-value > 0.05 were removed from the model. Treatment sum of squares (SST) values were calculated for statistically significant factors. SST describes the degree to which each treatment contributes to the variability in the output parameter. The full factorial design allowed estimation of model parameters, including individual factor coefficients and interaction parameter coefficients.

Individual relationships between experimental variables and ssHDX kinetic parameters were also evaluated using the simple linear regression function in the GraphPad Prism software. F-tests were used to compare regression parameters and to determine whether the slopes of the regression lines were significantly different from zero. In these analyses, a p-value < 0.05 was used to determine statistical significance. The mono- and biexponential kinetic models for ssHDX were compared with an F-test using the GraphPad Prism software.

### 4.3.4 Sample Preparation

The frozen mAb stock solution was thawed at room temperature, and the protein solution was then buffer exchanged into three formulations containing 2.5 mM potassium phosphate buffer, pH 7.5, 25 mg/mL trehalose, and either 0%, 5% or 10% (w/w) glycerol (reported as a percent of trehalose concentration). Buffer exchange was carried out using Amicon Ultra Centrifugal Filter Units containing regenerated cellulose membranes (MilliporeSigma, Burlington, MA). Samples were spun at 4k rpm for 30-60 min using an Allegra X-15R benchtop centrifuge (Beckman Coulter, Brea, CA). Fresh buffer was added to the supernatant and three rounds of exchange were

performed to ensure >99% buffer exchange. mAb concentration was measured by UV absorption at 280 nm and concentrations adjusted to a target of 25 mg/mL.

Each formulation was filled into clear glass vials at a volume of 250  $\mu$ L. The lyophilization cycle consisted of freezing at -50  $^{\circ}$ C with a 2 h hold; primary drying at -45  $^{\circ}$ C and 40 mTorr; a 0.2  $^{\circ}$ C/min ramp to 25  $^{\circ}$ C; and secondary drying at 25  $^{\circ}$ C and 40 mTorr for 6 hours. The end of primary drying was determined by the convergence of the capacitance manometer and Pirani gauge. The lyophilized samples were stoppered under vacuum.

#### 4.3.5 Solid-State Hydrogen-Deuterium Exchange Mass Spectrometry (ssHDX-MS)

ssHDX studies were carried out by placing uncapped vials containing lyophilized mAb formulations into sealed desiccators at controlled RH and temperature. The three RH levels (6, 23, 43%) were controlled using saturated salt solutions (LiBr,  $\text{KCH}_3\text{CO}_2$ , and  $\text{K}_2\text{CO}_3$ , respectively). Samples were incubated at different temperatures (5, 25, 40  $^{\circ}$ C) by placing the desiccators in temperature-controlled ovens. Vials were removed at designated time intervals (6h, 12h, 24h, 5 days and 10 days), capped, quenched by flash freezing in liquid  $\text{N}_2$  and stored at -80  $^{\circ}$ C. An additional time point was included for each of the two extreme conditions (i.e., where the reaction is slowest and fastest): 360 h for 5  $^{\circ}$ C, 6% RH and 6 h for 40  $^{\circ}$ C, 43% RH. Deuterium uptake of the quenched samples was measured using an LC-MS system (Agilent G6230B TOF, ZORBAX 300SB-C18 column, 1.0  $\times$  50 mm, particle size 3.5  $\mu$ m; Agilent Technologies, Santa Clara, CA) equipped with a custom refrigeration unit capable of maintaining low temperatures to minimize deuterium back exchange. Prior to injection, quenched samples were reconstituted with 250  $\mu$ L of ice-cold quench buffer (0.2% formic acid and 5% methanol in water, pH 2.5) and diluted 100-fold. Injected samples were held on a peptide microtrap (Michrom Biosources, Inc., Auburn, CA) and desalted for 1.8 min with 0.1% formic acid in water at a flow rate of 0.3 mL/min (isocratic) before elution onto the LC column. Gradient flow lasting for 9 minutes consisted of 0.1% formic acid in MS-grade water and 0.1% formic acid in MS-grade acetonitrile. Mass spectra were obtained over a 200-20,000  $m/z$  range.

Samples were analyzed using MassHunter Workstation software equipped with the BioConfirm package (Agilent Technologies, Version B.04.00) to obtain the masses of deuterated mAb. Deuterium uptake was calculated by subtracting the mass of the undeuterated mAb from the mass of the deuterated samples. The data were then fit to a biexponential kinetic model (Eq. 4.2)

$$D(t) = D_{fast}(1 - e^{-k_{fast}t}) + D_{slow}(1 - e^{-k_{slow}t}) \quad 4.2$$

where  $D(t)$  is the deuterium uptake at labelling time  $t$ ,  $D_{fast}$  and  $D_{slow}$  are the number of exchanging amides in the fast and slow pools, respectively, and  $k_{fast}$  and  $k_{slow}$  are the apparent first-order rate constants of the “fast” and “slow” exchanging amide groups, respectively. During preliminary analysis, the data were also fit to a monoexponential model (not shown). The biexponential model was a better fit for all conditions according to a sum of squares F-test (p-value = 0.0003).

#### 4.3.6 Moisture Content by Karl Fischer Titration (KF)

A C20S Karl Fischer titrator (Mettler Toledo, Columbus, OH) was used to measure the moisture content of the samples after lyophilization and after 10 d incubation at each ssHDX condition. Anhydrous methanol was used to reconstitute the lyophilized samples. The moisture content (in ppm) of the anhydrous methanol and the reconstituted samples was recorded. The sample moisture content was calculated accordingly and reported as a weight percentage (%w/w).

#### 4.3.7 Modulated Differential Scanning Calorimetry (DSC)

Thermal analysis of lyophilized samples was performed using a differential scanning calorimeter (DSC 2500, TA Instruments, New Castle, DE). The resulting data were analyzed using Trios software (Version 4.2.1, TA Instruments). 5-10 mg of sample was hermetically sealed in a Tzero pan using a Tzero hermetic lid in a dry glove box. Samples were cooled to -5 °C, held for 5 min, and then heated from -5 °C to 150 °C at a ramp rate of 1 °C/min under nitrogen gas flow. Temperature modulation of ±0.5 °C every 60 s was applied. An empty, crimped aluminum pan was used as a reference.

#### 4.3.8 Solid-State Fourier Transform Infrared Spectroscopy (FTIR)

Solid-state FTIR was used to probe the secondary structure of all formulations after lyophilization and after 10 days incubation in ssHDX desiccators. The FTIR spectra were acquired using a Nexus FTIR spectrometer (Thermo Nicolet Corp., Madison, WI) equipped with a smart

iTR single bounce attenuated total reflectance (ATR) sampling accessory. Approximately 1-2 mg of solid sample was placed on the ATR crystal, compressed with a metal anvil, and spectra were collected at a resolution of  $4\text{ cm}^{-1}$  with 36 scans. A continuous nitrogen gas purge was used to reduce interference by atmospheric moisture. The amide-I region was extracted, and the results processed using baseline correction, normalization, and second derivatization in the Opus software (Version 6.5, Bruker Optics, Billerica, MA).

#### **4.3.9 Powder X-ray Diffraction (PXRD)**

PXRD was used to characterize the physical state of mAb formulations after lyophilization and after 10 days incubation in HDX desiccators. The x-ray diffractograms were collected using a Rigaku SmartLab (XRD 6000) diffractometer (The Woodlands, TX) at a 0.154505 wavelength. Diffraction patterns were collected from  $5^\circ$  to  $40^\circ$   $2\theta$  at a step size of  $0.02^\circ$  and speed of  $10^\circ\text{C}/\text{min}$ .

#### **4.3.10 Dynamic Vapor Sorption (DVS)**

Water vapor sorption behavior was characterized using DVS (Surface Measurement Systems LTD, Wembley, UK) for each formulation and ssHDX-MS labeling condition. Approximately 3-4 mg of sample was placed in the sample pan and equilibrated to 0% RH to remove loosely bound water. Equilibration was carried out for 3 hours. The RH was then increased stepwise to each ssHDX-MS RH condition (6, 23, 43% RH). At each step, the sample was equilibrated until the mass change was less than 0.002% for 10 minutes or for a maximum of 3 h. Experiments were carried out at 5, 25, and  $40^\circ\text{C}$ . Data for a single sample was collected at 5 and  $40^\circ\text{C}$ . Triplicate measurements were taken at  $25^\circ\text{C}$ . The instrument was calibrated using a 100 mg calibration standard at each temperature.

### **4.4 Results**

#### **4.4.1 Secondary Structure by FTIR**

Solid-state FTIR was performed to assess the effects of experimental parameters (glycerol content, temperature,  $\text{D}_2\text{O}$  % RH) on mAb secondary structure during ssHDX-MS. Spectra were

acquired after lyophilization (T0) and after 10 d incubation in ssHDX-MS desiccators at each experimental condition. The second-derivative spectra of all samples showed peaks at  $\sim 1630\text{ cm}^{-1}$  and  $\sim 1690\text{ cm}^{-1}$  (Figure C-1) indicating that the  $\beta$ -sheet secondary structure of the mAb is largely intact throughout ssHDX. Peak broadening and differences in the intensity of the  $1630\text{ cm}^{-1}$  band among samples are consistent with minor changes in secondary structure.

#### **4.4.2 Physical Characterization by PXRD**

PXRD was performed on samples after lyophilization (T0) and on samples incubated for 10 d at each ssHDX experimental condition. All samples exhibited smooth, broad, featureless spectra indicative of amorphous solids without crystallinity (Figure C-2).

#### **4.4.3 Water Vapor Sorption Behavior by DVS**

DVS was used to analyze the water sorption behavior of solid formulations at each of the ssHDX-MS experimental conditions. The mass change measured at each condition is listed in Table C-1. The dependence of moisture uptake on temperature and glycerol content was explored using two-way ANOVA at each RH condition (6, 23, 43 %). Mass change due to moisture uptake did not show a significant dependence on either factor or on the interaction between temperature and glycerol content at fixed RH (p-value < 0.1) (Table C-2).

#### **4.4.4 Moisture Content by KF**

The moisture content of each formulation was measured after lyophilization (T0) and after 10 d incubation in ssHDX-MS desiccators at each experimental condition. Moisture content was less than 1% (w/w) after lyophilization, increased with storage RH after 10 d incubation and overall was independent of glycerol content and temperature (Figure 4-1A). RH makes the greatest contribution to the observed variation in moisture content followed by temperature, as indicated by SST by ANOVA effects tests (Table C-3). There is a slight decrease in moisture content with temperature at a fixed RH. This may be due to a slight decrease in RH with temperature of the saturated salt solutions used to create controlled RH environments in the HDX desiccators.<sup>27</sup> Glycerol content does not have a significant effect on moisture content over the range studied (Figure 4-1A, Table C-3).

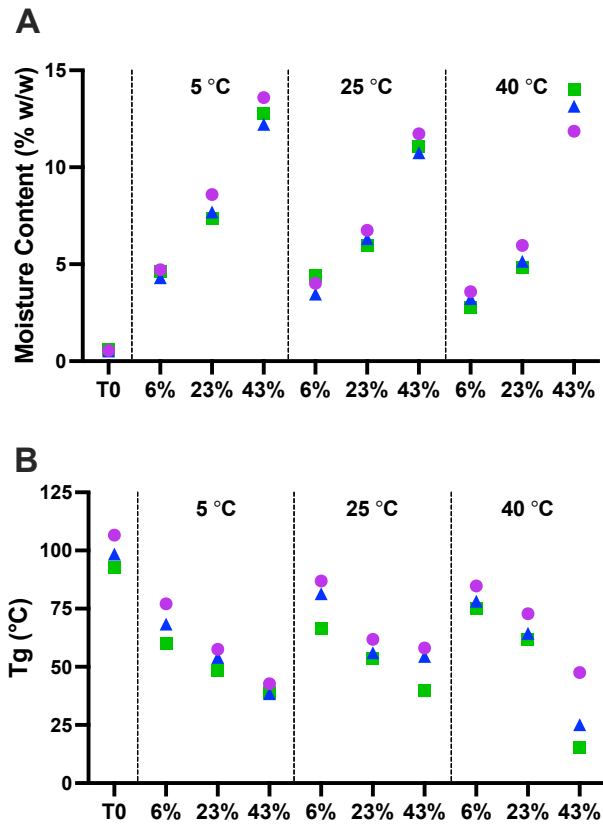


Figure 4-1. Moisture content (A) and Tg values (B) of lyophilized mAb formulations containing 0% (purple circles), 5% (blue triangles), or 10% (green squares) glycerol as a function of RH and temperature. T0 indicates values post-lyophilization before ssHDX incubation. (moisture content  $n = 3$ , mean  $\pm$  SD; Tg  $n = 1$ ; error bars not shown when less than the height of the symbol)

#### 4.4.5 Modulated DSC

The Tg of each formulation was measured post-lyophilization and after 10 d incubation at each experimental condition (Figure 4-1B). After lyophilization, the Tg values were 106.7, 98.5, and 92.9 °C for 0, 5 and 10% glycerol formulations, respectively. After 10 d incubation, the Tg values decreased and ranged from 15.5 to 86.7 °C. Overall, Tg decreased with increasing storage RH and with increasing glycerol content. RH makes the greatest contribution to the observed variation in Tg, followed by glycerol, as indicated by SST by ANOVA effect tests (Table C-3). Storage temperature does not have a significant effect on Tg over the range of temperatures studied (Figure 4-1B, Table C-3).

#### 4.4.6 ssHDX-MS

ssHDX-MS kinetic data for the three mAb formulations carried out at various temperature (5, 25, 40 °C) and RH (6, 23, 43%) conditions are presented in Figure 4-2. Deuterium incorporation increased biexponentially with time and was most noticeably dependent on temperature and RH. Biexponential fits were compared across glycerol levels for each RH and temperature condition using an extra-sum-of-squares F test (GraphPad Prism 9) to determine if one fit could be used for all glycerol levels. For all RH and temperature conditions, except 40 °C with 43% RH, the results indicated that a separate fit should be used for each of the three glycerol formulations ( $p < 0.01$ ). For 40 °C with 43% RH, one model can be used for all three formulations, indicating that the effects of glycerol are insignificant under these conditions. The most noticeable differences among the three glycerol levels are evident at select RH and temperature conditions, namely 5 °C with 43% RH, 25 °C with 23% RH, and 40 °C with 23% RH (Figure 4-2C,E,H). Here the addition of glycerol causes a small, but clear, increase in deuterium incorporation.

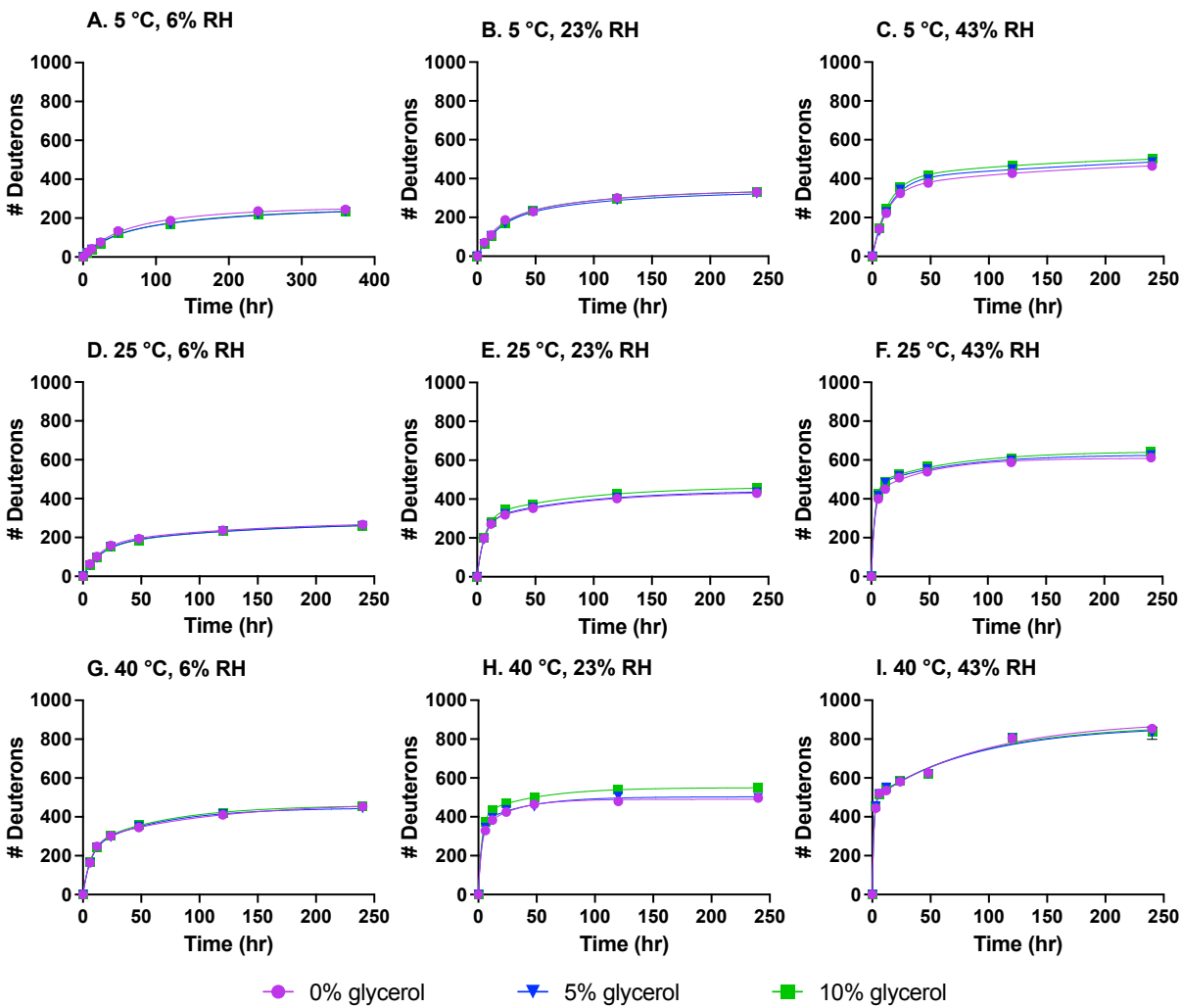


Figure 4-2. ssHDX-MS of trehalose-mAb formulations without glycerol (purple circle), and containing 5% glycerol (blue triangle), and 10% glycerol (green square) carried out at 5, 25 and 40 °C and 6, 23, and 43% RH.  $n=3$ , mean  $\pm$ SD; error bars are not when less than the height of the symbol.

Kinetic parameters,  $D_{\text{fast}}$ ,  $D_{\text{slow}}$ ,  $k_{\text{fast}}$ , and  $k_{\text{slow}}$  were generated for each temperature, RH, and glycerol content level according to Equation 4.2 **Error! Reference source not found.** using the non-linear regression platform in JMP® Pro 16.0.  $D_{\text{fast}}$  and  $k_{\text{fast}}$  values are plotted against RH and temperature for all conditions in Figure 4-3 and Figure 4-4. Regression parameters for Figure 4-3 and Figure 4-4 are presented in Appendix C (Table C-4, Table C-5). There is a clear effect of RH and temperature on both the rate and extent of deuterium incorporation in the fast phase, as our group has shown previously for myoglobin and unstructured peptides.<sup>4,8,23</sup> For  $D_{\text{fast}}$ , the effect of temperature decreases slightly as RH increases as indicated by slightly shallower slopes at 43% RH (Figure 4-3A, Table C-4). The slopes in Figure 4-3B are not significantly different among the three temperatures, indicating that the effect of RH does not change with temperature (Table C-4 and Table C-5). For  $k_{\text{fast}}$ , the effects of RH and temperature are interdependent as indicated by increasing and significantly different slopes across RH (Figure 4-4A) and across temperature (Figure 4-4B, Table C-4). The effect of temperature is greater at higher RH (Figure 4-4A) and the effect of RH is greater at higher temperatures (Figure 4-4B). The effects of temperature and RH on  $D_{\text{slow}}$  and  $k_{\text{slow}}$  are inconsistent across the formulations and experimental conditions (Figure C-3, Figure C-4). Regression parameters for  $D_{\text{slow}}$  and  $k_{\text{slow}}$  versus temperature and RH are presented in SI (Table C-6). Linearity is poor and many relationships have a slope that is not significantly different from zero, suggesting that the slow phase of ssHDX is independent of temperature and RH, as we have shown previously for lyophilized myoglobin.<sup>23</sup>

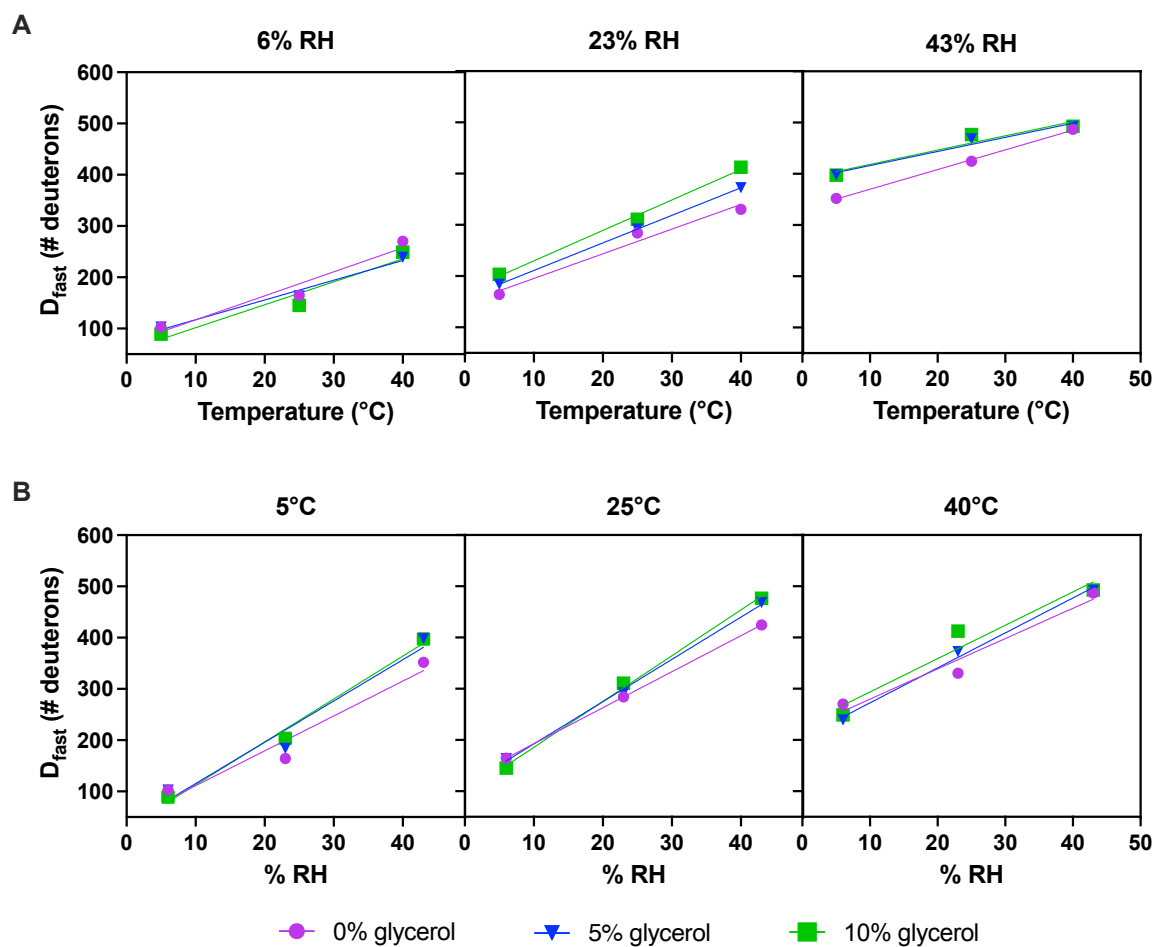


Figure 4-3.  $D_{fast}$  values (Eq 4.2) as a function of temperature (A) and RH (B) for trehalose-mAb formulations containing 0% glycerol (purple circles), 5% glycerol (blue triangles), and 10% glycerol (green squares).

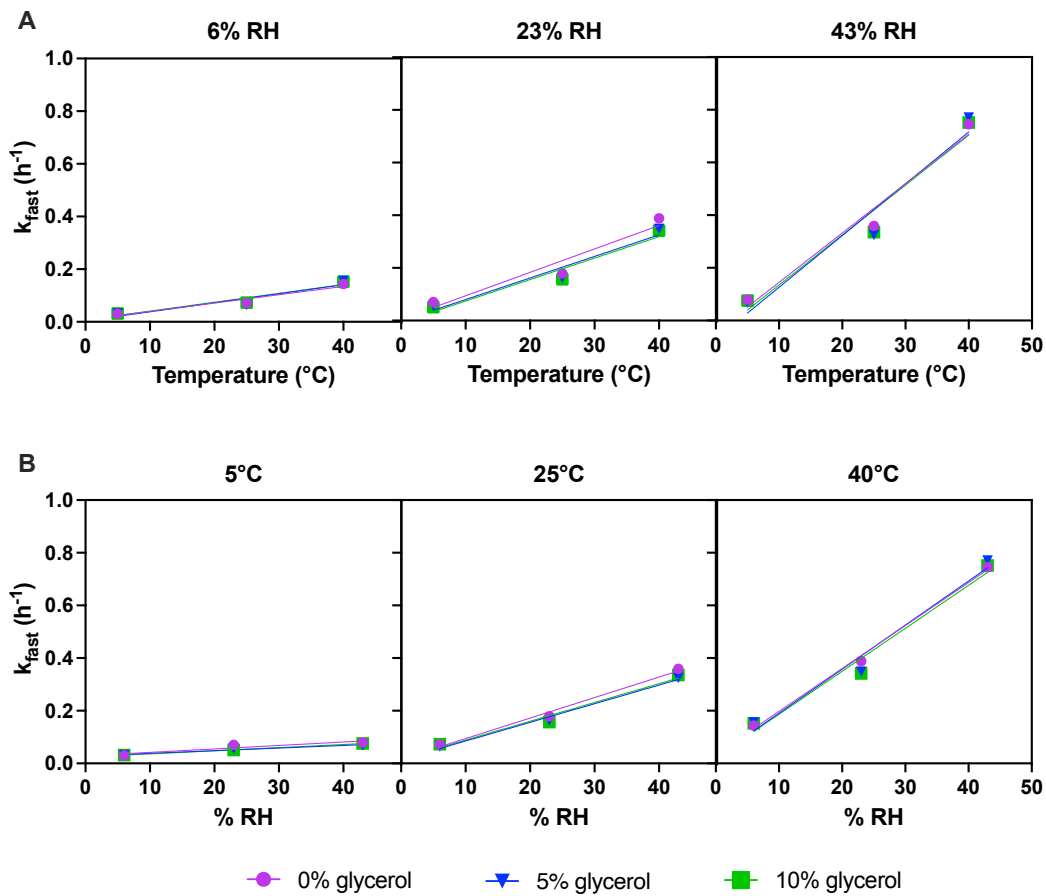


Figure 4-4.  $k_{fast}$  values (Eq 4.2) as a function of temperature (A) and RH (B) for trehalose-mAb formulations containing 0% glycerol (purple circles), 5% glycerol (blue triangles), and 10% glycerol (green squares).

To further investigate the effects and possible interactions of the experimental parameters (temperature, RH, and glycerol content), three-way ANOVA was performed for each of the ssHDX kinetic parameters ( $D_{\text{fast}}$ ,  $k_{\text{fast}}$ ,  $D_{\text{slow}}$ ,  $k_{\text{slow}}$ ). Model terms with treatment p-value  $< 0.05$  were considered significant and retained in the model. ANOVA results indicated that  $D_{\text{fast}}$  and  $k_{\text{fast}}$  were significantly affected by the experimental parameters (ANOVA table p-value  $< 0.0001$ ) (Table 4-1).  $D_{\text{fast}}$  showed a significant dependence on temperature and RH, and  $k_{\text{fast}}$  showed a significant dependence on temperature, RH and the interaction between the two factors (treatment p-value  $< 0.05$ ). The effect of the interaction between RH and temperature on  $k_{\text{fast}}$  is apparent in Figure 4-4, and corresponds to the interdependence described above. Comparing SST (Table 4-1) reveals that RH contributes more to the variability in  $D_{\text{fast}}$  than does temperature. This is also shown in Figure 4-3 by the greater slopes when  $D_{\text{fast}}$  is plotted against RH (Figure 4-3B) than when plotted against temperature (Figure 4-3A, Table C-4). For  $k_{\text{fast}}$ , SST values (Table 4-1) indicate that temperature makes the greatest contribution to  $k_{\text{fast}}$  values followed by RH and then by the interaction between RH and temperature. These effects agree with the trends shown in Figure 4-4. ANOVA results also showed that experimental variables contributed less significantly to  $D_{\text{slow}}$  and  $k_{\text{slow}}$  (Table C-7). Hereinafter, analysis will focus on kinetic parameters from the fast process because these parameters showed a clearer dependence on RH and temperature. Moreover, for lyophilized myoglobin, it has been proposed that RH and temperature effects can be incorporated into the fast terms, while slow terms remain independent of RH and temperature, because the fast phase makes the greater contribution to the calculated deuterium incorporation over the time course of typical ssHDX-MS experiments.<sup>23</sup> To verify this hypothesis in the present study, contributions of the fast and slow exponential terms (Eq. 4.2) to the total deuterium uptake were calculated for each time point of each data set using the calculated biexponential regression parameters following the procedure described by Tukra et al. (Table C-8). In 122 of 164 timepoints (~75%) the fast phase contributed to at least 70% of the total deuterium incorporation.

Glycerol was added to lyophilized mAb formulations as a plasticizer to investigate mobility effects on ssHDX-MS. Despite reducing Tg (Figure 4-1), ANOVA results indicate that glycerol does not significantly contribute to ssHDX kinetic parameters as indicated by a treatment p-value greater than 0.05, suggesting that molecular mobility in the form of  $\alpha$ -relaxation is not important for this reaction.<sup>28,29</sup>

Table 4-1. ANOVA of the treatment variables RH, temperature, and glycerol content on ssHDX-MS kinetic parameters  $D_{fast}$  and  $k_{fast}$ . Treatment variables with  $p > 0.05$  were eliminated from the fit model.

<b>Output Parameter</b>	<b>Treatment Variable</b>	<b>Parameter Estimate</b>	<b>Std Error</b>	<b>SST</b>	<b>p-value</b>
<b><math>D_{fast}</math></b>	<b>RH</b>	137.09	4.95	339038.51	<0.0001
	<b>Temp</b>	74.93	6.05	101738.57	<0.0001
<b><math>k_{fast}</math></b>	<b>RH</b>	0.147	0.012	0.39	<0.0001
	<b>Temp</b>	0.184	0.011	0.611	<0.0001
	<b>RH*Temp</b>	0.139	0.014	0.235	<0.0001

To further investigate the role of mobility in the ssHDX reaction, the dependence of kinetic parameters on T-Tg and moisture content was assessed. In the ssHDX experiments, these variables were manipulated indirectly through experimental factors, temperature, RH and glycerol content.  $D_{fast}$  and  $k_{fast}$  show similar dependence on moisture content (Figure 4-5A,B), though the trends are better defined for  $D_{fast}$ . Overall,  $D_{fast}$  and  $k_{fast}$  increase with increasing moisture content, however, at constant RH (6, 23, 43% RH) the trend is reversed (i.e., increasing moisture content reduces  $D_{fast}$  and  $k_{fast}$ ) and linearity is strong ( $R^2 = 0.751$  at 6% RH,  $R^2 = 0.967$  at 23% RH for  $D_{fast}$ ;  $R^2 = 0.749$  at 6% RH,  $R^2 = 0.722$  at 23% RH for  $k_{fast}$ ). The slopes of the regression lines of  $D_{fast}$  versus moisture content at 6% and 23% RH are not significantly different ( $p = 0.275$ ) nor are the slopes of  $k_{fast}$  versus moisture content at 6% and 23% RH ( $p = 0.482$ ), indicating that moisture content affects ssHDX kinetic parameters equally regardless of  $D_2O$  activity (Table C-9). The intercepts, which are significantly different ( $p < 0.0001$ ), represent the values of  $D_{fast}$  and  $k_{fast}$  in the absence of moisture for each RH level (Table C-9).

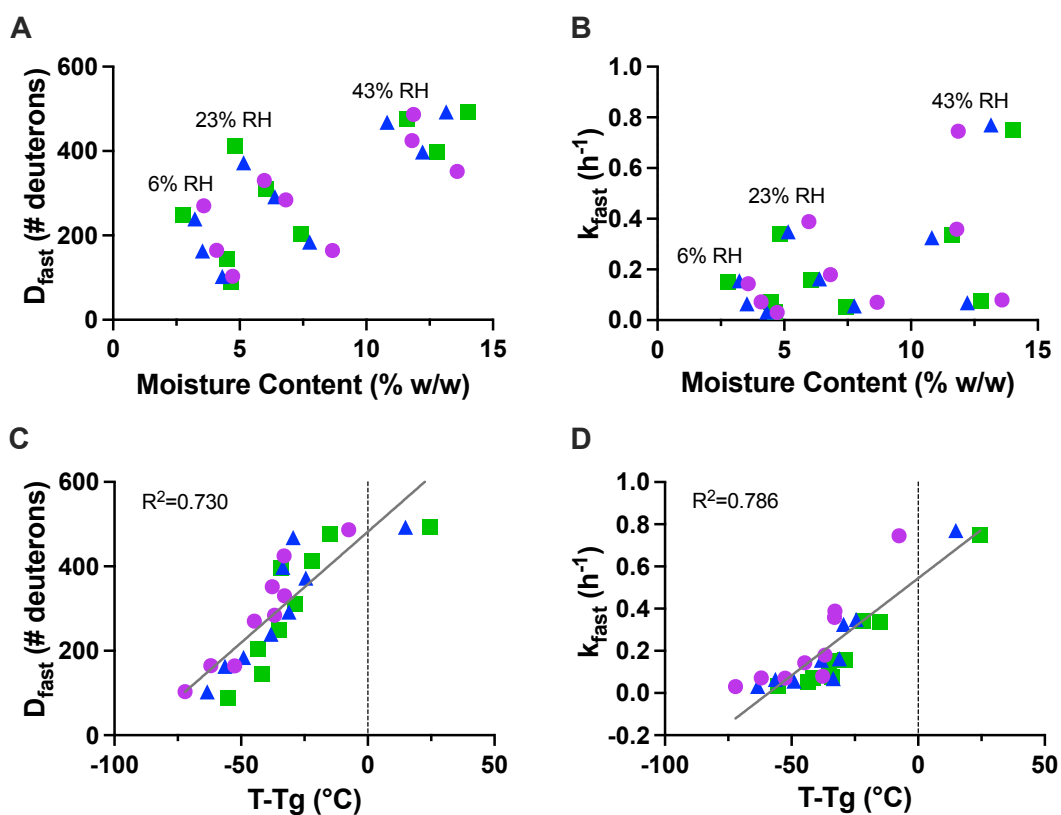


Figure Panel	Relationship	RH	Slope $\pm$ SE	y-intercept $\pm$ SE	$R^2$
A	$D_{fast}$ vs moisture content	6%	$-86.5 \pm 18.8$	$509 \pm 75$	0.751
		23%	$-67.6 \pm 4.7$	$727 \pm 31$	0.967
B	$k_{fast}$ vs moisture content	6%	$-0.067 \pm 0.058$	$0.35 \pm 0.06$	0.749
		23%	$-0.091 \pm 0.021$	$0.79 \pm 0.14$	0.722
C	$D_{fast}$ vs $T-T_g$	N/A	$5.26 \pm 0.64$	$481.9 \pm 26.02$	0.730
D	$k_{fast}$ vs $T-T_g$	N/A	$0.009 \pm 0.001$	$0.54 \pm 0.04$	0.786

Figure 4-5  $D_{fast}$  (A,C) and  $k_{fast}$  (B,D) values (Eq. 4.2) as a function of moisture content (A,B) and  $T-T_g$  (C,D) for lyophilized mAb formulations containing 0% glycerol (purple circles), 5% glycerol (blue triangles), and 10% glycerol (green squares). Solid lines represent linear fit for all data points

Both  $D_{\text{fast}}$  and  $k_{\text{fast}}$  increase with  $T-T_g$  (Figure 4-5C,D) with  $R^2$  values 0.730 and 0.786, respectively. This linear relationship is more prominent in the glassy region ( $T-T_g < 0$ ) suggesting that ssHDX reactivity depends on mobility in glassy solids. Linearity may be lost in the rubbery region ( $T-T_g > 0$ ), or the dependence on mobility may change, as has been shown previously, although the current data are limited in the rubbery regime and do not allow definitive conclusions.<sup>30</sup> There is a subtle sigmoidal behavior in the dependence of  $D_{\text{fast}}$  and  $K_{\text{fast}}$  on  $T-T_g$  (Figure 4-5D); at low  $T-T_g$  values ( $\sim -50$  °C), the dependence of  $D_{\text{fast}}$  and  $k_{\text{fast}}$  on  $T-T_g$  is small, but becomes more pronounced as  $T-T_g$  increases towards zero.

#### 4.5 Discussion

In the studies reported here, the mechanism of ssHDX was investigated in lyophilized mAb formulations, with a focus on temperature, RH and mobility effects. Initial analysis of the experimental parameters showed that temperature and RH had significant effects on the overall rate and extent of exchange, as measured by  $k_{\text{fast}}$  and  $D_{\text{fast}}$ . ssHDX involves a chemical reaction in which a deuterium atom from a donor is transferred to an amide bond on a peptide or protein. In the solid state, the process requires the initial sorption of  $D_2O$  from the vapor phase into the solid matrix before the exchange reaction can begin. Previous work has shown that the initial sorption process is complete within 2-6 h, with faster sorption at higher RH.<sup>9</sup>

Mechanistically, there are several possible explanations for the effects of RH (i.e.,  $D_2O$  activity) on the deuteration process observed here. First, a change in the activity of any reactant is expected to have a direct effect on reactivity, with rates increasing with increasing reactant activity.<sup>31</sup> Second, the RH dependence may be due to an increase in the rate and extent of  $D_2O$  vapor sorption into the solid and the reduction of any mass transport contributions to the observed rate. Third, the  $D_2O$  activity could influence deuterium incorporation by changing the local protein conformation and dynamics and/or by acting as a plasticizer.<sup>4</sup>

Similarly, it is not surprising that the rate of deuterium incorporation increases with temperature. It is well understood that reactivity increases with temperature, often in accordance with the Arrhenius rate law. In addition, the rate of exchange is temperature dependent in solution HDX.<sup>32,33</sup> It is reasonable to expect a similar trend in the solid state, and it has been observed previously in lyophilized myoglobin formulations.<sup>23</sup> Temperature can also affect the rate of deuterium incorporation by increasing water vapor activity and by increasing mobility in the solid

state (i.e., by decreasing  $T-T_g$ ).<sup>23,34,35</sup> For  $k_{fast}$ , the interaction parameter for the combined effects of RH and temperature is significant, indicating that the two effects are synergistic and not simply additive.

It is somewhat surprising that the extent of deuterium incorporation increased with temperature. This may be in part due to the increase in water vapor activity mentioned above. Another explanation is that the hydrogen bond network may be more disrupted at higher temperatures. Deuteration occurs through the breaking of an amide hydrogen bond in order for the deuterium ion to replace the hydrogen. It is possible that hydrogen bonds that were securely formed and unperturbed during ssHDX at low temperatures are more easily broken at higher temperatures, thus increasing the number of hydrogen bonds accessible to deuteration.

The experimental variable with the greatest impact on  $D_{fast}$  differed from that for  $k_{fast}$ , as determined by ANOVA.  $D_{fast}$  was most dependent on RH and  $k_{fast}$  was most dependent on temperature. Increased deuterium activity in the solid matrix resulting from increased RH may increase both total deuterium incorporation and the number of amide groups in the fast-exchanging pool ( $D_{fast}$ ). On the other hand, the classical Arrhenius dependence of reaction rate on temperature may explain the dependence of  $k_{fast}$  on temperature, though temperature dependent changes in the solid matrix may complicate this relationship.

Glycerol was added to the formulations as a plasticizer in an attempt to manipulate molecular mobility in the solid matrix. ANOVA results showed that glycerol did not have a significant effect on any of the ssHDX kinetic parameters despite reducing  $T_g$ , suggesting that mobility (here,  $\alpha$ -relaxation) is not important for ssHDX in the parameter range studied. It is not surprising that ssHDX is unaffected by mobility in the solid state, as the reaction depends on the availability of protons and deuterons and the diffusion of these small molecules typically is not coupled to viscosity.<sup>31</sup> Yet ssHDX kinetic parameters,  $D_{fast}$  and  $k_{fast}$ , are strongly correlated to  $T-T_g$  (Figure 4-5). An explanation for this discrepancy may be that  $T-T_g$ , while representative of mobility, also incorporates both temperature and RH, which are clear drivers of the ssHDX reaction.

At constant temperature, ssHDX in unstructured peptides has been described by a first-order reversible kinetic model,<sup>8</sup>

$$\frac{k_f}{k_b} A \rightleftharpoons B \quad 4.3$$

where A and B are the number or percentage of exchangeable amide groups and deuterated amide groups, respectively, and  $k_f$  and  $k_b$  are the forward and reverse reaction rate constants, respectively. The forward reaction rate is assumed to be proportional to  $D_2O_{(g)}$  activity ( $a_D$ ) (i.e., RH in  $D_2O$ ) so that

$$k_f = k_f^* \times (a_D) \quad 4.4$$

where  $k_f^*$  is the forward reaction rate in the absence of RH effects. The rate constant for the reverse reaction,  $k_b$ , is assumed to be independent of RH. The apparent rate constant for deuterium incorporation measured in ssHDX-MS experiments ( $k_{ap}$ ) then depends on  $a_D$  and on the forward and reverse reaction rate constants:

$$k_{ap} = k_f^*(a_D) + k_b \quad 4.5$$

In this model, the extent of deuterium incorporation at equilibrium is related to  $a_D$  by

$$\frac{A_0}{D_{max}} = 1 + \frac{1}{K} \left( \frac{1}{a_D} \right) \quad 4.6$$

where  $A_0$  is the total number of exchangeable amide groups, ( $D_{max}/A_0$ ) is the fraction of the total number of exchangeable amide groups deuterated at large  $t$ , and  $K$  is a pseudo-equilibrium constant equal to the ratio of the forward and reverse rate constants (i.e.,  $K = k_f^*/k_b$ ).<sup>8</sup>

In the data presented here, deuterium incorporation in the fast-exchanging pool is consistent with this first-order kinetic model, where  $k_{ap}$  represents  $k_{fast}$  and  $D_{max}$  represents  $D_{fast}$ . Here,  $A_0$  was determined from fully deuterated solution controls prepared by diluting each formulation 1:9 (v/v) with HDX labelling solution containing 2.5 mM potassium phosphate buffer in  $D_2O$  and storing at 40 °C for 72 h. At constant temperature, there is a linear relationship ( $R^2 \geq 0.85$ ) between  $k_{fast}$  and  $a_D$  and between  $A_0/D_{fast}$  and  $1/a_D$  (Figure C-5) suggesting that the

reversible first-order kinetic model can also be applied to ssHDX in large, structured proteins as well as to the small unstructured peptides studied previously. There is a strong linear relationship between temperature and the slopes of these relationships (Figure C-5A,  $R^2 = 0.96$ ; Figure C-5B,  $R^2 = 1.00$ ) suggesting that the rate and extent of ssHDX also depend on temperature.

Typically, reaction rates depend exponentially on reciprocal temperature as described by the Arrhenius equation. However, over a narrow temperature range and with a low activation energy, the Arrhenius equation can be approximated by a linear relationship between rate constant and temperature (see Appendix C),

$$k = Z(T - T_o) \quad 4.7$$

where  $T$  is the experimental temperature,  $T_o$  is the reference temperature for linearization, and  $Z$  is a constant combining activation energy,  $E_a$ , the pre-exponential constant from the Arrhenius equation,  $A$ , the universal gas constant  $R$ , and  $T_o$ .

With the observed linear dependence of reaction rate on temperature, we propose a kinetic model that extends Equation **Error! Reference source not found.** to incorporate both RH and temperature, using Equation 4.7:

$$k_f = k_f^* \times (a_D)(\mathbb{T} \times Z) \quad 4.8$$

where the dimensionless temperature,  $\mathbb{T}$  represents the temperature term from Equation 4.7 normalized across the range 273 to 373 K (i.e.,  $\mathbb{T} = (T - T_o)/(373 - 273)$ ). This range represents the temperatures accessible to ssHDX experiments and creates a dimensionless term with a range of 0 to 1, similar to  $a_D$ . The reverse rate constant,  $k_b$ , is assumed independent of RH and temperature (see Appendix C) so that

$$k_{ap} = k_f^*(a_D)(\mathbb{T} \times Z) + k_b \quad 4.9$$

Derivation of the integrated rate law for the first-order kinetic model (Eq. 4.3) and substituting in Equation 4.8 (see Appendix C) provides a relationship between  $D_{\text{fast}}$ ,  $a_D$ , and temperature at large time,  $t$ , (i.e., at the plateau of ssHDX kinetic plots),

$$\frac{A_0}{D_{fast}} = 1 + \frac{1}{K} \left( \frac{1}{a_D} \right) \left( \frac{1}{T \times Z} \right) \quad 4.10$$

where  $K$  is the ratio of the forward and reverse rate constants (i.e.,  $K = k_f^*/k_b$ ). The modified kinetic model predicts that plots of  $k_{ap}$  versus  $(a_D \times T)$  and of  $(A_0/D_{fast})$  versus  $(1/(a_D \times T))$  will be linear and can serve as a test for the consistency of the model with experimental data.

Figure 4-6A shows a linear regression of  $k_{ap}$  as a function of  $a_D \times T$  for ssHDX-MS data for lyophilized mAb formulations at all RH (6, 23, 43%) and temperature (5, 25, 40 °C) conditions. Linearity is confirmed ( $R^2 = 0.95$ ) in agreement with Equation 4.9, where the slope given by  $k_f^* \times Z$ . The y-intercept, which is predicted to be equal to  $k_b$  (Eq. 4.9), is not significantly different from zero, suggesting that the reverse reaction rate constant is much less than the forward rate constant.

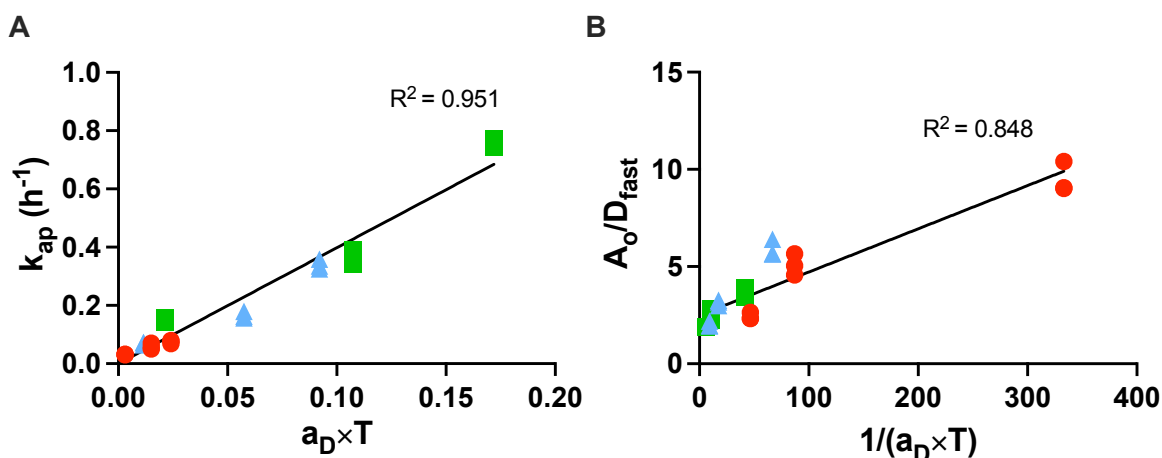


Figure 4-6. Apparent exchange rate constant ( $k_{ap}$ ) as a function of  $a_D \times T$  (A) and  $A_0/D_{fast}$  as a function of  $1/(a_D \times T)$  (B) for lyophilized mAb formulations at 5 °C (red), 25 °C (blue), and 40 °C (green) where  $a_D = (\% \text{ RH}/100)$  at equilibrium. Solid lines represent best fit lines for all data points.

**Figure 4-6B** shows linear regression of  $(A_0/D_{fast})$  as a function of  $(1/(a_D \times T))$  for ssHDX-MS data of lyophilized mAb formulations at all RH (6, 23, 43%) and temperature (5, 25, 40 °C) conditions. Linearity is confirmed ( $R^2 = 0.85$ ) in agreement with Equation 4.10, where the slope represents  $k_b/(k_f^* \times Z)$ . The absolute value for the forward exchange rate cannot be calculated from this model because it cannot be decoupled from the constant,  $Z$ . However, since

Z is not expected to vary within the experimental conditions of ssHDX, the model allows comparison of relative forward reaction rate constants among formulations.

The data show a better fit to Equation 4.9 than Equation 4.10 as indicated by the  $R^2$  values (Figure 4-6), suggesting the model describes the rate of exchange better than the extent of exchange. The divergence from linearity with  $D_{\text{fast}}$  in (Figure 4-6B) could reflect several assumptions made in the model. First, the assumption that  $k_b$  is independent of temperature may be incorrect. Second, the linear approximation of the Arrhenius equation diverges from the Arrhenius equation itself at higher temperatures (Figure C-6) and may contribute to the loss of linearity. Third, this model assumes that  $D_2O_{(g)}$  activity ( $a_D$ ) is independent of temperature, which may be incorrect and contribute to the lower  $R^2$ -value in Equation 4.10 (Figure 4-6B).

The proposed model has implications for understanding ssHDX on a mechanistic level and for designing ssHDX experiments. Figure 4-6 demonstrates that for lyophilized mAb formulations the ssHDX kinetics are consistent with a reversible first-order kinetic model in which the forward reaction rate constant depends linearly on temperature. The functional effects of RH and temperature can be anticipated in designing ssHDX experiments. For example, increasing temperature and/or RH may result in larger differences in the extent of exchange among formulations (i.e., in  $D_{\text{fast}}$ ), which may be masked at lower temperature and RH. The effectiveness of the proposed model also suggests that the correlation of these parameters with  $T-T_g$  does not necessarily represent coupling of the reaction to mobility (i.e.,  $\alpha$ -relaxation), and that an alternative explanation is possible. That is, ssHDX kinetic parameters may show a linear dependence on mobility ( $T-T_g$ ) simply because both RH and temperature are imbedded in this relationship, a finding that has implications for other solid-state reactions that show apparent dependence on mobility.

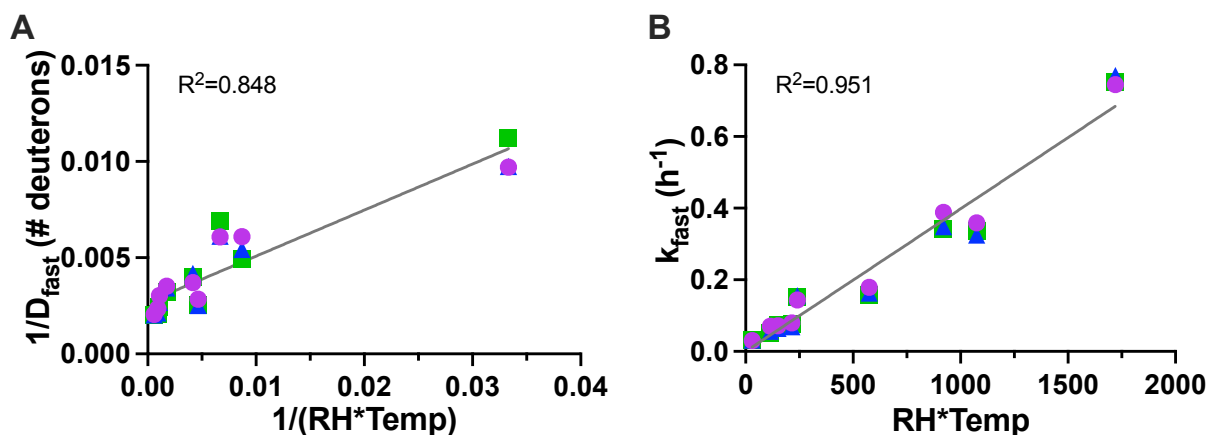


Figure 4-7. The inverse of  $D_{fast}$  (A) and  $k_{fast}$  (B) values (Eq. 4.2) as a function of the inverse of the product of ssHDX RH and temperature and as the product of RH and temperature, respectively, for lyophilized mAb formulations containing 0% glycerol (purple circles), 5% glycerol (blue triangles), and 10% glycerol (green squares). Solid lines represent linear fit for all data points.

#### 4.6 Conclusions

Formulations of a lyophilized mAb plasticized with varying levels of glycerol were subjected to ssHDX-MS at different RH and temperature conditions in order to investigate the effects of mobility, temperature and RH on the exchange. Kinetic parameters for exchange were determined by fitting to a biexponential model. The kinetic parameters,  $D_{fast}$  and  $k_{fast}$ , depended on RH and temperature, but not on glycerol content, although a correlation was observed between kinetic parameters and mobility ( $T-T_g$ ). A reversible first-order kinetic model for deuterium incorporation by ssHDX-MS was proposed in which the forward rate constant depends linearly on RH and temperature and is consistent with experimental data. That the dependence of kinetic parameters on RH and temperature is better described by this model than by a linear dependence on  $T-T_g$  suggests that the apparent mobility dependence of ssHDX may simply be because RH and temperature are imbedded in  $T-T_g$ .

## 4.7 References

1. Li, Y., Williams, T. D. & Topp, E. M. Effects of Excipients on Protein Conformation in Lyophilized Solids by Hydrogen/Deuterium Exchange Mass Spectrometry. *Pharmaceutical Research* 25, 259–267 (2008).
2. Moorthy, B. S., Iyer, L. K. & Topp, E. M. Mass Spectrometric Approaches to Study Protein Structure and Interactions in Lyophilized Powders. *JoVE* 52503 (2015) doi:10.3791/52503.
3. Moussa, E. M., Singh, S. K., Kimmel, M., Nema, S. & Topp, E. M. Probing the Conformation of an IgG1 Monoclonal Antibody in Lyophilized Solids Using Solid-State Hydrogen–Deuterium Exchange with Mass Spectrometric Analysis (ssHDX-MS). *Mol. Pharmaceutics* 15, 356–368 (2018).
4. Sophocleous, A. M. & Topp, E. M. Localized Hydration in Lyophilized Myoglobin by Hydrogen–Deuterium Exchange Mass Spectrometry. 2. Exchange Kinetics. *Molecular Pharmaceutics* 9, 727–733 (2012).
5. Moorthy, B. S. et al. Solid-State Hydrogen–Deuterium Exchange Mass Spectrometry: Correlation of Deuterium Uptake and Long-Term Stability of Lyophilized Monoclonal Antibody Formulations. *Mol. Pharmaceutics* 15, 1–11 (2018).
6. Moorthy, B. S., Schultz, S. G., Kim, S. G. & Topp, E. M. Predicting Protein Aggregation during Storage in Lyophilized Solids Using Solid State Amide Hydrogen/Deuterium Exchange with Mass Spectrometric Analysis (ssHDX-MS). *Mol Pharmaceutics* 11, 1869–1879 (2014).
7. Iyer, L. K., Sacha, G. A., Moorthy, B. S., Nail, S. L. & Topp, E. M. Process and Formulation Effects on Protein Structure in Lyophilized Solids Using Mass Spectrometric Methods. *Journal of Pharmaceutical Sciences* 105, 1684–1692 (2016).
8. Kammari, R. & Topp, E. M. Solid-State Hydrogen–Deuterium Exchange Mass Spectrometry (ssHDX-MS) of Lyophilized Poly- D , L -Alanine. *Mol. Pharmaceutics* 16, 2935–2946 (2019).
9. Sophocleous, A. M., Zhang, J. & Topp, E. M. Localized Hydration in Lyophilized Myoglobin by Hydrogen–Deuterium Exchange Mass Spectrometry. 1. Exchange Mapping. *Mol. Pharmaceutics* 9, 718–726 (2012).
10. Sinha, S., Li, Y., Williams, T. D. & Topp, E. M. Protein Conformation in Amorphous Solids by FTIR and by Hydrogen/Deuterium Exchange with Mass Spectrometry. *Biophysical Journal* 95, 5951–5961 (2008).
11. Li, Y., Williams, T. D., Schowen, R. L. & Topp, E. M. Characterizing protein structure in amorphous solids using hydrogen/deuterium exchange with mass spectrometry. *Analytical Biochemistry* 366, 18–28 (2007).

12. Kammari, R. & Topp, E. M. Effects of Secondary Structure on Solid-State Hydrogen–Deuterium Exchange in Model  $\alpha$ -Helix and  $\beta$ -Sheet Peptides. *Mol. Pharmaceutics* 17, 3501–3512 (2020).
13. Wilson, N. E., Topp, E. M. & Zhou, Q. T. Effects of drying method and excipient on structure and stability of protein solids using solid-state hydrogen/deuterium exchange mass spectrometry (ssHDX-MS). *International Journal of Pharmaceutics* 567, 118470 (2019).
14. Hvidt, A. & Linderstrom-Lang, K. The kinetics of the deuterium exchange of insulin with D<sub>2</sub>O; an amendment. *Biochim Biophys Acta* 16, 168–169 (1955).
15. Hvidt, A. & Linderstrøm-Lang, K. Exchange of hydrogen atoms in insulin with deuterium atoms in aqueous solutions. *Biochimica et Biophysica Acta* 14, 574–575 (1954).
16. Bai, Y., Milne, J. S., Mayne, L. & Englander, S. W. Primary structure effects on peptide group hydrogen exchange. *Proteins* 17, 75–86 (1993).
17. Jensen, P. F. & Rand, K. D. Hydrogen exchange: a sensitive analytical window into protein conformation and dynamics. in *Hydrogen exchange mass spectrometry of proteins: Fundamentals, methods and applications* 1–15 (John Wiley & Sons, Ltd, 2016).
18. Truhlar, S. M. E., Croy, C. H., Torpey, J. W., Koeppe, J. R. & Komives, E. A. Solvent accessibility of protein surfaces by amide H/ <sup>2</sup>H exchange MALDI-TOF mass spectrometry. *J. Am. Soc. Mass Spectrom.* 17, 1490–1497 (2006).
19. Katta, V. & Chait, B. T. Hydrogen/deuterium exchange electrospray ionization mass spectrometry: a method for probing protein conformational changes in solution. *J. Am. Chem. Soc.* 115, 6317–6321 (1993).
20. Zhang, Z. & Smith, D. L. Determination of amide hydrogen exchange by mass spectrometry: A new tool for protein structure elucidation: Amide hydrogen exchange by mass spectrometry. *Protein Science* 2, 522–531 (1993).
21. Nguyen, D., Mayne, L., Phillips, M. C. & Walter Englander, S. Reference Parameters for Protein Hydrogen Exchange Rates. *J. Am. Soc. Mass Spectrom.* 29, 1936–1939 (2018).
22. Li, Y., Williams, T. D., Schowen, R. L. & Topp, E. M. Trehalose and calcium exert site-specific effects on calmodulin conformation in amorphous solids. *Biotechnol. Bioeng.* 97, 1650–1653 (2007).
23. Tukra, R., Gardner, S. & Topp, E. M. Effects of temperature and relative humidity in D<sub>2</sub>O on solid-state hydrogen deuterium exchange mass spectrometry (ssHDX-MS). *International Journal of Pharmaceutics* 596, 120263 (2021).
24. Yoshioka, S. & Aso, Y. Correlations between Molecular Mobility and Chemical Stability During Storage of Amorphous Pharmaceuticals. *Journal of Pharmaceutical Sciences* 96, 960–981 (2007).

25. Duddu, S. & Dal Monte, P. Effect of glass transition temperature on the stability of lyophilized formulations containing a chimeric therapeutic monoclonal antibody. *Pharmaceutical Research* 14, 591–595 (1997).
26. Roy, M. L., Pikal, M. J., Rickard, E. C. & Maloney, A. M. The effects of formulation and moisture on the stability of a freeze-dried monoclonal antibody-vinca conjugate: a test of the WLF glass transition theory. *Dev Biol Stand* 74, 323–339 (1992).
27. Greenspan, L. Humidity fixed points of binary saturated aqueous solutions. *J. RES. NATL. BUR. STAN. SECT. A.* 81A, 89 (1977).
28. Cicerone, M. T. & Douglas, J. F. Beta-relaxation governs protein stability in sugar-glass matrices. *Soft Matter* 8, 2983–2991 (2012).
29. Cicerone, M. T. & Soles, C. L. Fast Dynamics and Stabilization of Proteins: Binary Glasses of Trehalose and Glycerol. *Biophysical Journal* 86, 3836–3845 (2004).
30. Lai, M. C. et al. Chemical stability of peptides in polymers. 2. Discriminating between solvent and plasticizing effects of water on peptide deamidation in poly(vinylpyrrolidone). *Journal of Pharmaceutical Sciences* 88, 1081–1089 (1999).
31. Shalaev, E. Y. & Zografi, G. How Does Residual Water Affect the Solid-state Degradation of Drugs in the Amorphous State? *Journal of Pharmaceutical Sciences* 85, 1137–1141 (1996).
32. Gallagher, E. S. & Hudgens, J. W. Mapping Protein–Ligand Interactions with Proteolytic Fragmentation, Hydrogen/Deuterium Exchange-Mass Spectrometry. in *Methods in Enzymology* vol. 566 357–404 (Elsevier, 2016).
33. Englander, S. W. Hydrogen exchange and mass spectrometry: A historical perspective. *J. Am. Soc. Mass Spectrom.* 17, 1481–1489 (2006).
34. Umprayn, K. & Mendes, R. W. Hygroscopicity and Moisture Adsorption Kinetics of Pharmaceutical Solids: A Review. *Drug Development and Industrial Pharmacy* 13, 653–693 (1987).
35. Grant, A. et al. Effects of Temperature on Sorption of Water by Wheat Gluten Determined Using Deuterium Nuclear Magnetic Resonance. *Cereal Chemistry* 76, 219–226 (1999).

## CHAPTER 5. CONCLUSIONS AND RECOMMENDATIONS

The positive impact of therapeutic proteins on global health is irrefutable. Over the past 40 years since the first approval, therapeutic proteins have grown rapidly to become a significant portion of the pharmaceutical market due to their applicability to a wide array of disease conditions. While the use of biopharmaceuticals continues to grow their formulation and development remains challenging due to the complexity of the molecules. One approach for molecules with persistent physicochemical instabilities is to formulate in the solid state. However, instabilities may still occur. Many aspects of solid-state reactivity are not well understood and there is a lack of high-resolution analytical techniques to probe the solid matrix.

This work addresses gaps in both our understanding of solid-state reactivity and analytical techniques used to assess stability in the solid state. First, the mechanism of pGlu formation, a form of chemical instability, was explored. Formulation strategies for preventing pGlu formation were demonstrated in both the solid and solution state. ssHDX-MS was examined as a tool for assessing formulations for their potential to form pyroglutamate. Lastly, the effects of temperature, RH, and mobility on ssHDX were investigated to better understand the mechanism of exchange in this reaction.

### 5.1 Main Findings

In Chapter 2 and Chapter 3 the effects of ‘pH’ and excipient on pGlu formation from Glu were investigated in both the solid and solution states. The results demonstrate the importance of formulation ‘pH’ for this degradation pathway. ‘pH’-rate profiles differed markedly between the solid and solutions states. In solution, the U-shaped profile indicated acid and base catalysis with a minimum at ‘pH’ 5.5-6, while in the solid-state pGlu formation was generally independent of ‘pH’ from 4 to 7 with a minimum in the basic region at ‘pH’ 9. Moreover, at ‘pH’ 5.5-6, a region common to mAb formulation, solid reaction rates surpassed solution rates, suggesting stability may not be enhanced in a solid formulation in this region. These ‘pH’ trends were unchanged with excipient type across those investigated: sucrose, trehalose, dextran, and hydroxyectoine. Solution stability was also unaffected by excipient, however notable differences were observed in the solid

state. pGlu formation rates were lowest when stabilized by hydroxyectoine, suggesting that small, low molecular weight excipients may prevent pGlu formation.

The effects of moisture and Tg on solid-state pGlu formation were also investigated in Chapter 3. pGlu formation showed a clear dependence on moisture content, suggesting maintenance of a dry product is crucial for stability. Accordingly, pGlu formation increased when formulations were plasticized with water, however an increase was not observed when formulations were plasticized by glycerol, meaning there was not a clear effect of Tg on pGlu formation. These findings suggest that water may influence pGlu formation as a reaction medium (i.e., by altering polarity or the solvent dielectric) and Tg alone doesn't determine pGlu reactivity, leaving the opportunity for other forms of mobility.

Also in Chapter 3, peptide formulations with varying excipient and 'pH' were subjected to ssHDX-MS to determine a correlation, if any, with pGlu formation rates. The extent of deuterium incorporation ( $D_{\text{fast}}$  and  $D_{\text{fast}}+D_{\text{slow}}$ ) showed a moderate correlation with pGlu formation rates, which was most notable when comparing excipients. The results suggest that ssHDX-MS could be used as a broad screening tool for pGlu-prone formulations.

Despite the correlation between stability and ssHDX-MS here and elsewhere, the mechanism of exchange in ssHDX is not well understood. To meet this need, the final study in this dissertation investigated the effect of temperature, RH, and mobility on ssHDX kinetics. For lyophilized mAb formulated with varying levels of glycerol there was a strong linear correlation between kinetic parameters,  $D_{\text{fast}}$  and  $k_{\text{fast}}$ , and temperature and RH, but not on glycerol content, suggesting that mobility is not important for this reaction. However, there was a strong correlation with mobility (i.e., T-Tg). Next, a reversible first-order model for deuterium incorporation by ssHDX-MS was proposed in which the forward rate constant depends linearly on RH and temperature and is consistent with the results of this study. The model indicates that deuterium incorporation kinetic parameters are jointly proportional to RH and temperature. The dependence of kinetic parameters on RH and temperature is better described by this model than by a linear dependence on T-Tg. This finding suggests that the apparent mobility (T-Tg) dependence may simply be because both RH and temperature are imbedded in T-Tg. Moreover, the proposed model has implications for designing ssHDX-MS studies and a mechanistic interpretation of results.

## 5.2 Recommendations for Future Research

Given the outcomes of the present studies several recommendations can be made to deepen our understanding of pGlu formation and of ssHDX-MS as an analytical tool for probing solid-state protein formulations.

The 'pH'-rate profiles generated in Chapter 2 revealed a faster reaction rate in the solid state than solution state for pGlu formation in the range 'pH' 5.5-6, an unexpected finding. One hypothesis is that the opposing charges, on the Glu side chain and primary amine, that inhibit ring closure in the solution state in this 'pH' range are diminished in the solid environment. The barrier to ring closure is lessened and reaction rates are higher. Understanding the behavior of charge states in a solid environment is essential to understanding solid-state reactivity not only for pGlu formation, but also for other chemical instabilities of biopharmaceuticals.

To study pGlu formation, a model, unstructured peptide was used so that the mechanism could be investigated in the absence of higher order structure. The downside to this approach is that formulations were limited to low concentrations and solid content. A natural next step is to expand the investigation to larger, structured molecules. Differences in pGlu formation in IgG mAbs has previously been attributed to the local microenvironment created by the surrounding amino acids, specifically on its effect on the affinity for ring closure.<sup>1</sup> It is reasonable to assume that the formulation trends observed here, in particular 'pH', may also be affected by higher order structure.

In Chapter 3, the results suggest that pGlu formation does not depend on mobility as measured by Tg but leaves the possibility of influence from other forms of mobility (i.e.,  $\beta$ -relaxation). In this study, formulations were limited to low levels of glycerol (i.e., a narrow Tg range) due to the low peptide concentration and solid content. To repeat this investigation using a mAb would allow a wider Tg range and confirmation of the mobility effects observed here. Moreover, understanding the role that  $\beta$ -relaxation plays in the mechanism of pGlu formation, through neutron scattering or solid-state nuclear magnetic resonance (ssNMR), would benefit formulations scientists working to prevent this instability.

Hydroxyectoine was shown to provide greater protection against pGlu formation than trehalose in the solid state. This result is somewhat surprising considering the number of hydrogen bonding sites on trehalose compared to hydroxyectoine. Due to the low peptide concentration, these formulations were prepared at a S/P (i.e., sugar to protein weight ratio) higher than that

typically recommended for pharmaceutical stability (15 (w/w)).<sup>2</sup> Protection from stabilizing excipients is often concentration dependent, thus assessing other S/P may provide different results and a better understanding of the effectiveness of each excipient.<sup>3</sup>

Also in Chapter 3, a moderate correlation of the extent of deuterium incorporation with rates of pGlu formation was observed. To better understand ssHDX-MS as a potential screening tool for chemical instabilities, other degradation reactions should be examined. Two limitations of pGlu as a model reaction are that the amide hydrogen involved in the reaction is not captured by ssHDX-MS and that the reaction rates don't vary widely (~1-2 orders of magnitude) across the formulations investigated. Different results, and perhaps a better correlation, may be observed for proton transfer reactions that don't have these limitations. One such suggestion is asparagine deamidation, which has a well understood mechanism.

Many other facets of ssHDX-MS still need to be unraveled. In Chapter 4, a relationship between ssHDX-MS kinetic parameters and RH and temperature was established for formulations mainly in the glassy region. Extending this relationship into the rubbery region may reveal a different relationship and more about the mechanism of ssHDX. Moreover, this work described the effect of RH and temperature on the overall extent of deuterium incorporation, yet the effect on individual deuteration sites is still unclear. To understand whether deuteration sites are changing or simply increasing in number would improve interpretation of ssHDX-MS results. Lastly, understanding the 'pH'-dependence of the rate of exchange in ssHDX-MS would improve the application for formulations with varying 'pH'.

### 5.3 References

1. Seifert, F. et al. Glutaminyl Cyclases Display Significant Catalytic Proficiency for Glutamyl Substrates. *Biochemistry* 48, 11831–11833 (2009).
2. Carpenter, J., Pikal, M., Chang, B. & Randolph, T. Rational Design of Stable Lyophilized Protein Formulations.pdf. *Pharm. Res.* 14, 969–975 (1997).

## APPENDIX A. SUPPORTING INFORMATION FOR CHAPTER 2

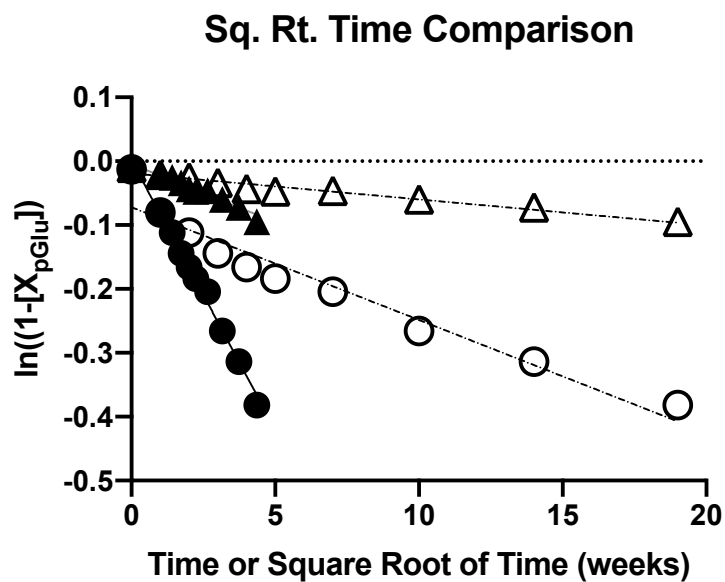


Figure A.1. Examples of kinetics of pGlu formation from EVQL peptide in solid formulations at ‘pH’ 4 (circles) and ‘pH’ 8 (triangles) at 50°C comparing square root of time and first order kinetics. Open symbols are plots versus time and filled symbols are plots versus the square root of time.

Table A.1. R-squared values of linear regression to fit first order kinetics and square root of time kinetics.

R-squared of Linear Regression		
‘pH’	First Order Kinetics	Square Root of Time Kinetics
4.0	0.9392	0.9887
8.0	0.9230	0.9388

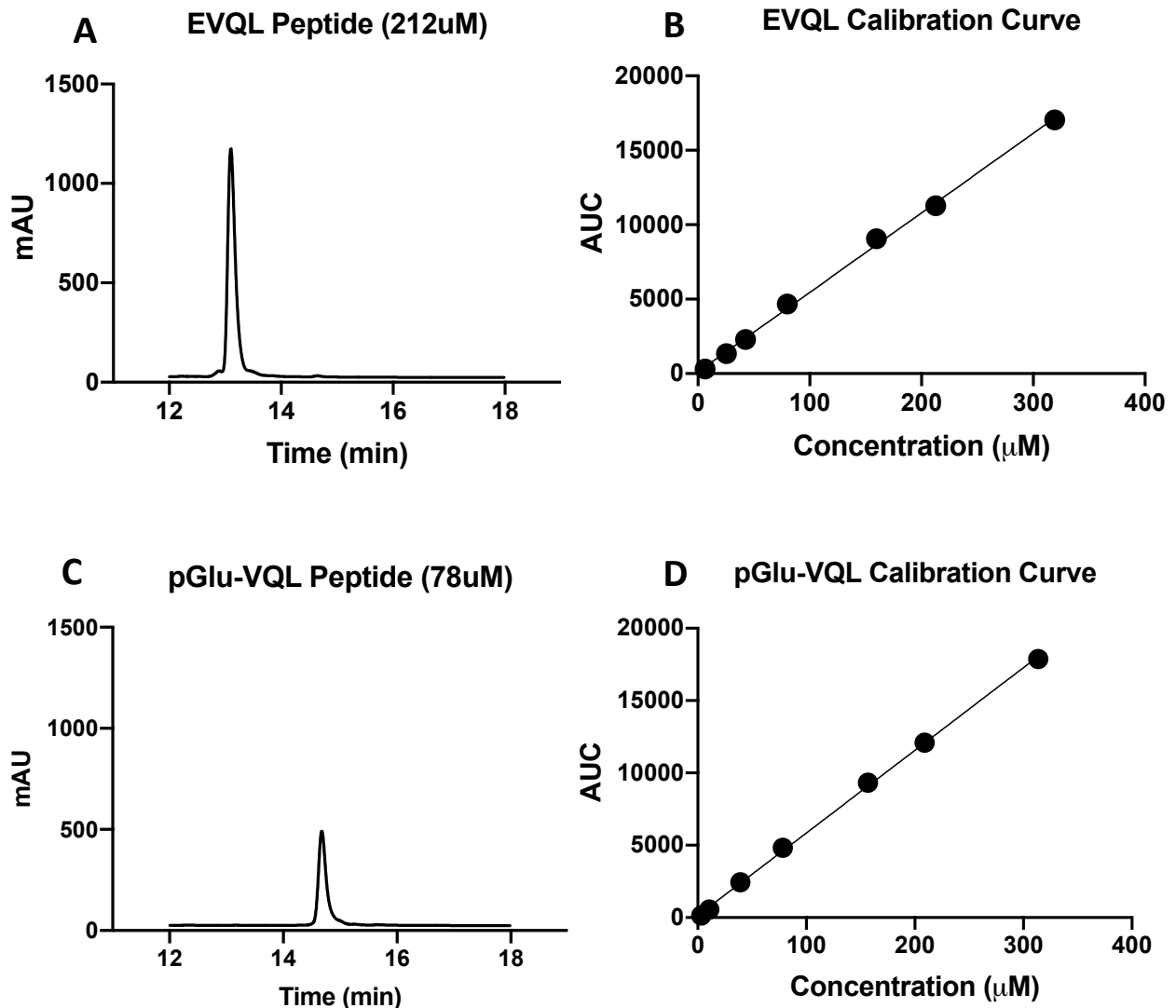


Figure A.2. Quantitation of EVQL and pGlu-VQL peptides by rp-HPLC. Representative rp-HPLC chromatogram for the EVQL peptide (EVQLVESGGGLVQPGGSLR) (A) and corresponding calibration curve relating peak area (AUC) to concentration. The regression line is  $AUC=53.42[EVQL]+111.8$  with an R-squared value of 0.9983 (B). Representative rp-HPLC chromatogram for the pGlu-VQL peptide (pGlu-VQLVESGGGLVQPGGSLR) (C) and corresponding calibration curve relating peak area (AUC) to concentration. The regression line is  $AUC=57.12*[pGlu-VQL]+137.1$  with an R-squared value of 0.9992. See text for chromatographic conditions. The y-intercepts of the regression lines represent the quantitation limit of this method. The limit is approximately  $2\mu M$  for both the EVQL and pGlu-VQL peptides. Values below this absorbance were not observed for either peptide throughout the study.

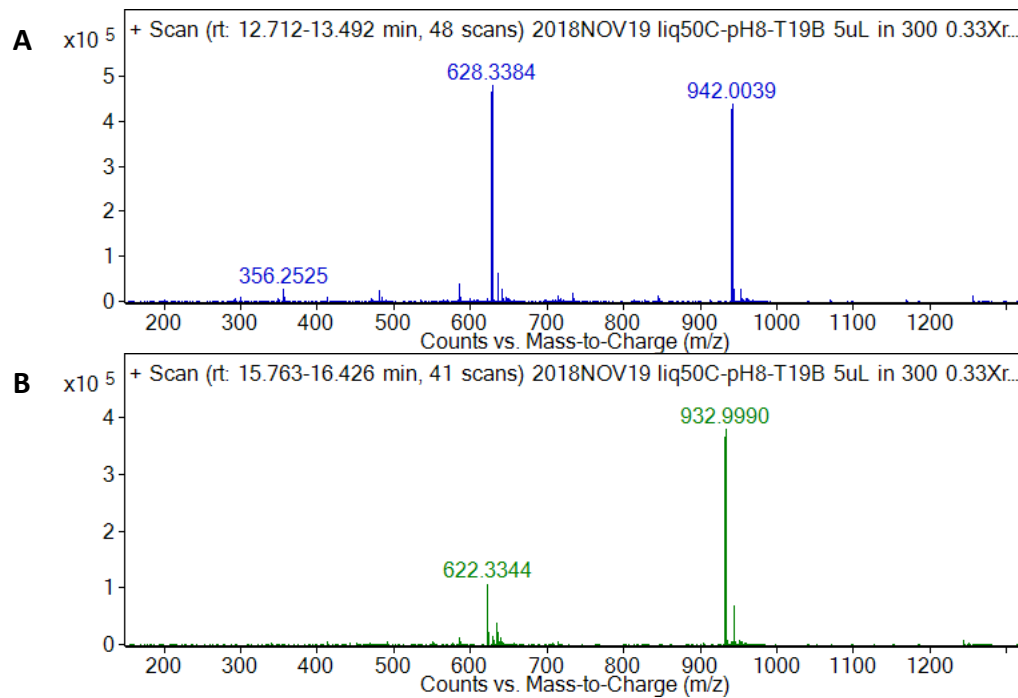


Figure A.3. Mass spectra of EVQL (A) and pGlu-VQL (B) in doubly and triply charged states. Peaks with  $m/z$  628.3384 and 942.0039 (A) correspond to a peptide mass of 1882 Da. Peaks with  $m/z$  622.3344 and 932.9990 (B) correspond to a peptide mass of 1864 Da, an 18 Da loss from the parent molecule.

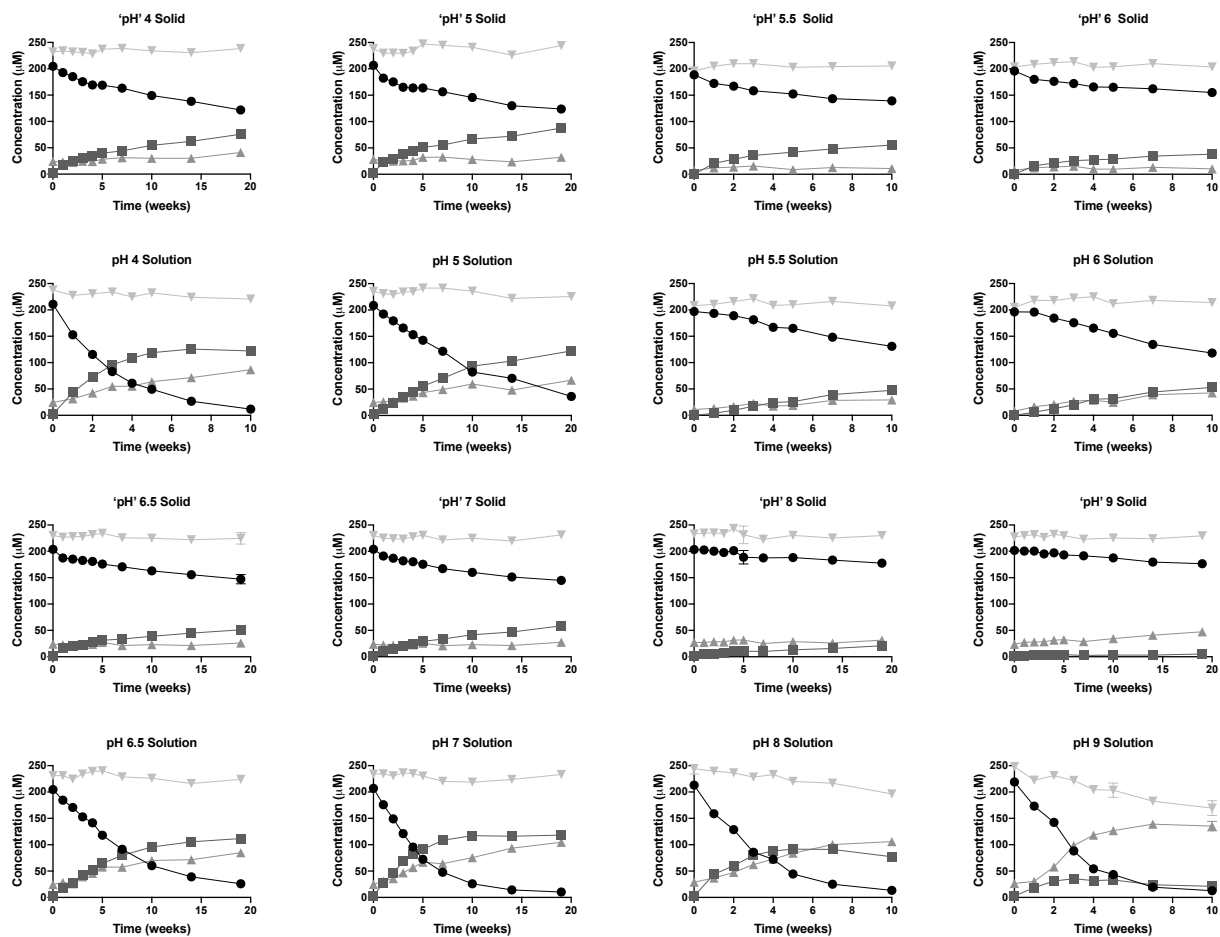


Figure A.4. Peptide concentration versus time profiles. Peptide concentrations including EVQL peptide (black circle), pGlu-VQL peptide (dark gray square), summed side products (gray triangle), and total peptide concentration (light gray inverted triangle) after incubation at 50°C formulated as a solid (A-D, I-L) and in solution (E-H, M-P) at ‘pH’ 4 (A, E), ‘pH’ 5 (B, F), ‘pH’ 5.5 (C, G), ‘pH’ 6 (D, H) ‘pH’ 6.5 (I, M), ‘pH’ 7 (J, N), ‘pH’ 8 (K, O), and ‘pH’ 9 (L, P). n=9 (3 replicate measurements of 3 vials), mean  $\pm$  S.D.

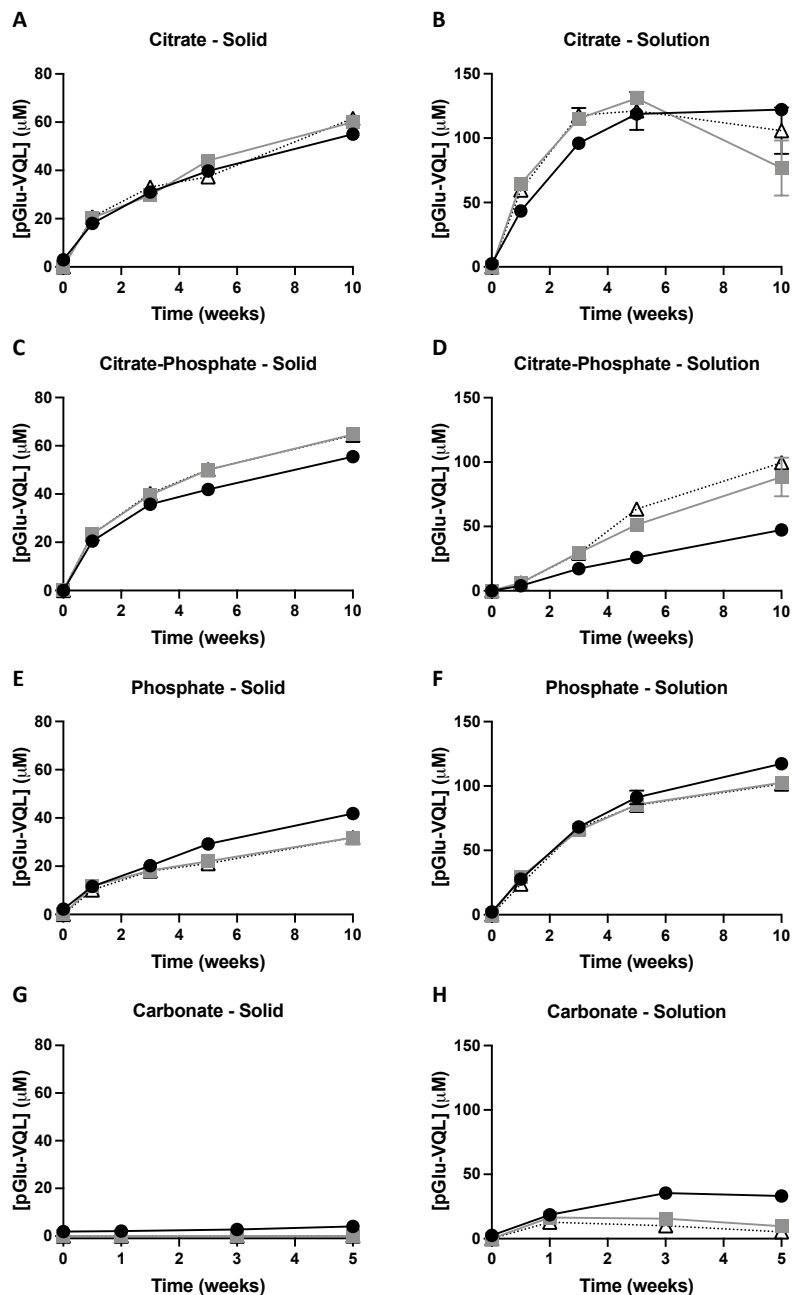


Figure A.5. pGlu-VQL peptide concentration in formulations with 20 mM (black circle), 40 mM (gray square), and 60 mM (open triangle) citrate buffer (A,B), citrate-phosphate buffer (C,D), phosphate buffer (E,F), and carbonate buffer (G,H) stored at 50°C as lyophilized solid (A,C,E,G) and in solution (B,D,F,H). n=9 (3 replicate measurements of 3 vials), mean ± S.D.

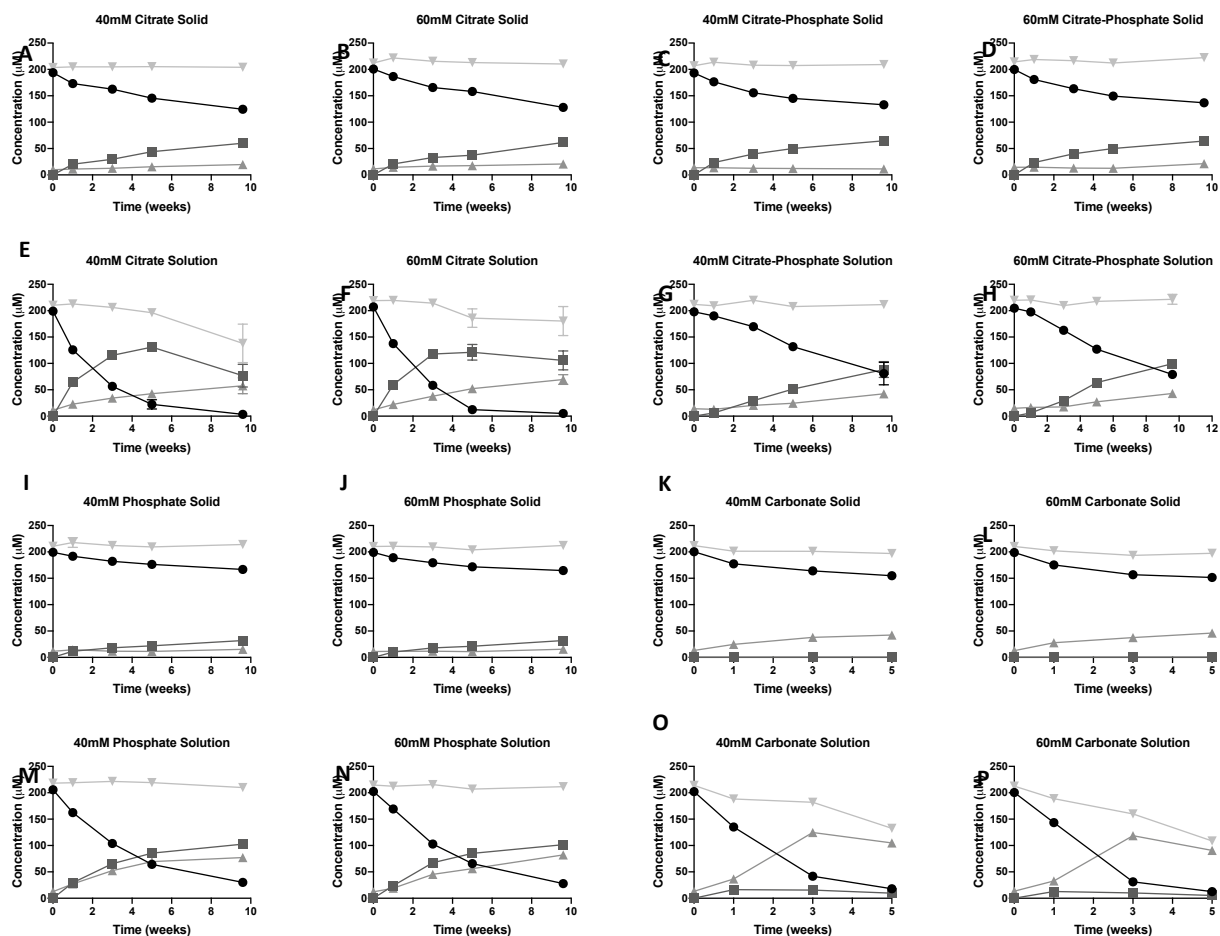


Figure A.6. Peptide concentration versus time profiles. Peptide concentrations including EVQL peptide (black circle), pGlu-VQL peptide (dark gray square), summed side products (gray triangle), and total peptide concentration (light gray inverted triangle) after incubation at 50°C formulated as a solid (A-D, I-L) and in solution (E-H, M-P). Formulations contain citrate (A, B, E, F), citrate-phosphate (C, D, G, H), phosphate (I, J, M, N), or carbonate (K, L, O, P) buffer at concentrations of 40 mM (A, C, E, G, I, K, M, O) or 60 mM (B, D, F, H, J, L, N, P).  $n=9$  (3 replicate measurements of 3 vials), mean  $\pm$  S.D.

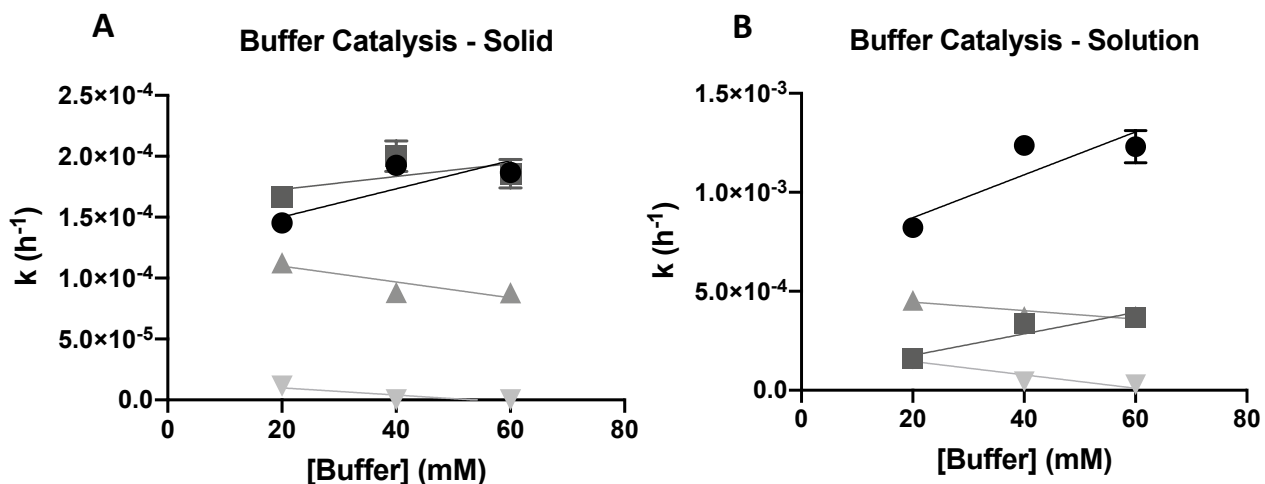


Figure A.7. pGlu formation rate constants ( $k$ ) versus buffer concentration for citrate (black circle), citrate-phosphate (dark gray square), phosphate (gray triangle), and carbonate (light gray inverted triangle) buffer systems with linear regression analysis. Rate constants determined by first order kinetics (Equation 2.1) for EVQL peptide stored as a lyophilized solid (A) and in solution (B). Error bars represent standard error of the regression fit to Equation 2.1.

Table A.2. Statistical analysis output of pGlu react rate versus buffer concentration linear regression.

Slope Significantly Non-Zero P-values				
Buffer System	Solid		Solution	
	Slope	P-Value	Slope	P-Value
Citrate	$1.16 \times 10^{-6}$	0.0008	$1.08 \times 10^{-5}$	0.0005
Citrate-Phosphate	$5.32 \times 10^{-7}$	0.2005	$5.43 \times 10^{-6}$	<0.0001
Phosphate	$-6.50 \times 10^{-7}$	0.0005	$-2.15 \times 10^{-6}$	0.0039
Carbonate	$-2.95 \times 10^{-7}$	<0.0001*	$-3.38 \times 10^{-6}$	0.0002

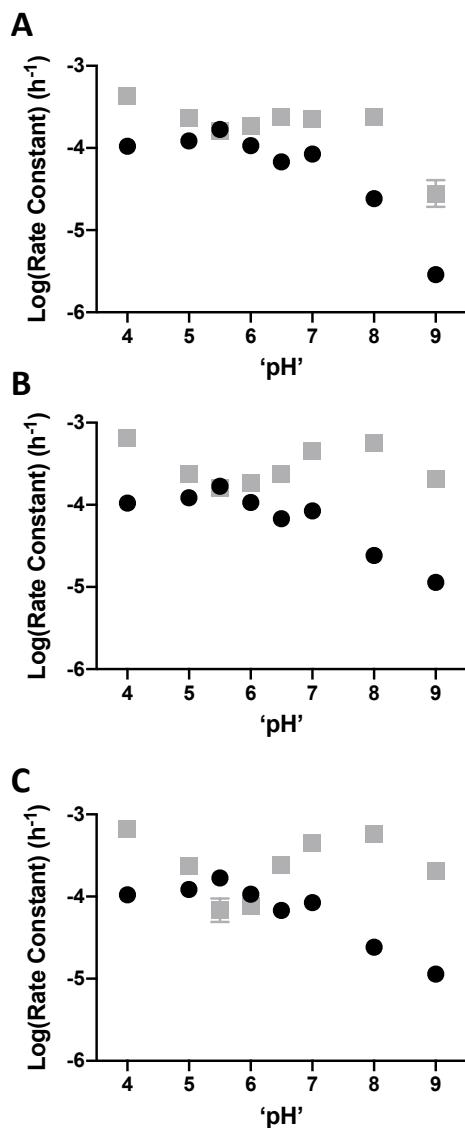


Figure A.8. 'pH'-rate profile for pGlu formation in lyophilized solid (black circle) and in solution (gray square) at 50°C. Rate constants are determined by a first order kinetic model (Equation 2.1). Absolute rate constants (A) include all time points and do not account for buffer catalysis. Truncated rate constants (B) exclude some later time points during regression analysis as described in the text. Rate constants were adjusted to zero buffer concentration (C) where applicable as described in text. Figure C is a duplicate of Figure 5 from the text for ease of comparison. Error bars represent standard error of the regression fit. Regardless of how the data is analyzed the overall 'pH' trends remain the same.

Table A.3. Tabulated rate constants for pGlu formation following first-order kinetics ( $k_{\text{obs}}$ ,  $k_{\text{trunc}}$ ,  $k_0$ ) and square root of time kinetics ( $k_{\text{sqrt}}$ ).

Rate Constant, k (h <sup>-1</sup> )							
'pH'	Buffer System	Observed ( $k_{\text{obs}}$ )		Truncated ( $k_{\text{trunc}}$ )		Adjusted to Zero Buffer Concentration ( $k_0$ )	Square Root Kinetics ( $k_{\text{sqrt}}$ )
		Solid	Solution	Solid	Solution	Solution	Solid
4	Citrate	1.05(±.03)*10 <sup>-4</sup>	4.36(±.29)*10 <sup>-4</sup>	--	6.58(±.25)*10 <sup>-4</sup>	--	6.51(±.07)*10 <sup>-3</sup>
5		1.22(±.04)*10 <sup>-4</sup>	2.35(±.04)*10 <sup>-4</sup>	--	--	--	7.74(±.07)*10 <sup>-3</sup>
5.5	Citrate-Phosphate	1.68(±.09)*10 <sup>-4</sup>	1.61(±.03)*10 <sup>-4</sup>	--	--	6.81(±2.26)*10 <sup>-5</sup>	7.73(±.07)*10 <sup>-3</sup>
6		1.07(±.06)*10 <sup>-4</sup>	1.86(±.03)*10 <sup>-4</sup>	--	--	7.71(±1.44)*10 <sup>-5</sup>	5.02(±.06)*10 <sup>-3</sup>
6.5	Phosphate	6.79(±.25)*10 <sup>-5</sup>	2.40(±.03)*10 <sup>-4</sup>	--	--	--	4.36(±.05)*10 <sup>-3</sup>
7		8.41(±.20)*10 <sup>-5</sup>	2.26(±.17)*10 <sup>-4</sup>	--	4.54(±.13)*10 <sup>-4</sup>	--	5.21(±.08)*10 <sup>-3</sup>
8		2.42(±.08)*10 <sup>-5</sup>	2.36(±.25)*10 <sup>-4</sup>	--	5.73(±.25)*10 <sup>-4</sup>	--	1.40(±.04)*10 <sup>-3</sup>
9	Carbonate	2.88(±.35)*10 <sup>-6</sup>	2.80(±.10)*10 <sup>-4</sup>	1.14(±.05)*10 <sup>-5</sup>	2.07(±.13)*10 <sup>-4</sup>	--	3.20(±.22)*10 <sup>-4</sup>

Table A.4. Moisture content (%) of solid samples as determined by Karl Fischer.

Moisture Content (%)							
'pH'	Buffer System	Buffer Concentration					
		20mM		40mM		60mM	
		Start	End	Start	End	Start	End
4	Citrate	0.52±0.74	2.04±0.44	1.03±0.12	--	1.04±0.02	1.00±0.10
5		2.26±1.22	2.38±0.31	--	--	--	--
5.5	Citrate-Phosphate	2.61±1.89	--	1.43±0.21	1.27±0.82	1.26±0.31	1.45±0.30
6		2.91±1.00	2.70±1.13	--	--	--	--
6.5	Phosphate	2.45±0.66	2.50±0.83	--	--	--	--
7		0.68±0.82	2.00±1.45	0.55±0.34	1.73±0.45	0.98±0.34	1.37±0.78
8		1.47±0.72	2.73±0.50	--	--	--	--
9	Carbonate	4.96±0.99	10.05±0.82	6.63±0.87	7.13±0.32	5.73±0.26	5.15±0.63

## APPENDIX B. SUPPORTING INFORMATION FOR CHAPTER 3

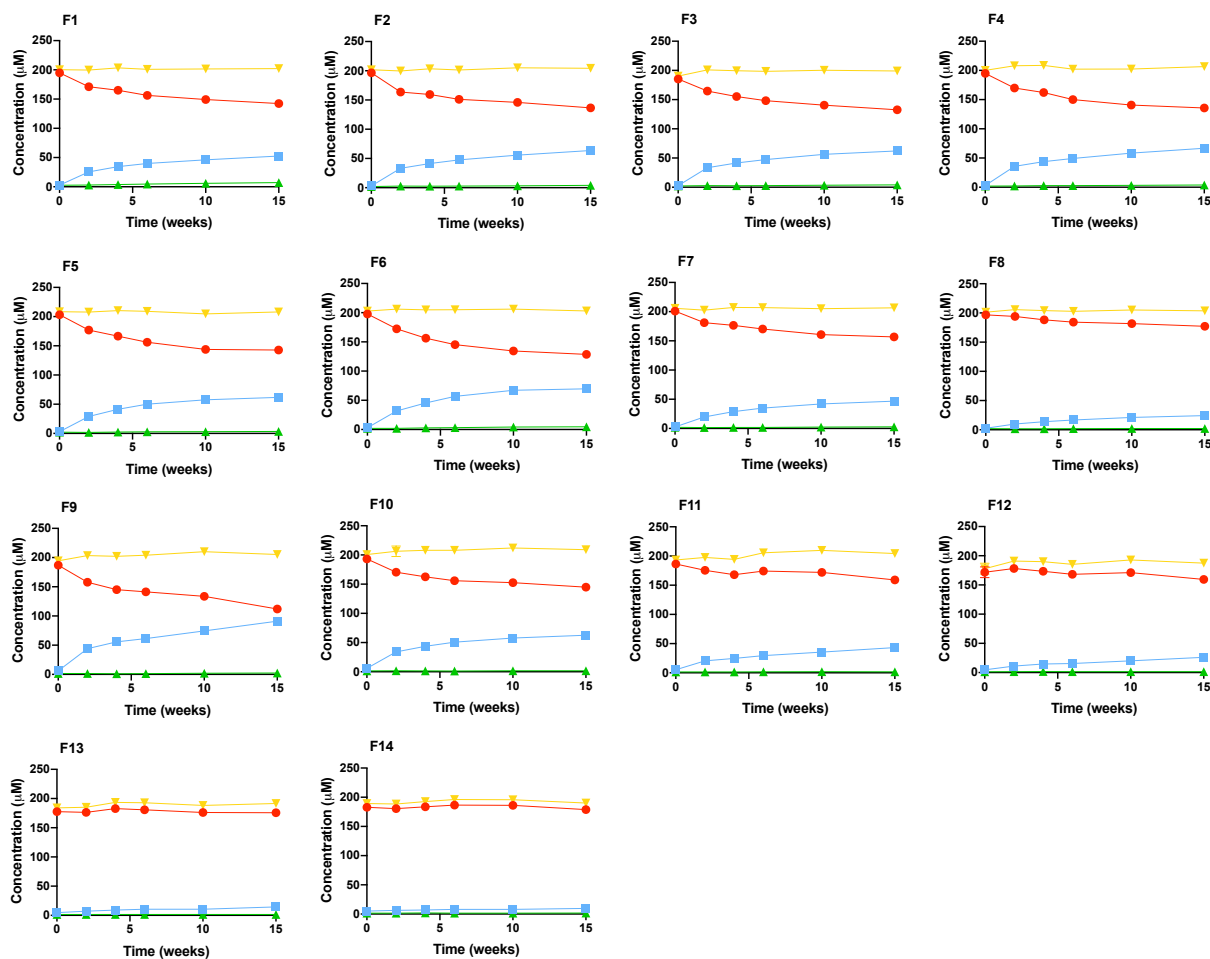


Figure B-1. Peptide concentration versus time profiles for lyophilized formulations. Peptide concentrations, including EVQL peptide (circles), pGlu-VQL peptide (squares), summed side products (triangles), and total peptide concentration (inverted triangles) after incubation at 50 °C. Formulations are defined in Table 3-1. n=9 (3 replicate measurements of 3 vials), mean  $\pm$  S.D.

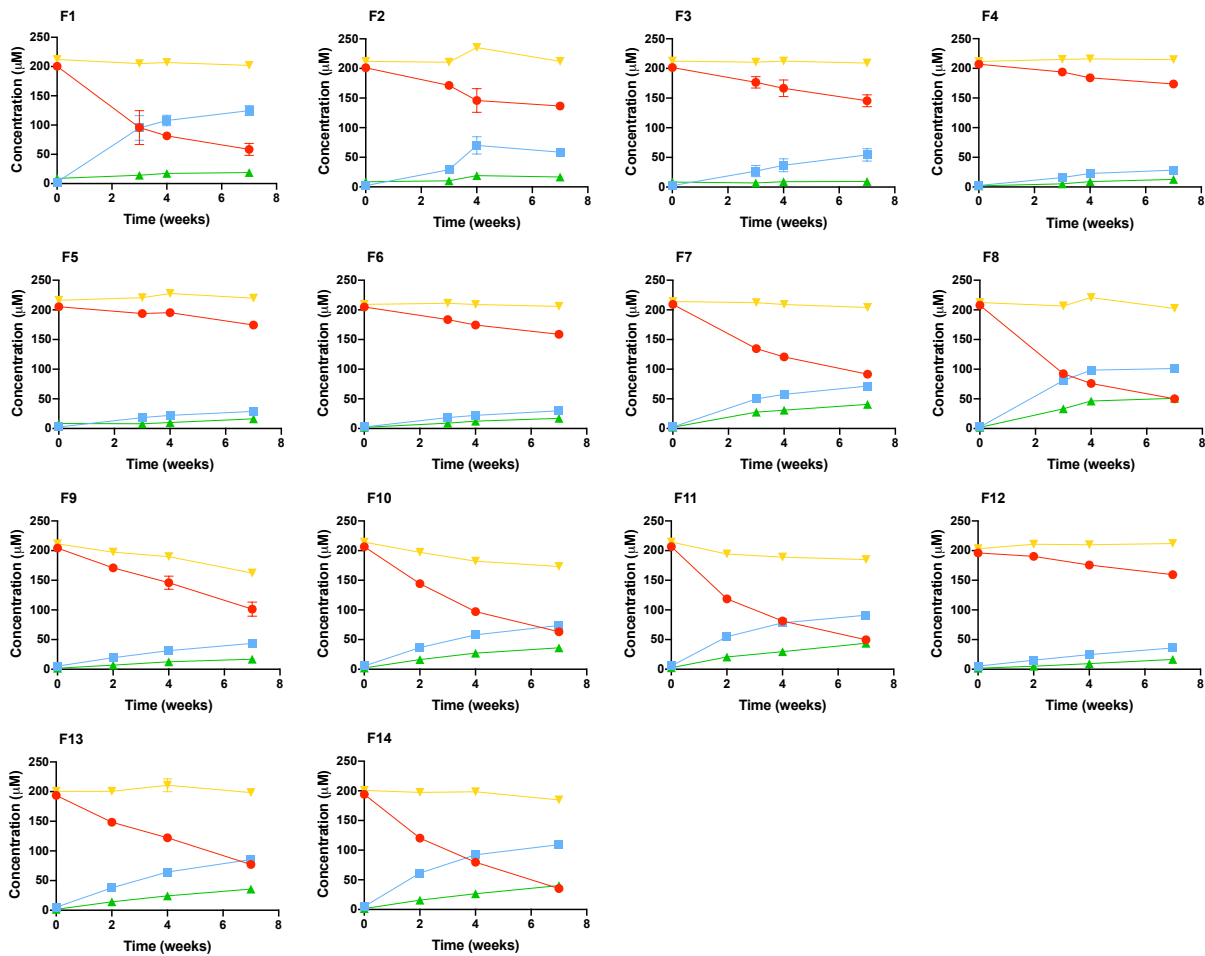


Figure B-2. Peptide concentration versus time profiles for solution controls. Peptide concentrations, including EVQL peptide (circles), pGlu-VQL peptide (squares), summed side products (triangles), and total peptide concentration (inverted triangles) after incubation at 50 °C. Formulations are defined in Table 3-1. n=9 (3 replicate measurements of 3 vials), mean  $\pm$  S.D.

Table B-1. Rate constants ( $k_{obs}$ ) calculated using a first-order kinetic model for pGlu formation in EVQL peptide in the solid and solution states and moisture content measured by Karl Fischer for all formulations at select timepoints (n=3, 3 replicate measurements of 1 vial, mean  $\pm$  S.D.)

Formulation ID	pH	Excipient	Rate Constant ( $k_{obs}$ )		Moisture Content		
			Solid	Solution	T0	10 weeks	15 weeks
F1	4	Trehalose	$1.00(\pm.07)*10^{-4}$	$5.79(\pm.91)*10^{-4}$	$2.80 \pm 0.48$	$2.10 \pm 0.05$	$2.04 \pm 0.14$
F2	5		$1.22(\pm.08)*10^{-4}$	$2.18(\pm.57)*10^{-4}$	$2.62 \pm 0.06$	$2.37 \pm 0.18$	$2.47 \pm 0.21$
F3	5		$1.24(\pm.08)*10^{-4}$	$2.41(\pm.36)*10^{-4}$	$2.79 \pm 0.33$	$2.70 \pm 0.14$	$2.19 \pm 0.34$
F4	5.5		$1.30(\pm.08)*10^{-4}$	$9.68(\pm.69)*10^{-5}$	$3.02 \pm 0.19$	$2.49 \pm 0.07$	$2.52 \pm 0.09$
F5	6		$1.23(\pm.08)*10^{-4}$	$8.83(\pm.40)*10^{-5}$	$2.85 \pm 0.24$	$2.82 \pm 0.32$	$2.68 \pm 0.17$
F6	6		$1.49(\pm.10)*10^{-4}$	$1.05(\pm.04)*10^{-4}$	$3.11 \pm 0.64$	$2.39 \pm 0.02$	$2.47 \pm 0.24$
F7	7		$8.92(\pm.50)*10^{-5}$	$2.77(\pm.15)*10^{-4}$	$3.17 \pm 0.23$	$2.87 \pm 0.11$	$3.53 \pm 0.49$
F8	8		$4.21(\pm.19)*10^{-5}$	$3.72(\pm.40)*10^{-4}$	$3.21 \pm 0.48$	$3.21 \pm 0.13$	$3.25 \pm 0.42$
F9	6	Dextran	$1.91(\pm.09)*10^{-4}$	$2.58(\pm.44)*10^{-4}$	$0.56 \pm 0.00$	2.67*	$3.14 \pm 0.54$
F10	7		$1.12(\pm.08)*10^{-4}$	$4.38(\pm.11)*10^{-4}$	$0.93 \pm 0.29$	2.29*	$3.08 \pm 0.97$
F11	8		$7.27(\pm.35)*10^{-5}$	$4.88(\pm.29)*10^{-4}$	$1.16 \pm 0.16$	2.42*	$1.84 \pm 0.82$
F12	6	Hydroxy-ectoine	$4.70(\pm.25)*10^{-5}$	$1.34(\pm.04)*10^{-4}$	$3.83 \pm 0.35$	4.11*	$3.55 \pm 0.69$
F13	7		$1.84(\pm.13)*10^{-5}$	$4.44(\pm.07)*10^{-4}$	$5.80 \pm 0.03$	4.54*	$5.35 \pm 0.61$
F14	8		$8.48(\pm.68)*10^{-6}$	$6.93(\pm.22)*10^{-4}$	$5.88 \pm 0.19$	4.91*	$4.30 \pm 0.70$

\*n=1, replicate measurements not collected.

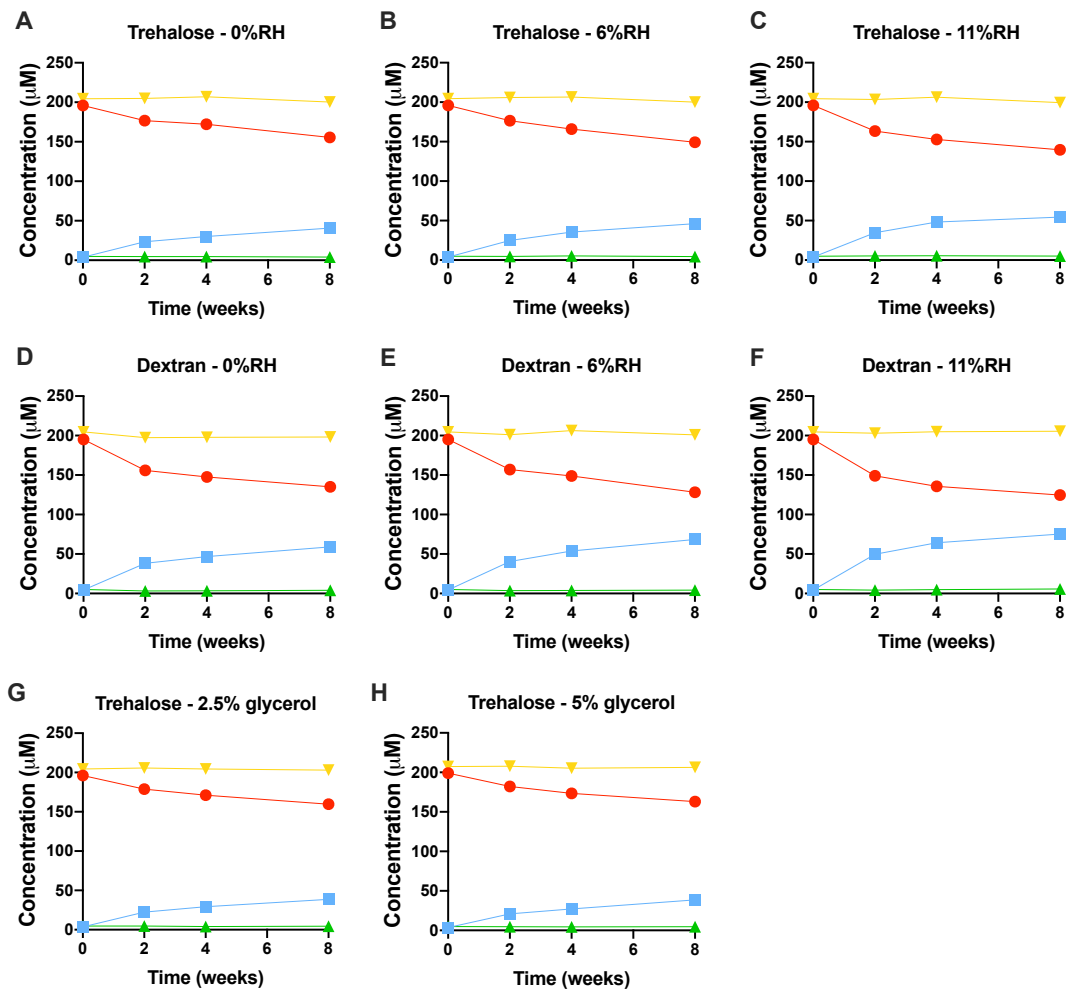


Figure B-3. Peptide concentration versus time profiles for moisture content and mobility investigation. Peptide concentrations, including EVQL peptide (circles), pGlu-VQL peptide (squares), summed side products (triangles), and total peptide concentration (inverted triangles) after incubation at 50 °C. Formulations are defined in Table 3-2. n=9 (3 replicate measurements of 3 vials), mean ± S.D.

Table B-2. Moisture content (%) of solid samples as determined by Karl Fischer. n=3 (3 replicate measurements of 1 vial), mean  $\pm$  S.D.

Excipient	Glycerol Content <sup>1</sup>	Storage RH	T0*	2 weeks	4 weeks	8 weeks
Trehalose	0	0% <sup>2</sup>	2.63	2.06 $\pm$ 0.44	1.56 $\pm$ 0.10	1.87 $\pm$ 0.28
		6%	--	3.12 $\pm$ 0.43	3.44 $\pm$ 0.36	3.65 $\pm$ 0.28
		11%	--	4.81 $\pm$ 0.55	4.99 $\pm$ 0.44	5.90 $\pm$ 0.74
Dextran	0	0% <sup>2</sup>	0.66	2.31 $\pm$ 0.87	1.63 $\pm$ 0.30	1.95 $\pm$ 0.44
		6%	--	3.84 $\pm$ 0.45	3.37 $\pm$ 0.70	3.63 $\pm$ 0.52
		11%	--	5.14 $\pm$ 0.81	5.73 $\pm$ 0.99	6.18 $\pm$ 0.37
Trehalose	2.5	0% <sup>2</sup>	3.00	1.64 $\pm$ 0.64	1.19 $\pm$ 0.24	2.25 $\pm$ 0.29
	5		3.91	1.92 $\pm$ 0.47	1.28 $\pm$ 0.06	2.07 $\pm$ 0.10

\* n=1, replicate measurements not collected.

<sup>1</sup>reported as percent (w/w) of trehalose content (i.e., 5% indicates 5% of 5.65%)

<sup>2</sup>samples stored under desiccant

Table B-3. Statistical analysis of moisture content and Tg on pGlu concentration using an ANOVA effect test. Moisture content and pGlu concentration from the 8-week timepoint were used for analysis. SST represents a relative degree of contribution to the output parameter for each experimental variable. Treatment p-value < 0.05 are significant.

Treatments Parameters	Parameter Estimate	Std Error	SST	Treatment p-value
Moisture content	7.00	1.49	79.23	0.0008
Tg	0.27	0.22	5.42	0.2467
Moisture content * Tg	0.02	0.12	0.13	0.8513

## APPENDIX C. SUPPORTING INFORMATION FOR CHAPTER 4

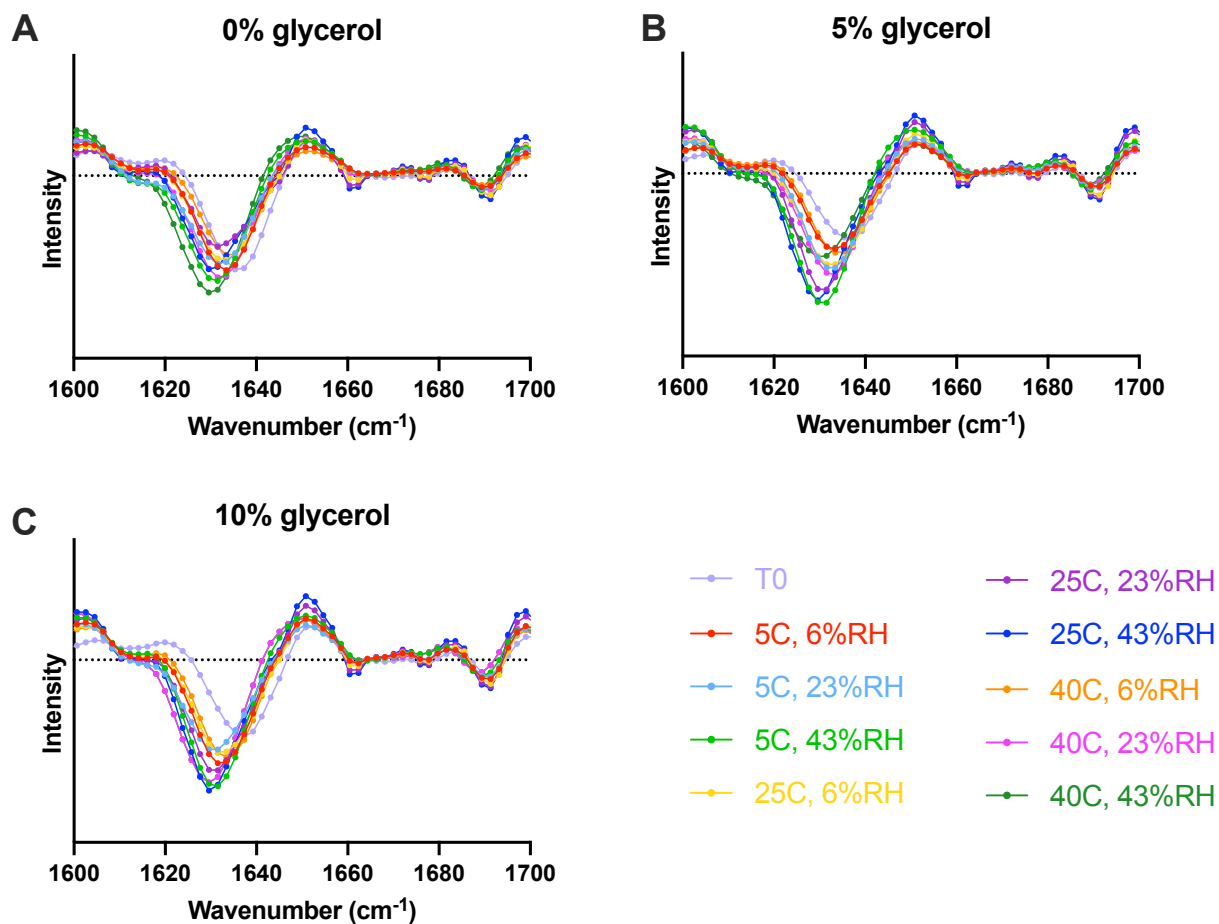


Figure C-1. Solid-state FTIR spectra of mAb formulations containing no glycerol (A), 5% glycerol (B), and 10% glycerol (C) immediately after lyophilization (T0) and after 10 d incubation at various combinations of temperature (5, 25, or 40 °C) and D<sub>2</sub>O RH (6, 23, or 43%).

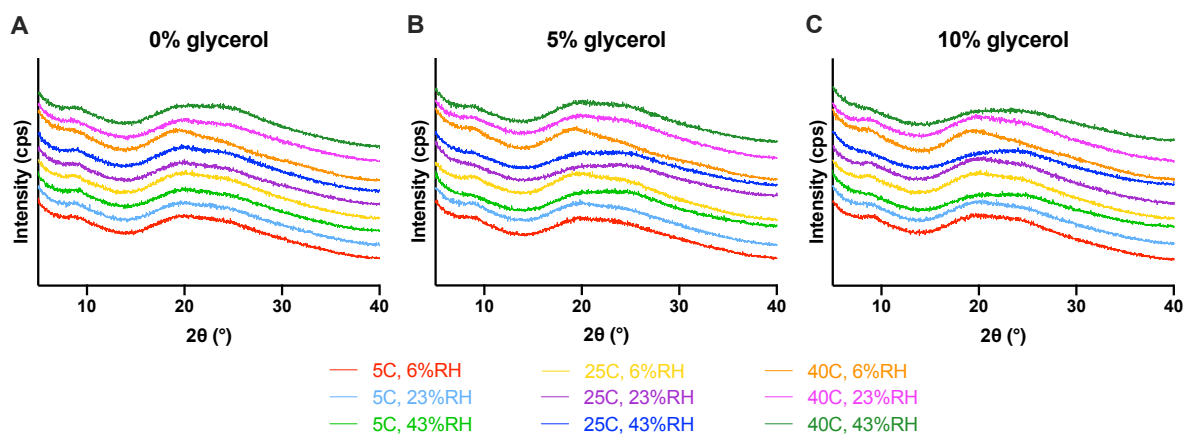


Figure C-2. PXRD diffractograms of lyophilized mAb containing no glycerol (A), 5% glycerol (B), and 10% glycerol (C) after 10 d incubation at various combinations of temperature (5, 25, or 40 °C) and D<sub>2</sub>O RH (6, 23, or 43%).

Table C-1. Mass change (%) of lyophilized mAb formulations containing 0%, 5%, and 10% glycerol measured by dynamic vapor sorption under fixed RH (6, 23, 43% RH) and temperature (5, 25, 40 °C) conditions. Samples were measured in triplicate at 25 °C to determine instrument variability.

RH	Temperature (°C)	Glycerol Content		
		0%	5%	10%
6%	5	2.380	2.033	2.600
	25	2.741	2.728	2.410
		3.020	2.663	2.700
		3.390	2.947	2.576
	40	2.137	2.352	2.120
23%	5	5.710	5.050	6.070
	25	6.313	5.986	5.630
		6.530	5.643	5.820
		7.200	6.129	5.671
	40	4.833	5.472	4.770
43%	5	9.690	8.691	11.420
	25	9.813	9.774	9.900
		10.510	9.220	10.230
		11.420	9.991	9.981
	40	7.844	9.625	9.150

Table C-2. P-values for two-way ANOVA of the effect of glycerol content and temperature on moisture uptake.

<b>RH</b>	<b>Factor</b>	<b>Prob &gt;  t </b>
<b>6%</b>	<b>Glycerol Content</b>	0.539
	<b>Temp</b>	0.577
	<b>Temp*Glycerol Content</b>	0.867
<b>23%</b>	<b>Glycerol Content</b>	0.205
	<b>Temp</b>	0.431
	<b>Temp*Glycerol Content</b>	0.888
<b>43%</b>	<b>Glycerol Content</b>	0.125
	<b>Temp</b>	0.421
	<b>Temp*Glycerol Content</b>	0.904

Table C-3. ANOVA effect tests of experimental variables (treatments), RH, glycerol content, and temperature, on moisture content and Tg values. SST represents a relative degree of contribution to the output parameter for each experimental variable. Treatment p-value < 0.05 are significant.

<b>Output Parameter</b>	<b>Experimental Factors</b>	<b>Parameter Estimate</b>	<b>Std Error</b>	<b>SST</b>	<b>Treatment p-value</b>
Moisture content	RH	4.28	0.25	331.11	<0.0001
	Glycerol content	-0.14	0.25	0.34	0.5853
	Temperature	7.99	0.25	7.10	0.0138
Tg	RH	-17.64	1.86	5614.77	<0.0001
	Glycerol content	-7.16	1.86	921.49	0.0008
	Temperature	2.45	1.85	108.75	0.1992

Table C-4. Linear regression parameters and statistical analysis for non-zero slopes for ssHDX kinetic parameters  $D_{\text{fast}}$  and  $k_{\text{fast}}$  versus experimental variables temperature and RH. Preliminary analysis revealed that regression slopes were not significantly different across glycerol levels for each condition, thus glycerol levels were pooled for each experimental condition during regression. (i.e., one slope and y-intercept are reported for 0, 5, and 10% glycerol at each condition). Statistical significance determined as  $p < 0.05$ .

Reference Figure in Text	ssHDX kinetic parameter	Primary variable (x-values)	Secondary variable level	Slope $\pm$ SE	y-intercept $\pm$ SE	R <sup>2</sup>	Significantly non-zero slope
Figure 3A	$D_{\text{fast}}$	Temperature	6% RH	$4.34 \pm 0.44$	$68.4 \pm 12.1$	0.93	Significant, $p < 0.0001$
			23% RH	$5.38 \pm 0.59$	$158.2 \pm 16.3$	0.92	Significant, $p < 0.0001$
			43% RH	$3.13 \pm 0.51$	$370.2 \pm 13.7$	0.85	Significant, $p < 0.0001$
Figure 3B		RH	5 °C	$7.74 \pm 0.66$	$35.7 \pm 18.8$	0.95	Significant, $p < 0.0001$
			25 °C	$8.07 \pm 0.39$	$109.5 \pm 11.0$	0.98	Significant, $p < 0.0001$
			40 °C	$6.42 \pm 0.53$	$217.8 \pm 15.1$	0.95	Significant, $p = 0.0004$
Figure 4A	$k_{\text{fast}}$	Temperature	6% RH	$0.0033 \pm 0.0004$	$0.006 \pm 0.010$	0.92	Significant, $p = 0.0002$
			23% RH	$0.0084 \pm 0.0009$	$0.008 \pm 0.024$	0.93	Significant, $p < 0.0001$
			43% RH	$0.0191 \pm 0.0016$	$0.019 \pm 0.002$	0.96	Significant, $p < 0.0001$
Figure 4B		RH	5 °C	$0.0012 \pm 0.0001$	$0.027 \pm 0.005$	0.88	Significant, $p < 0.0001$
			25 °C	$0.0073 \pm 0.0004$	$0.016 \pm 0.012$	0.98	Significant, $p < 0.0001$
			40 °C	$0.0165 \pm 0.0009$	$0.027 \pm 0.025$	0.98	Significant, $p < 0.0001$

Table C-5. Statistical analysis of slopes of  $D_{fast}$  and  $k_{fast}$  versus RH and temperature (Figure 4-3, Figure 4-4). Glycerol levels were pooled for each experimental condition during regression.

<b>Reference Figure in Text</b>	<b>Statistical comparison</b>	<b>F-value</b>	<b>p-value</b>	<b>Significant difference between slopes</b>
Figure 3A	6, 23, and 43 %RH for $D_{fast}$ vs temperature	4.768	0.0196	Significant
Figure 3B	5, 25, and 40 °C for $D_{fast}$ vs RH	2.644	0.0946	Not significant*
Figure 4A	6, 23, and 43 %RH for $k_{fast}$ vs temperature	58.11	<0.0001	Significant
Figure 4B	5, 25, and 40 °C for $k_{fast}$ vs RH	182.7	<0.0001	Significant

\*Because the slopes are not different, test if the intercepts are also equal? F-value = 74.44, p-value < 0.0001. The difference between intercepts is extremely significant.

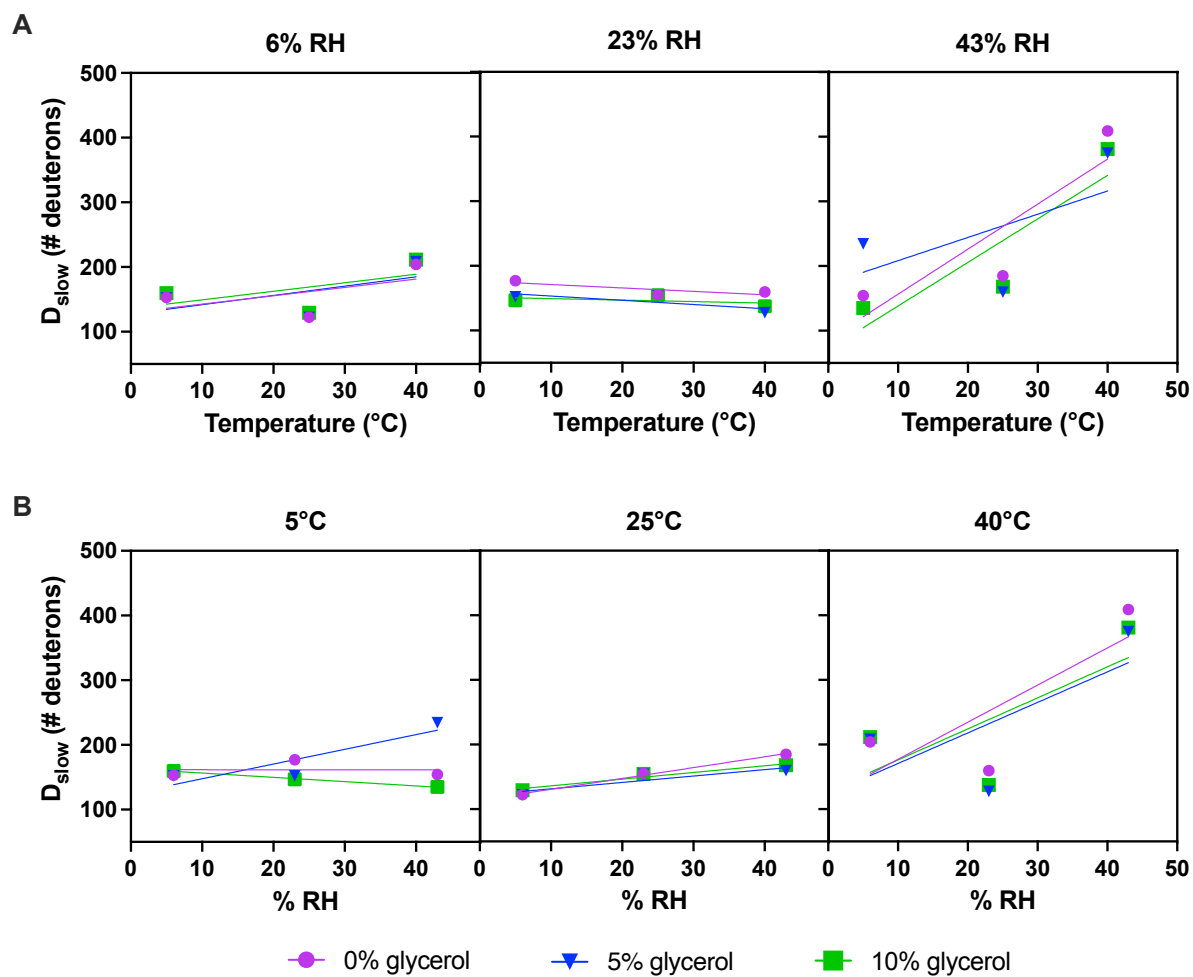


Figure C-3.  $D_{\text{slow}}$  values (Eq 4.1) as a function of temperature (A) and RH (B) for trehalose-mAb formulations containing 0% glycerol (purple circles), 5% glycerol (blue triangles), and 10% glycerol (green squares).

Table C-6. Linear regression parameters and statistical analysis for non-zero slopes for  $D_{\text{slow}}$  and  $k_{\text{slow}}$  versus experimental variables temperature and RH. Preliminary analysis revealed that regression slopes were not significantly different across glycerol levels for each condition, thus glycerol levels were pooled for each experimental condition during regression. (i.e., one slope and y-intercept are reported for 0, 5, and 10% glycerol at each condition). Statistical significance determined as  $p < 0.05$ .

Reference Figure	ssHDX kinetic parameter	Primary variable (x-values)	Secondary variable level	Slope $\pm$ SE	y-intercept $\pm$ SE	R <sup>2</sup>	Significantly non-zero slope
Figure S3A	$D_{\text{slow}}$	Temperature	6% RH	$1.35 \pm 0.76$	$131.1 \pm 20.7$	0.31	Not significant, $p = 0.1176$
			23% RH	$-0.47 \pm 0.30$	$162.6 \pm 8.09$	0.27	Not significant, $p = 0.1551$
			43% RH	$5.77 \pm 1.71$	$110.0 \pm 46.9$	0.62	Significant, $p = 0.0120$
Figure S3B		RH	5 °C	$0.54 \pm 0.65$	$149.9 \pm 18.5$	0.09	Not significant, $p = 0.4401$
			25 °C	$1.24 \pm 0.19$	$120.4 \pm 5.34$	0.86	Significant, $p = 0.0003$
			40 °C	$5.09 \pm 1.78$	$123.8 \pm 50.5$	0.54	Significant, $p = 0.0243$
Figure S4A	$k_{\text{slow}}$	Temperature	6% RH	$1.84(\pm 0.56) \cdot 10^{-4}$	$0.0049 \pm 0.0015$	0.61	Significant, $p = 0.0131$
			23% RH	$4.70(\pm 1.45) \cdot 10^{-4}$	$0.0053 \pm 0.0040$	0.60	Significant, $p = 0.0140$
			43% RH	$2.11(\pm 1.18) \cdot 10^{-4}$	$0.0059 \pm 0.0032$	0.32	Not significant, $p = 0.0120$
Figure S4B		RH	5 °C	$-6.29(\pm 6.23) \cdot 10^{-5}$	$0.0085 \pm 0.0018$	0.13	Not significant, $p = 0.3460$
			25 °C	$2.45(\pm 0.45) \cdot 10^{-4}$	$0.0062 \pm 0.0013$	0.81	Significant, $p = 0.0010$
			40 °C	$-0.81(\pm 2.04) \cdot 10^{-4}$	$0.0192 \pm 0.0058$	0.02	Not significant, $p = 0.7021$

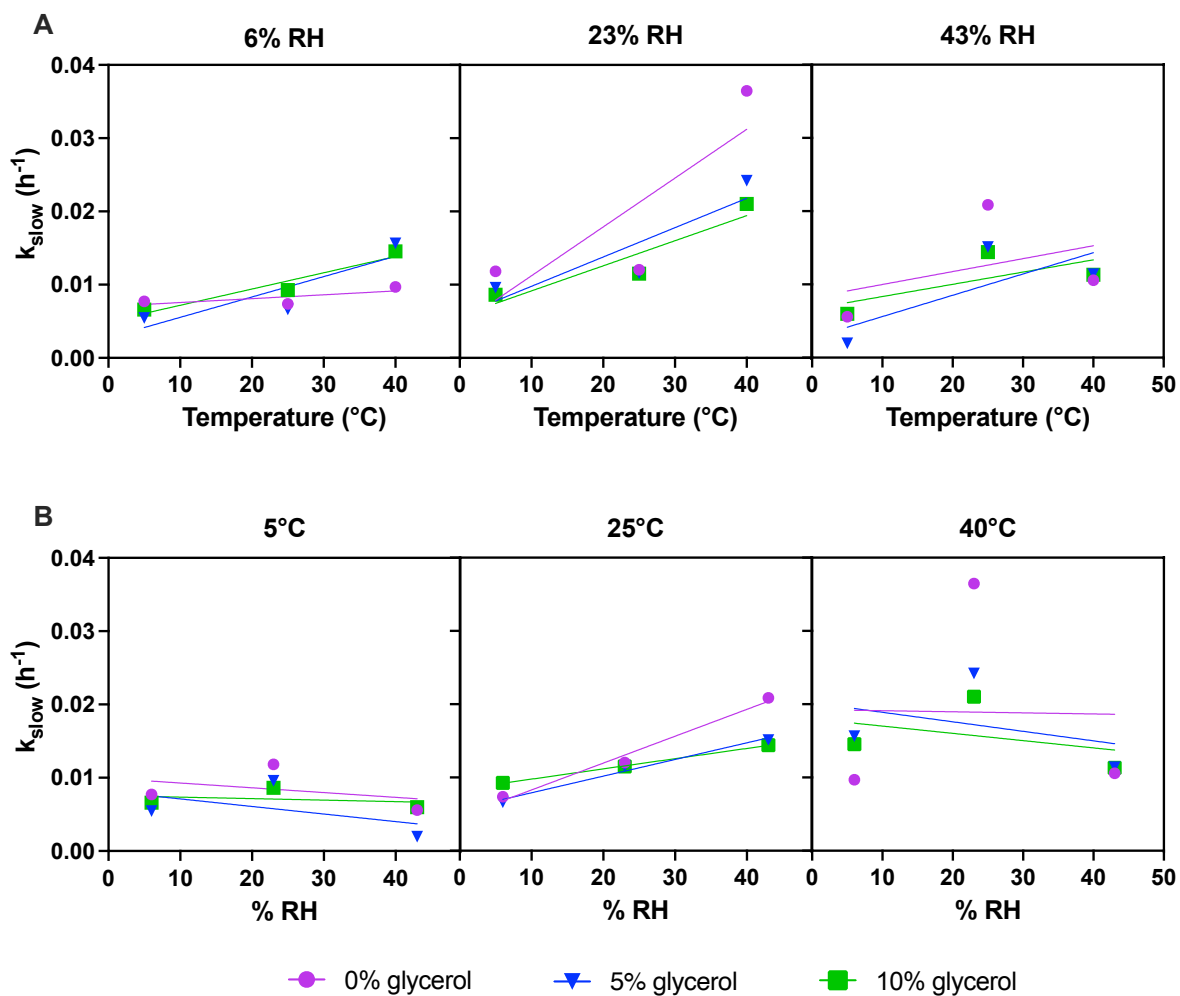


Figure C-4.  $k_{slow}$  values (Eq. 4.2) as a function of temperature (A) and RH (B) for trehalose-mAb formulations containing 0% glycerol (purple circles), 5% glycerol (blue triangles), and 10% glycerol (green squares).

Table C-7. ANOVA of experimental factors (treatments) RH, temperature, and glycerol content on ssHDX-MS parameters  $D_{\text{slow}}$  and  $k_{\text{slow}}$ . Variables with  $p > 0.05$  were eliminated from the fit model.

<b>Output Parameter</b>	<b>ANOVA p-value</b>	<b>Experimental Factors</b>	<b>Parameter Estimate</b>	<b>Std Error</b>	<b>SST</b>	<b>Treatment p-value</b>
<b><math>D_{\text{slow}}</math></b>	<b>0.001</b>	<b>RH</b>	40.38	13.81	29314.49	0.0076
		<b>Temp</b>	39.85	13.76	28744.26	0.0082
		<b>RH*Temp</b>	40.48	16.83	19838.13	0.0246
<b><math>k_{\text{slow}}</math></b>	<b>0.001</b>	<b>Temp</b>	$5.05 \cdot 10^{-3}$	$1.36 \cdot 10^{-3}$	$4.62 \cdot 10^{-4}$	0.001

Table C-8. Contribution of the fast process to total deuterium uptake for all formulations calculated using the biexponential model (Eq. 4.2). In 122 of 164 time points (~75%) the fast process contributed to at least 70% of the overall deuterium incorporation and are highlighted in green.

	0% Glycerol				5% Glycerol				10% Glycerol			
	Time (h)	Calculated values		% due to fast phase	Time (h)	Calculated values		% due to fast phase	Time (h)	Calculated values		% due to fast phase
		Fast portion	Slow portion			Fast portion	Slow portion			Fast portion	Slow portion	
5 °C, 6% RH	6	17.22	6.93	71%	6	17.80	4.91	78%	6	15.54	6.21	71%
	12	31.56	13.55	70%	12	32.52	9.65	77%	12	28.37	12.18	70%
	24	53.46	25.90	67%	24	54.73	18.70	75%	24	47.73	23.43	67%
	48	79.20	47.41	63%	48	80.27	35.09	70%	48	69.93	43.42	62%
	120	100.41	92.50	52%	120	100.34	73.16	58%	120	87.29	87.45	50%
	240	103.01	129.15	44%	240	102.56	111.14	48%	240	89.19	127.03	41%
	360	103.08	143.67	42%	360	102.61	130.86	44%	360	89.23	144.94	38%
5 °C, 23% RH	6	56.58	12.12	82%	6	52.68	8.50	86%	6	53.33	7.41	88%
	12	93.68	23.41	80%	12	90.28	16.53	85%	12	92.68	14.44	87%
	24	133.93	43.73	75%	24	136.28	31.26	81%	24	143.13	27.46	84%
	48	158.67	76.66	67%	48	171.65	56.10	75%	48	185.56	49.78	79%
	120	164.24	134.21	55%	120	183.84	103.95	64%	120	202.97	94.66	68%
	240	164.27	166.73	50%	240	184.05	136.84	57%	240	203.43	128.27	61%
5 °C, 43% RH	6	134.06	5.08	96%	6	134.80	2.73	98%	6	145.29	4.76	97%
	12	217.05	9.98	96%	12	223.91	5.43	98%	12	237.46	9.35	96%
	24	300.24	19.32	94%	24	321.75	10.74	97%	24	333.05	18.05	95%
	48	344.34	36.22	90%	48	383.20	20.99	95%	48	387.01	33.68	92%
	120	351.91	75.25	82%	120	397.60	49.00	89%	120	397.39	69.14	85%
	240	351.94	113.78	76%	240	397.70	87.76	82%	240	397.44	102.90	79%

Table C-8 continued

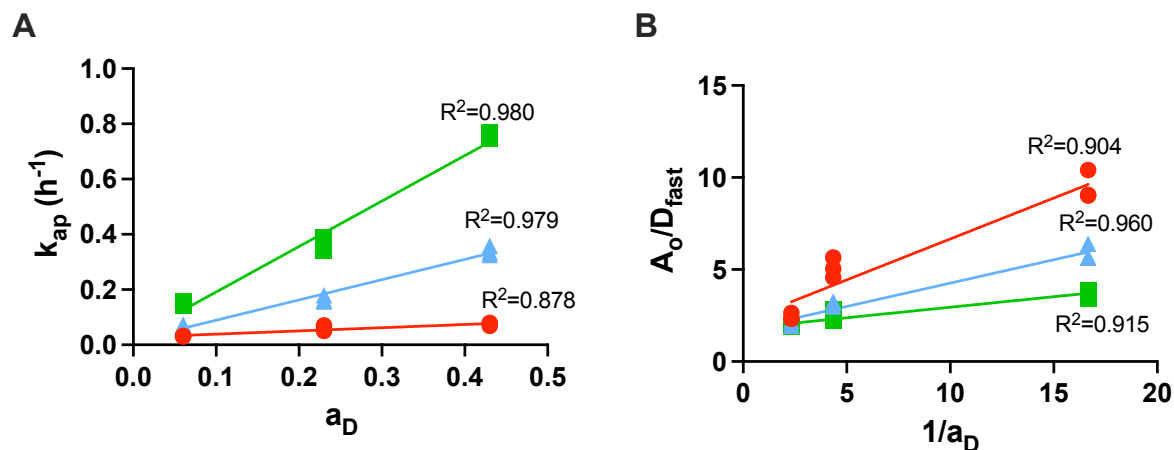
<b>25 °C, 6% RH</b>	6	57.61	5.31	92%	6	52.35	4.77	92%	6	51.59	6.99	88%
	12	95.05	10.39	90%	12	87.94	9.36	90%	12	84.84	13.60	86%
	24	135.20	19.89	87%	24	128.58	18.00	88%	24	120.09	25.77	82%
	48	159.31	36.55	81%	48	156.04	33.34	82%	48	140.83	46.40	75%
	120	164.52	71.99	70%	120	163.42	67.11	71%	120	145.13	86.74	63%
	240	164.55	101.68	62%	240	163.50	97.37	63%	240	145.15	115.27	56%
<b>25 °C, 23% RH</b>	6	187.15	10.83	95%	6	181.87	10.31	95%	6	189.69	10.30	95%
	12	250.98	20.91	92%	12	250.35	19.93	93%	12	263.64	19.92	93%
	24	280.17	39.00	88%	24	285.83	37.28	88%	24	303.71	37.27	89%
	48	283.96	68.22	81%	48	291.57	65.54	82%	48	310.73	65.55	83%
	120	284.01	118.75	71%	120	291.69	115.48	72%	120	310.89	115.63	73%
	240	284.01	146.73	66%	240	291.69	144.36	67%	240	310.89	144.70	68%
<b>25 °C, 43% RH</b>	6	375.29	21.75	95%	6	401.67	13.84	97%	6	412.85	13.93	97%
	12	418.89	40.94	91%	12	458.71	26.47	95%	12	468.05	26.70	95%
	24	424.54	72.80	85%	24	467.96	48.56	91%	24	476.42	49.15	91%
	48	424.62	116.92	78%	48	468.15	82.35	85%	48	476.57	83.92	85%
	120	424.62	169.68	71%	120	468.15	133.63	78%	120	476.57	138.22	78%
	240	424.62	183.54	70%	240	468.15	155.45	75%	240	476.57	162.71	75%
<b>40 °C, 6% RH</b>	6	155.86	11.53	93%	6	145.05	18.65	89%	6	149.13	17.70	89%
	12	221.81	22.41	91%	12	202.11	35.63	85%	12	208.98	33.92	86%
	24	261.52	42.35	86%	24	233.38	65.16	78%	24	242.64	62.40	80%
	48	269.90	75.90	78%	48	238.97	109.94	68%	48	248.93	106.40	70%
	120	270.18	140.25	66%	120	239.10	176.36	58%	120	249.10	174.73	59%
	240	270.18	184.04	59%	240	239.10	203.37	54%	240	249.10	205.19	55%
<b>40 °C, 23% RH</b>	6	298.37	31.38	90%	6	326.32	17.26	95%	6	359.42	16.30	96%
	12	327.35	56.60	85%	12	366.66	32.18	92%	12	405.77	30.66	93%
	24	330.43	93.14	78%	24	372.26	56.26	87%	24	412.51	54.49	88%
	48	330.46	131.96	71%	48	372.34	87.72	81%	48	412.63	87.40	83%
	120	330.46	157.71	68%	120	372.34	120.68	76%	120	412.63	126.51	77%
	240	330.46	159.69	67%	240	372.34	127.28	75%	240	412.63	136.67	75%

Table C-8 continued

<b>40 °C, 43% RH</b>	3	434.79	12.77	97%	3	443.70	12.60	97%	3	441.03	12.72	97%
	6	481.28	25.15	95%	6	487.72	24.77	95%	6	487.30	25.01	95%
	12	486.78	48.74	91%	12	492.51	47.91	91%	12	492.66	48.38	91%
	24	486.85	91.68	84%	24	492.56	89.69	85%	24	492.72	90.61	84%
	48	486.85	162.81	75%	48	492.56	157.91	76%	48	492.72	159.68	76%
	120	486.85	294.03	62%	120	492.56	279.29	64%	120	492.72	283.03	64%
	240	486.85	376.68	56%	240	492.56	350.39	58%	240	492.72	355.86	58%

In Figure C-5A, the slopes of the fit lines ( $k_f^*$ ) increase with temperature indicating a stronger dependence of  $k_f^*$  on  $a_D$  at higher temperature and thus  $k_f^*$  is also dependent on temperature. In fact, there is a strong linear dependence ( $R^2=0.963$ ) of the slopes of Figure C-5A ( $k_f^*$ ) on temperature, suggesting a linear relationship between ssHDX exchange rates and temperature. Moreover, the y-intercepts, representing  $k_b$ , (Equation 4.5, Chapter 4) are not significantly different from each other and at 25 °C and 40 °C the values are not significantly different from zero (Figure C-5A), which suggests that either  $k_b$  is independent of temperature or that  $k_b$  values are too small to observe a notable temperature effect.

In Figure C-5B, the slopes of the fit lines ( $k_b/k_f^*$ ) also trend linearly with temperature ( $R^2=1.00$ ) further supporting a linear dependence of ssHDX on temperature. Because the slope here is a ratio of the forward and reverse rate constants, the change in slope with temperature also suggests that temperature does not influence the forward and reverse reactions equally. The  $k_b$  values for each temperature can be estimated as the product of slopes in Figure C-5A and Figure C-5B (i.e.,  $k_b = (1/K)k_f^*$ ). The resulting values are not significantly different, again suggesting that  $k_b$  is independent of temperature, at least in the practical range of ssHDX experiments.



Temperature (°C)	$K_{ap}$ versus $a_D$ (Panel A)			$A_0/D_{fast}$ versus $1/a_D$ (Panel B)		
	Slope $\pm$ SE (h <sup>-1</sup> )	Y-intercept $\pm$ SE (h <sup>-1</sup> )	R <sup>2</sup>	Slope $\pm$ SE (h <sup>-1</sup> )	Y-intercept $\pm$ SE (h <sup>-1</sup> )	R <sup>2</sup>
5	0.12 $\pm$ 0.02	0.027 $\pm$ 0.005	0.89	0.45 $\pm$ 0.05	2.21 $\pm$ 0.51	0.92
25	0.73 $\pm$ 0.04	0.016 $\pm$ 0.012	0.98	0.25 $\pm$ 0.02	1.73 $\pm$ 0.20	0.96
40	1.65 $\pm$ 0.88	0.027 $\pm$ 0.025	0.98	0.11 $\pm$ 0.01	1.81 $\pm$ 0.14	0.90

Figure C-5. Apparent exchange rate constant ( $k_{ap}$ ) as a function of  $a_D$  (A) and  $A_0/D_{fast}$  as a function of  $1/a_D$  (B) for lyophilized mAb formulations analyzed at 5 °C (red), 25 °C (blue), and 40 °C (green), where  $a_D = (\% \text{ RH}/100)$  at equilibrium. Solid lines represent best fit lines for each temperature.

Table C-9. Statistical analysis of  $D_{fast}$  and  $k_{fast}$  versus moisture content (Figure C-5A,B) testing the difference between slopes and y-intercepts at 6% and 23% RH.

<b>ssHDX Kinetic Parameter</b>	<b>Regression parameter tested</b>	<b>F-value</b>	<b>p-value</b>	<b>Statistically significant difference</b>
<b><math>D_{fast}</math></b>	<b>Slope</b>	1.289	0.275	Not significant
	<b>y-intercept</b>	173.0	<0.0001	Significant
<b><math>k_{fast}</math></b>	<b>Slope</b>	0.5211	0.482	Not significant
	<b>y-intercept</b>	55.57	<0.0001	Significant

## Linearization of Arrhenius Equation by Taylor Series Expansion

Taylor series expansion of the Arrhenius is presented in Equation C.1,

$$k = A \frac{E_a}{R} e^{-E_a/RT_o} \left[ \frac{1}{E_a/R} + \frac{E_a}{RT_o^2} \times \frac{(T - T_o)}{1!} + \left( \frac{E_a}{RT_o^4} - \frac{2}{T_o^3} \right) \times \frac{(T - T_o)^2}{2!} + \left( \frac{1}{T_o^6} - \frac{6}{T_o^5} + \frac{6}{T_o^4} \right) \times \frac{(T - T_o)^3}{3!} + \dots \right] \quad \text{C.1}$$

where  $A$  is a pre-exponential constant from the Arrhenius equation,  $E_a$  is the activation energy,  $R$  is the universal gas constant,  $T_o$  is the temperature around which the Taylor series is expanded, and  $T$  is the experimental temperature in Kelvin. In Equation C.1, with each additional term, the leading exponent in the denominator increases faster than the exponent in the numerator. Thus, the higher order terms go to zero revealing a constant leading term ( $1/\frac{E_a}{R}$ ) and the second term which is linear in temperature (Eq. C.2).

$$k = A \frac{E_a}{R} e^{-E_a/RT_o} \left[ \frac{1}{E_a/R} + \frac{E_a}{RT_o^2} \times \frac{(T - T_o)}{1!} \right] \quad \text{C.2}$$

Figure C-6 presents rate constant,  $k$ , versus temperature for the Arrhenius equation and the linear approximation (Eq. C.2) using values for  $E_a$  and  $A$  approximated from the present data and  $T_o$  of 273 K. The relationship can be further simplified to Equation C.3, where  $C$  is a constant equal to  $E_a/(RT_o)$ . The linear relationship between reaction rate and experimental temperature becomes more apparent.

$$k = Ae^{-C}[1 + C^2(T - T_o)] \quad \text{C.3}$$

When  $C^2 \gg 1$ , Equation C.3 can be further simplified to Equation C.4, revealing a relationship where  $k$  is proportional to temperature. Selecting  $T_o$  as 273 K and using the estimation of  $E_a$ , determined below,  $C^2$  is approximately 270, validating the simplification of Equation C.3 to Equation C.4.

$$k = Ae^{-C}C^2(T - T_o) \quad \text{C.4}$$

Since  $A$  and  $C$  are both constant, Equation C.4 can be further simplified to Equation C.5, where  $Z$  is a combined constant ( $Z = Ae^{-C}C^2$ ):

$$k = Z(T - T_o) \quad \text{C.5}$$

The linear relationship between  $k$  and temperature described by Equation C.5 is only valid over small temperature ranges, for temperatures greater than 0 °C (273 K), where the majority of ssHDX experiments are carried out, and for low activation energies (Figure C-6).

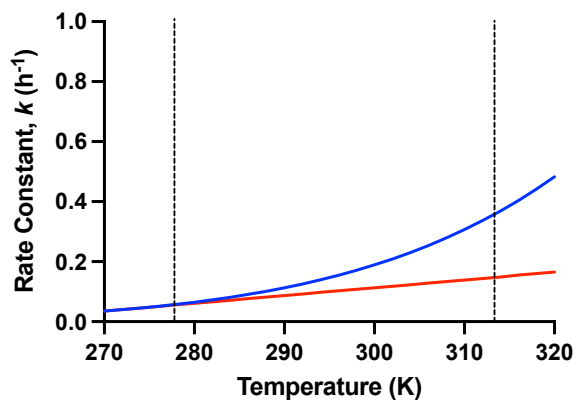


Figure C-6. Rate constant,  $k$ , versus temperature for ssHDX described by the Arrhenius equation (blue) and the linear approximation using Taylor series expansion (red). Values of  $E_a$  and  $A$  are approximated from the present data as described below. Dashed lines represent the temperature range of the current work.

### Estimation of Activation Energy for ssHDX

Activation energy,  $E_a$ , for ssHDX can be estimated from the plot of  $\ln(k)$  versus  $1/T$  based on the logarithmic form of the Arrhenius equation. The plot of  $\ln(k_{fast})$  versus  $1/T$  results in  $E_a$  of approximately 9 kcal/mol (Figure S7), which is similar to that for solution state HDX (17 kcal/mol).<sup>1</sup>

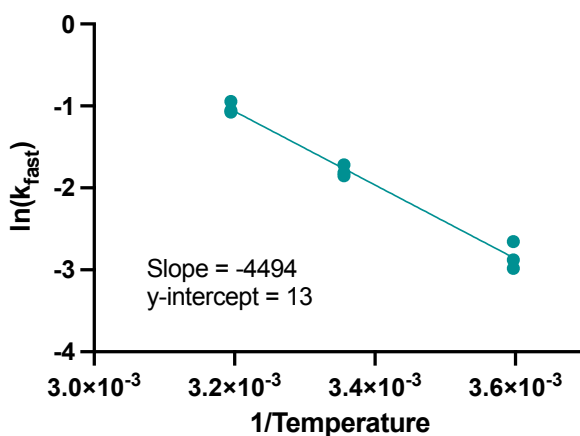
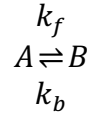


Figure C-7. The logarithm of  $k_{fast}$  as a function of inverse temperature, for lyophilized mAb subjected to ssHDX at 23 %RH. The solid line represents the linear fit with slope -4494 and y-intercept 13.

## Derivation of Equation 4.10

Derive a relationship between the number of deuterons,  $D_2O(g)$  activity ( $a_D$ ) and temperature (Eq. 4.10) based on the first-order reversible kinetic model described below.



where A and B are the number or percentage of exchangeable amide groups and deuterated amide groups, respectively, and  $k_f$  and  $k_b$  are the forward and reverse reaction rate constants, respectively.

The change in A with time is given by:

$$\frac{dA}{dt} = -k_f A + k_b B \quad (i)$$

Given the initial conditions:

$$A = A_0 \\ B = 0$$

And the boundary condition:

$$A_0 = A + B$$

Which is equivalent to:

$$B = A_0 - A \quad (ii)$$

Substitution of (ii) into (i) gives:

$$\frac{dA}{dt} = -k_f A + k_b(A_0 - A) \\ \frac{dA}{dt} = -(k_f + k_b)A + k_b A_0 \quad (iii)$$

Integration of (iii) gives:

$$A = \frac{k_b + k_f e^{-(k_f+k_b)t}}{k_f + k_b} A_0 \quad (iv)$$

Substitution of (iv) into (ii) gives:

$$B = A_0 - \frac{k_b + k_f e^{-(k_f+k_b)t}}{k_f + k_b} A_0 \\ B = A_0 \left[ 1 - \frac{k_b + k_f e^{-(k_f+k_b)t}}{k_f + k_b} \right]$$

$$\begin{aligned}
B &= A_0 \left[ \frac{k_f + k_b}{k_f + k_b} - \frac{k_b + k_f e^{-(k_f+k_b)t}}{k_f + k_b} \right] \\
B &= A_0 \left[ \frac{k_f(1 - e^{-(k_f+k_b)t})}{k_f + k_b} \right] \\
B &= \frac{k_f A_0}{k_f + k_b} [1 - e^{-(k_f+k_b)t}] \tag{v}
\end{aligned}$$

We assume the forward reaction is first-order in  $a_D$  (i.e., relative humidity (RH) in  $D_2O$ ) and dimensionless temperature,  $\mathbb{T}$ , which is normalized across the range from 273 to 373 K (i.e., 273 K = 0, 373 K = 1, and  $\mathbb{T} = T - 273/(373 - 273)$ ), where  $k_f^*$  is the forward rate constant in the absence of RH effects.

$$k_f = k_f^* \times (a_D)(\mathbb{T} \times Z) \tag{vi}$$

Substitution of (vi) into (v) gives:

$$B = \frac{k_f^*(a_D)(\mathbb{T} \times Z)A_0}{k_f^*(a_D)(\mathbb{T} \times Z) + k_b} [1 - e^{-(k_f^*(a_D)(\mathbb{T} \times Z) + k_b)t}] \tag{vii}$$

At large  $t$ , the exponential term goes to zero and B is the steady-state or plateau value,  $D_{fast}$ , giving:

$$\begin{aligned}
D_{fast} &= \frac{k_f^*(a_D)(\mathbb{T} \times Z)A_0}{k_f^*(a_D)(\mathbb{T} \times Z) + k_b} \\
\frac{A_0}{D_{fast}} &= \frac{k_f^*(a_D)(\mathbb{T} \times Z) + k_b}{k_f^*(a_D)(\mathbb{T} \times Z)} \\
\frac{A_0}{D_{fast}} &= \frac{k_f^*(a_D)(\mathbb{T} \times Z)}{k_f^*(a_D)(\mathbb{T} \times Z)} + \frac{k_b}{k_f^*(a_D)(\mathbb{T} \times Z)} \\
\frac{A_0}{D_{fast}} &= 1 + \frac{k_b}{k_f^*(a_D)(\mathbb{T} \times Z)} \tag{ix}
\end{aligned}$$

Define the pseudo equilibrium constant,  $K$ , as:

$$K = \frac{k_f^*}{k_b}$$

And substituting into (iv) gives:

$$\frac{A_0}{D_{fast}} = 1 + \frac{1}{K} \left( \frac{1}{a_D} \right) \left( \frac{1}{\mathbb{T} \times Z} \right) \quad (\text{x})$$

## References

1. Bai, Y., Milne, J. S., Mayne, L. & Englander, S. W. Primary structure effects on peptide group hydrogen exchange. *Proteins Struct. Funct. Genet.* 17, 75–86 (1993).